January 2008

The Effects of Sea Level Change on the Molecular and Isotopic Composition of Sediments in the Cretaceous Western Interior Seaway: Oceanic Anoxic Event 3, Mesa Verde, CO, USA

Jeff Salacup
University of Massachusetts - Amherst, jeff.salacup@gmail.com

THE EFFECTS OF SEA LEVEL CHANGE ON THE MOLECULAR AND ISOTOPIC COMPOSITION OF SEDIMENTS IN THE CRETACEOUS WESTERN INTERIOR SEAWAY: OCEANIC ANOXIC EVENT 3, MESA VERDE, CO, USA

A Thesis Presented

by

JEFFREY M. SALACUP

Submitted to the Graduate School of the
University of Massachusetts Amherst in partial fulfillment
of the requirements for the degree of

MASTER OF SCIENCE

September 2008

Department of Geosciecnes

THE EFFECTS OF SEA LEVEL CHANGE ON THE MOLECULAR AND ISOTOPIC COMPOSITION OF SEDIMENTS IN THE CRETACEOUS WESTERN INTERIOR SEAWAY: OCEANIC ANOXIC EVENT 3, MESA VERDE, CO, USA

A Thesis Presented

by

JEFFREY M. SALACUP

Approved as to style and content by:

Steven T. Petsch, Chair

R. Mark Leckie, Member

Stephen J. Burns, Member

Robert DeConto, Member

Laurie Brown, Department Head
Department of Geoscience

ABSTRACT

THE EFFECTS OF SEA LEVEL CHANGE ON THE MOLECULAR AND ISOTOPIC COMPOSITION OF SEDIMENTS IN THE CRETACEOUS WESTERN INTERIOR SEAWAY: OCEANIC ANOXIC EVENT 3, MESA VERDE, CO, USA

SEPTEMBER 2008

JEFFREY SALACUP, B.S., UNIVERSITY OF MASSACHUSETTS AMHERST

Directed by: Associate Professor Steven T. Petsch

Cretaceous Oceanic Anoxic Events (OAEs) represent periods of enhanced burial of organic matter in black shale in marine, continental margin, and epicontinental settings around the globe. Compared to other OAEs, comparatively little is known about the last of these widespread events, OAE 3 (Coniacian-Santonian). The Mancos Shale at Mesa Verde National Park is an Upper Cretaceous (Cenomanian-Campanian) formation containing marine sediments of the second-order Niobrara cyclothem and associated third-order transgressive-regressive events (T1-T4). The Coniancian-Santonian Niobrara interval is characterized as dark-gray, moderately to well laminated, calcareous shale and mudstone. Synthesis of new high-resolution bulk chemostratigraphy and biomarker analyses with the preexisting geochemical, lithological, and biostratigraphical framework suggest a temporally protracted oxygen minimum zone was largely responsible for the preservation of large quantities of organic matter contained in these sediments. Additionally, C/N and $\delta^{15}N_{bulk}$ values imply denitrification and nitrogen fixation were both important metabolic processes during periods when surface water nutrient profiles may have differed much from those of the modern ocean.

TABLE OF CONTENTS

Page

ABSTRACT.....iii

LIST OF TABLES.....vii

LIST OF FIGURES.....viii

CHAPTER

1. CRETACEOUS OCEANIC ANOXIC EVENTS AND SEA LEVEL……1

1.1 Cretaceous Oceanic Anoxic Events……...1

1.1.1 Controls on Organic Matter Accumulation and Utility in Paleo-reconstructions…….3
1.1.2 Oceanic Anoxic Event 1a……....7
1.1.3 Oceanic Anoxic Event 1b……...8
1.1.4 Oceanic Anoxic Event 1c and 1d……..……....9
1.1.5 Oceanic Anoxic Event 2……....9
1.1.6 Oceanic Anoxic Event 3……...11

1.2 High Global Sea Level and the Late-Cretaceous Western Interior Seaway…13

1.2.1 Depositional Patters and Cyclicity in the KWIS……...16
1.2.2 Paleoceanography of the KWIS……16
1.2.3 The San Juan Basin: Late-Cretaceous Depocenter……...19
1.2.4 The Niobrara Cyclothem and Mesa Verde……...20

2. SEA LEVEL, OXYGEN STRESS, AND WATER COLUMN ECOLOGY DURING OCEANIC ANOXIC EVENT 3……25

2.1 Hypothesis……....26

2.1.1 Objectives.....26

2.2 Methods.....27

2.2.1 Sampling, Biostratigraphy, and Age…….27
2.2.2 Bulk Analyses……...29
2.2.3 Molecular Analyses……..31

2.2.4 Consideration of Maturity and Biodegradation……32

2.2.4.1 Maturity……..33
2.2.4.2 Biodegradation……...35

2.2.5 Biomarker Utility in Environmental Reconstruction……35

2.3 Results……..38

2.3.1 Bulk Characteristics……..38
2.3.2 Molecular Characteristics……....44

2.3.2.1 Compound Distribution.....44
2.3.2.2 Sample Maturity and Biodegradation.....44
2.3.2.3 Saturated Hydrocarbons.....46
2.3.2.4 Aryl-Isoprenoids.....47

2.4 Discussion.....48

2.4.1 Correlation of Coniacian-Santonian Sea Level Change at Mesa Verde.....48
2.4.2 Terrestrial vs. Algal Ratio: Source Indicator or Diagenetic Imprint? 51
2.4.3 $\delta^{13}C_{carb}$: Timing of Oceanic Anoxic Event 3 at Mesa Verde.....54
2.4.4 Sediment Fabric.....56
2.4.5 Gamma Ray and Th/U Ratios.....57
2.4.6 C/N Ratios and Denitrification.....59
2.4.7 $\delta^{15}N_{bulk}$ and Nitrogen Fixation.....62
2.4.8 Photic Zone Euxinia.....64
2.4.9 Organic Matter.....65
2.4.10 $\delta^{13}C_{OM}$: A Mixing Model.....66

2.5 Conclusions.....70

3. FURTHER WORK.....73

APPENDICES

1: CORRELATIVE X/Y PLOTS.....75
2: BIOMARKER CONCENTRATIONS.....76
3: REPRESENTATIVE CHROMATOGRAMS (A) AND MASS FRAGMENTATION PATTERS (B) OF *N*-ALKANES (M/Z 57), HOPANES (M/Z 191), AND STERANES (M/Z 217).....78

REFERENCES...81

LIST OF TABLES

2.1 Biomarker Interpretation.....33

2.2 Bulk Geochemical Interpretation.....36

2.3 Supporting Data.....40

2.4 Bulk Geochemical Data.....41

2.5 Biomarker Results.....45

LIST OF FIGURES

1.1 Geographic occurrence of the various Oceanic Anoxic Events and their depositional facies. Added in red is our section at Mesa Verde during OAE 3. Adapted from Schlanger, 1976.....4

1.2 The mid-Cretaceous record of major black shales and OAEs and the associated carbon isotopic record (Erbacher et al., 1996; Bralower et al., 1999), changing global sea level (Haq et al., 1988), and seawater chemistry (Bralower et al., 1997). Short-term sea level changes are shown as the dark shaded line, and the long-term record of sea level is shown with the thick solid line (adapted from Haq et al. (1988)). Initiation of increased spreading rates drove the long-term (Albian-Turonian) rise of global sea level. (From Leckie, 2002).....5

1.3 Locations of organic carbon-rich intervals associated with OAE 3 superimposed on the paleogeographic map of the mid-Cretaceous at 80 Ma (of Hay *et al*., 1999; from Wagner *et al*., 2004).....12

1.4 Global paleogeography of the Late Cretaceous showing marine inundation of the continents (light blue).....14

1.5 Cretaceous sea level and OAEs listing a) Kaufamann's T1-T10 and b) Molenaar's T1-T4.....15

1.6 The rhythmically bedded limestone and mudstone of the Bridge Creek Limestone Member of the Mancos Shale exposed at Pueblo, CO. The author for scale.....17

1.7 Paleogeography of the Late Cretaceous Western Interior Seaway at ~ 85 ma. MV = Mesa Verde National Park, CO. Blue and red arrows show suggested paths of cool brackish northern and warm saline southern water masses (Kent, 1968; Scott and Taylor, 1977; Spearing, 1976; Boyles and Scott, 1982). Adapted from http://jan.ucc.nau.edu/~rcb7/namK100.jpg.....19

1.8 Chronostratigraphy of the Smoky Hill Member of the Mancos Shale at MVNP based on molluscan biostratigraphy and correlation with the Rock Canyon (Pueblo Reservoir), Colorado reference section and Raton Basin, New Mexico (based on Leckie et al., 1997). Transgressive-regressive (T-R) terminology from Molenaar (1983).....21

1.9 A) Estimates of sedimentation rate and a graphic of the Mancos Shale at Mesa Verde from Leckie *et al* (1997). Ranges in sedimentation rate reflect uncertainties in the placement of biozone boundaries. B) Stratigraphic column for the study interval at MVNP. Numbers relate to position in meters above the Dakota Sandstone. 22

1.10 Correlation of Mancos Shale at MVNP with other locations of the Colorado Plateau illustrating Molenaar's (1983; T1-T4) transgressive-regressive cycles (adapted from Leckie et al., 1997).....24

2.1 Aerial view of the study section at MVNP. Numbers correlate to sampling locations described in Leckie et al. (1997). North is at the top of the page. Image from googlemaps.com.....28

2.2 Oblique view of the study section. Numbers correlate to sampling locations described in Table 2.1 and Leckie (1997). The curving white line highlights the top of the prominent Niobrara Bench (289 m). Thick vertical white line included for scale. Image from googlemaps.com.....29

2.3 Idealized analytical flow chart for preparation of MVNP samples.....30

2.4 Plots of carbonate and total organic carbon. Note two broad maxima between 210 and 230 m and 270 and 300 m.....39

2.5 Illustration of changes in n-alkane distribution with respect to TAR.....46

2.6 Plots illustrating relationships between carbonate concentration, sterane/hopanes (x 10^8), % Quartz, and sea level. Smoothed dashed lines are 6^{th}-order polynomial regressions.....50

2.7 Plots illustrating relationships between the terrestrial vs. algal ratio, % sand, total organic carbon to total nitrogen (C/N), total organic carbon, photic zone euxinia, and sea level. Smoothed black line on C/N plot is a 6^{th}-order polynomial regression.....52

2.8 Water column schematic illustrating the effects of increasing current activity and oxygen exposure time on the terrestrial vs. algal ratio and grain size. Shaded gray area represents decreased oxygen minimum zone extent during periods of increased oxicity and current activity.....53

2.9 Comparison of the stable isotopic composition of carbonate at MVNP to those of the new reference section of Jarvis *et al*. (2006). ^{13}C-enrichment at the bottom of both records represents the global signal of OAE 3.....55

2.10 Plots illustrating relationships between the terrestrial vs. algal ratio, % sand (grain size), total organic carbon to total nitrogen (C/N), total organic carbon, gamma ray emission, photic zone euxinia, and sea level.....59

2.11 Water column schematic illustrating the impact of oxygen minimum zones and denitrification on C/N ratios.....60

2.12 A hypothetical model demonstrating depletion of nitrogen isotope values and increases in C/N during N-rich-exclusive degradation assuming the protein fraction of prokaryotic biomass is enriched in ^{15}N relative to the whole cell by 3‰ (Macko *et al*., 1986). Percentages represent the percent mass of the degradaing cells that are "N-rich" based on the averages for prokaryotic cells (Neidhardt *et al*., 1996). Kinetic isotope fractionations are ignored for this estimation (from Junium *et al*., 2007).....62

2.13 Comparison of ^{15}N values with those of other proxies. A weak negative correlation can be seen between ^{15}N and C/N ratios.....63

2.14 Plots illustrating the relationships between the stable carbon isotopes of organic matter and other proxies.....67

2.15 A water column schematic comparing the results of our simple two-end member mixing model with those of the in situ study of van Mooy (2002).....70

CHAPTER 1

CRETACEOUS OCEANIC ANOXIC EVENTS AND SEA LEVEL

1.1 Cretaceous Oceanic Anoxic Events

Cretaceous Oceanic Anoxic Events (OAEs) represent periods of enhanced burial of organic matter in black shale in marine, continental margin, and epicontinental settings around the globe (Schlanger and Jenkyns, 1976). The geologic sequestration of this organic matter directly impacted atmospheric carbon dioxide concentrations aiding in the transition from the Mesozoic Greenhouse to the Cenozoic Icehouse climates (Arthur *et al*., 1988). Cretaceous shales have been the subject of decades of detailed sedimentological, mineralogical, paleontological, and geochemical research. Initially, investigation into the processes responsible for the deposition of Cretaceous black shales was driven by economic interests in the large volumes of oil associated with these deposits. More recently, studies of the paleo-climatic and –oceanographic processes associated with deposition of Cretaceous OAE sediments have been driven by an increasing need to understand the behavior of the coupled ocean-atmosphere system during times of increased atmospheric greenhouse gas inventories. Elucidation of the triggers, feedbacks, maintenance, and termination of widespread deposition of organic matter-rich sediments, water column oxygen stress, and carbon dioxide drawdown during Greenhouse periods will aid in predictions of the response of the current ocean-atmosphere system to future high greenhouse gas scenarios.

Jenkyns (1980) recognized three periods of enhanced organic matter burial (OAEs) during the Cretaceous based on the presence of organic matter rich intervals in

marine, marginal, and epicontinental facies (Figure 1.1). Since then, the Deep Sea Drilling Program (DSDP), Ocean Drilling Program (ODP) and the Integrated Ocean Drilling Program (IODP) have recovered numerous cores of organic carbon rich Cretaceous strata (Arthur *et al*., 1985). These samples together with continental cores and outcrop samples have led to a more detailed understanding of the distribution and timing of OAEs. Today, at least six Cretaceous Oceanic Anoxic Events are recognized in sediments from around the world (Leckie, 2002). Two of them, the early Aptian OAE 1a (~120.5 Ma) and the Cenomanian-Turonian OAE 2 (~93.5 Ma), represent nearly global deposition of organic matter-rich black shale. The other four, OAE 1b (late-Aptian to early-Albian; ~ 113-109 Ma), OAE 1c and 1d (both late-Albian; ~102 and 99.2 Ma respectively), and OAE 3 (Coniacian-Santonian; ~87.3-84.6 Ma), represent more regional deposition of black shale (Leckie, 2002). OAE 1b and OAE 3 are prolonged events lasting on the order of 3-4 myr, unlike the others which range from 10's to 100's of thousands of years in duration.

OAEs are typically associated with rising sea-level, flooding of previously exposed continental settings, expansion of marginal shelf environments, and intensified primary productivity (Arthur *et al*., 1990; Erbacher *et al*., 1996). The sinking and microbial degradation of this primary product removes free oxygen from the water column aiding in the preservation of subsequently deposited organic matter. However, once oxygen limitation is achieved and organic matter can be efficiently buried, the removal of organic matter associated nutrients (N, S, Fe) from the water column inhibits future production. High global sea-level and the maintenance of nutrients in highly productive waters are probably linked in part to changes in tectonic activity (Figure 1.2).

For example, Leckie *et al*. (2002) concluded that submarine volcanism and emplacement of large igneous provinces directly and indirectly fostered the deposition of black shale during OAEs via increased nutrient availability and/or changes in ocean circulation. Periods displaying high rates of sea floor spreading and/or emplacement of large oceanic plateaus (Large Igneous Provinces or LIPs) experience rising sea level due to the increased buoyancy of new, warm, less dense oceanic crust. Additionally, intensified submarine volcanism would be an important source of dissolved ions to the world ocean during OAEs. Finally, high atmospheric carbon dioxide concentrations during the Cretaceous and enhanced hydrologic activity would result in higher rates of continental chemical weathering and delivery of dissolved nutrients to marine environments.

1.1.1 Controls on Organic Matter Accumulation and Utility in Paleo-reconstructions

Sedimentary organic matter concentrations are controlled by many variables such as production intensity, heterotrophic grazing and fecal packaging, eukaryotic diversity, sediment and water-column oxidation state, and related microbial degradation processes (Peters, 2003; Killops and Killops, 2005). In turn, these factors are each impacted by "extra-marine" atmospheric and environmental conditions such as nutrient delivery, water balance (E-P), atmospheric gas inventories, temperature, surface wind direction and currents, production of deep water masses and associated upwelling and downwelling. Due to this long but incomplete list, great care must be taken in the interpretation of organic geochemical records of all types.

In a summary of general conditions conducive to the accumulation of concentrated sedimentary organic matter Killops and Killops (2005) list:

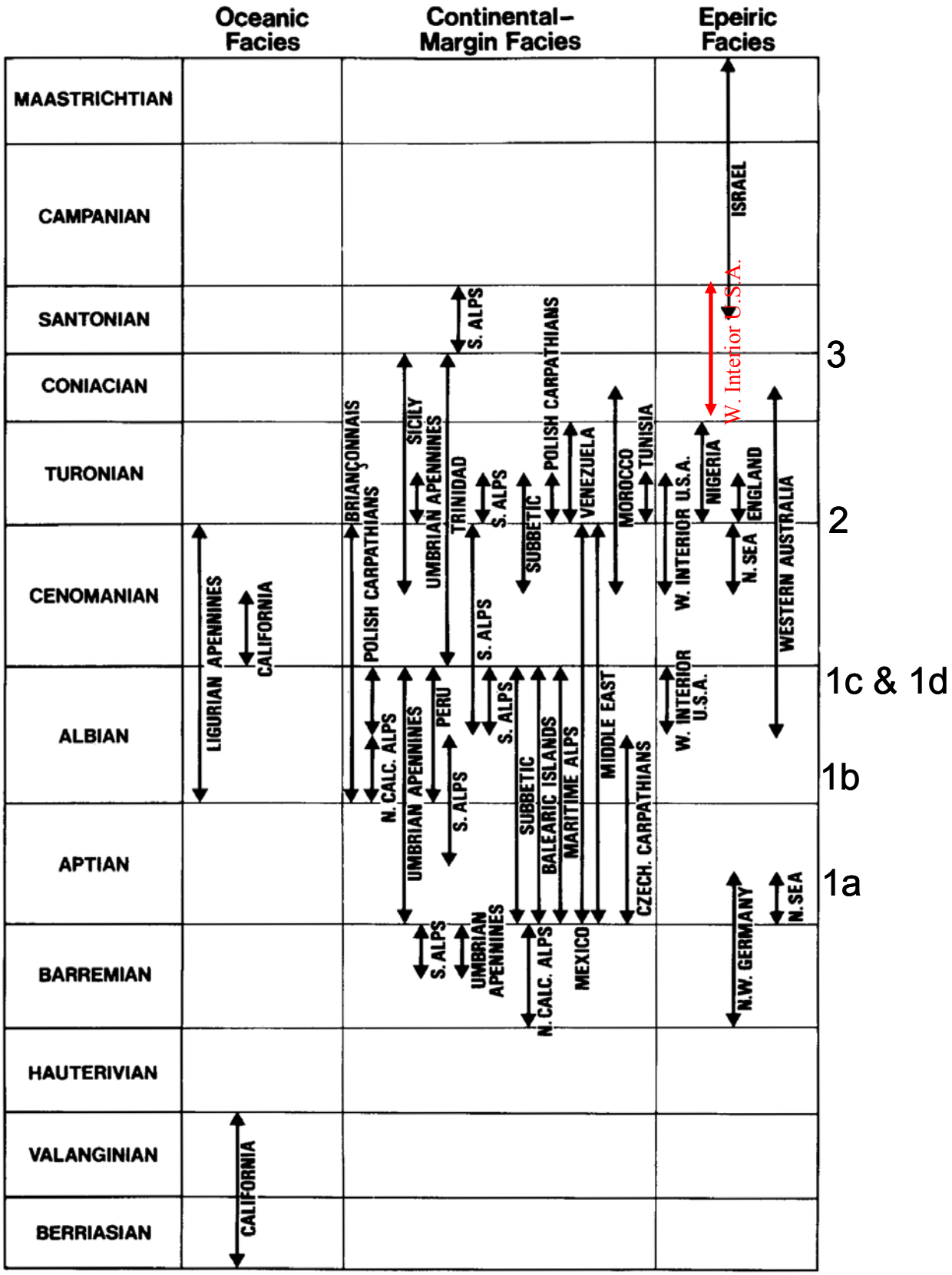

Figure 1.1 Geographic occurrence of the various Oceanic Anoxixc Events and their depositional facies. Added in red is our section at Mesa Verde during OAE 3. Adapted from Schlanger, 1976

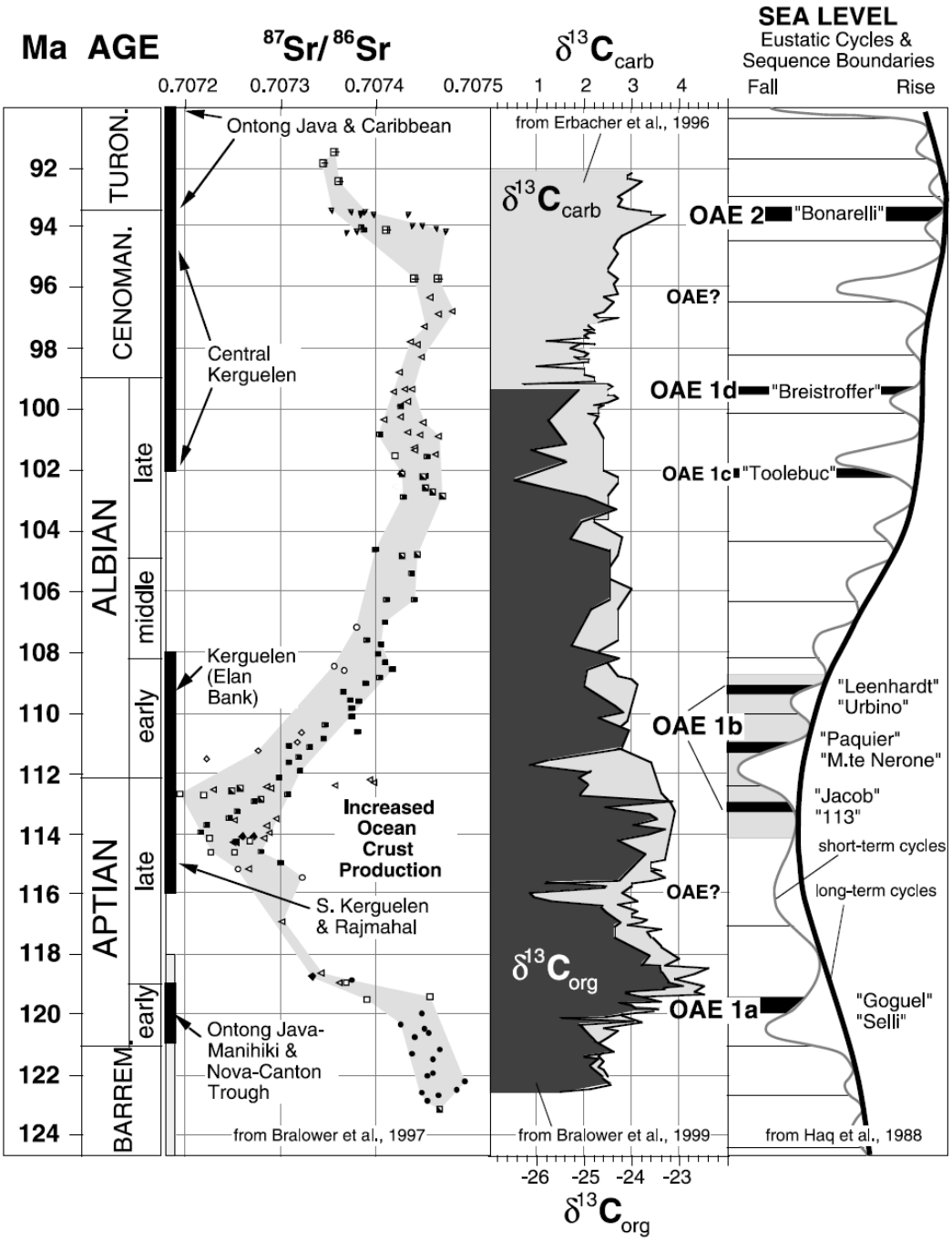

Figure 1.2 The mid-Cretaceous record of major black shales and OAEs and the associated carbon isotopic record (Erbacher et al., 1996; Bralower et al., 1999), changing global sea level (Haq et al., 1988), and seawater chemistry (Bralower et al., 1997). Short-term sea level changes are shown as the dark shaded line, and the long-term record of sea level is shown with the thick solid line (adapted from Haq et al. (1988)). Initiation of increased spreading rates drove the long-term (Albian-Turonian) rise of global sea level. (From Leckie et al., 2002)

1. high rates of primary production, fecal packaging, and removal from the euphotic zone,

2. a low energy depositional setting which allows the accumulation of low-density organic material,

3. low sediment contributions from inorganic sources such as carbonaceous and detrital material,

4. environmental condition poisonous to detritovores and decomposers; namely anoxia.

The integrity of biomarker source reconstructions, especially important in ancient rocks, is based on an increasing understanding of the relative reactivity of differing suites of organic molecules under various water-column and sediment redox conditions. Prior to diagenetic alteration and maturation of biomarker distributions (discussed below) a series of water column and sediment processes has been shown to alter the distribution of a wide-range of organic molecules. Hedges *et al* (1999) and Hartnett *et al* (1998) correlated "oxygen exposure time" in sediment pore-waters to the efficiency of organic matter burial. It has been shown that the "oxygen exposure time" of falling (Sinninghe-Damste *et al*., 2002) and sedimentary (Cowie *et al.*, 1995; Hoefs *et al.*, 1998; Cowie *et al*., 1998) particulate organic matter strongly influences not only its sediment concentration but also its molecular profile. These findings call into doubt the utility of labile (easily degraded) organic biomarkers in source reconstructions unless environmental conditions can be adequately constrained using independent inorganic proxies. In these studies, terrestrial *n*-alkanes were found to be among the best preserved biomarkers.

1.1.2 Oceanic Anoxic Event 1a

The beginning of the Early Aptian (~120.5 Ma) OAE 1a event is associated with a sharp negative $\delta^{13}C$ excursion in both organic and carbonate carbon, global transgression, and increased rates of ocean crust production including the emplacement of the Ontong Java Large Igneous Province (LIP) (Sliter, 1989a; Larson, 1991a, 1991b; Tarduno et al., 1991; Bralower et al., 1994,1997,1999; Erba, 1994; Föllmi et al., 1994; Jenkyns, 1995; Menegattiet al., 1998; Larson and Erba, 1999; Jones and Jenkyns, 2001; Leckie *et al.*, 2002). Using compound-specific stable isotope ratios of terrestrial and marine *n*-alkanes, van Breugel *et al.* (2007) found this excursion was coincident in the marine and terrestrial realms. Thus, they concluded the negative excursion was the result of injection of isotopically depleted carbon into the ocean-atmosphere system via either clathrate dissociation and/or thermal metamorphism of organic matter rich sedimentary rocks. Early characterization of organic matter from this event listed it as terrestrial (Simoneit, 1986) consistent with the restricted configuration of Tethys in the early Aptian. More recent organic geochemical assessment of Aptian sediments at Shatsky Rise (west central Pacific) implies an algal and bacterial origin in an Aptian "open marine" Pacific setting (Dumitrescu and Brassell, 2005).

After the negative excursion, the widespread burial of organic matter during OAE 1a resulted in a positive $\delta^{13}C$ excursion of >2‰ (Leckie *et al.*, 2002) and has been linked to the Ongtong-Java Pacific "superplume" eruption (Sliter, 1989a; Larson 1991a, 1991b; Tarduno et al., 1991; Bralower et al., 1994, 1997, 1999; Föllmi et al., 1994; Jenkyns, 1994; Menegatti et al., 1998; Jones and Jenkyns, 2001; Erba, 1994; Larson and Erba, 1999).

1.1.3 Oceanic Anoxic Event 1b

The latest-Aptian to earliest-Albian (113-109 Ma) OAE 1b event is a protracted interval of at least three separate depositional events experienced in western (Mexico and N. Atlantic) and eastern (Mediterranean) Tethys regions (Arthur and Premoli Silva, 1982; Bréhéret et al., 1986; Premoli Silva et al., 1989; Bralower et al., 1993, Leckie, 2002; Wagner *et al.* 2008). OAE 1b is characterized by an initial depletion and subsequent enrichment of $\delta^{13}C$ in both carbonates and organic matter. The negative excursion is attributed to global cooling, ice sheet advance, and sea-level fall in response to prolonged burial of organic matter and carbon dioxide drawdown (Weissert and Lini, 1991). Recently, compound specific analyses of terrestrial and marine biomarkers in early Albian sediments (NW Africa; DSDP Site 545) revealed a -1.5‰ excursion in terrestrial realms leading a similar change in the marine realm by 1-3 kyr (Wagner *et al.*, 2008). The abruptness of the excursion led the authors to conclude that, similar to OAE 1a, it was linked to the rapid release of isotopically depleted carbon into the atmosphere with later (1-3 kyr) incorporation into the oceanic dissolved inorganic carbon (DIC) pool.

Similar to OAE 1a, organic matter from this event was initially listed as terrestrial (Simoniet, 1986). However, advances in both analytical and organic geochemistry as well as microbiology have expanded our understanding of biomarkers in marine sediments. For example, Kuypers *et al*. (2001) detected large contributions of membrane lipids associated with chemoautotrophic Crenarchaeota in sediments from the western North Atlantic (near Florida; ODP Hole 1049C) and the Vocontian Basin of southeast France. The authors hypothesized the large concentration of such lipids was linked to extreme water column oxygen stress and that the relative enrichment of archaeal lipids in ^{13}C

relative to algal lipids accounts for much of the enrichment encountered in bulk $\delta^{13}C$ measurement of organic matter in OAE 1b.

1.1.4 Oceanic Anoxic Event 1c and 1d

Oceanic Anoxic Event 1c is a late Albian (102 Ma) short-lived episode recognized in sediments from central Italy and Australia. It is associated with the beginning of Central Kerguelen volcanism and short-term regression. Organic matter from this event is terrestrial in nature (Pratt and King, 1986; Bralower et al., 1993; Coccioni and Galeotti, 1993; Haig and Lynch, 1993; Erbacher et al., 1996).

Alternatively, OAE 1d is recognized across the Tethyan Basin with a more sparse record in the South Atlantic, South Indian, and East Pacific Basins, (Bréhéret and Delamette, 1989; Bréhéret, 1994; Erbacher et al., 1996; Wilson and Norris, 2001). Organic matter from this event is marine and its deposition may have been aided by the breakdown of water column stratification (Wilson and Norris, 2001) and delivery of nutrients to the photic zone.

1.1.5 Oceanic Anoxic Event 2

Oceanic Anoxic Event 2 (Cenomanian-Turonian; 93.5 Ma) represents a truly global and large perturbation of the global carbon cycle. Analyses of stable carbon isotopes of bulk organic matter from this event display a rapid and large positive excursion (~ 6 ‰; Erbacher, 2005). Marine deposition of high concentrations of organic matter in black shale during this time has been linked to transgression (White and Arthur, 2006), increased seafloor and continental volcanism (Kauffman, 1984; Kauffman and

Caldwell, 1993), and iron fertilization associated with mantle plume volcanism (Sinton and Duncan, 1997; Kerr, 1998, Leckie et al, 1998; Snow et al, 2005), all leading to the development of a "volcanically spiked nutrient-rich water column" (Leckie et al., 2002). Vertical delivery of nutrients to the photic zone may have been aided by the emplacement of a very warm (~ 20°C) intermediate/deep water mass weakening vertical density gradients (Huber et al., 1999, 2002). Additionally, the creation of a deep water mass connection between the North and South Atlantic may have aided in the delivery of nutrients via the ventilation of bottom water masses (Arthur and Natland, 1979; Tucholke and Vogt, 1979; Summerhayes, 1981, 1987; Cool, 1982; Zimmerman et al., 1987; Leckie et al., 1998; Poulsen et al., 2001).

Bulk and molecular analyses of organic matter deposited during OAE 2 suggest a marine source (Scholle and Arthur, 1980; Summerhayes, 1981, 1987; Pratt and Threlkeld, 1984; Arthur et al., 1987, 1990; Schlanger et al., 1987; Jarvis et al., 1988; Hilbrecht et al., 1992; Thurow et al., 1992; Gale et al., 1993; Pratt et al., 1993; Jenkyns et al., 1994; Sugarman et al., 1999). OAE 2 has been linked with emplacement of the Caribbean LIP and rising global sea level (Sinton and Duncan, 1997; Kerr, 1998; Leckie et al., 1998; Snow et al., 2001). Rates of organic matter burial during this event display characteristics consistent with orbital forcing (Gale et al., 1993; Sageman et al., 1998).

Because of its pronounced and widespread character, OAE 2 is the most studied Cretaceous OAE. In the Western Interior Seaway, OAE 2 is expressed in Cenomanian-Turonian deposits of the lower Mancos Shale and the correlative deposits of the Bridge Creek Limestone Member of the Greenhorn Formation. Previous bulk and molecular investigations of organic matter source to the southern KWIS during OAE 2 concluded

western locations were dominated by terrestrial input which became increasingly marine/algal to the east (Pratt and Threlkeld, 1984; Hayes et al., 1989; Curaile, 1994; Pancost et al., 1998). Vertical lithologic variations in *n*-alkane distributions were ascribed to the increased lability of marine algally-derived compounds and/or decreased marine productivity during times of carbonate deposition.

1.1.6 Oceanic Anoxic Event 3

In comparison to the Cenomanian-Turonian boundary event, OAE 3 (Coniacian-Santonian; 87.3-84.6 Ma) is longer-duration, spatially-restricted, and less-pronounced in the isotopic record. For these reasons, mechanisms of initiation and maintenance for this event are still poorly understood. It is thought that by this time in the Cretaceous, water column oxygen stress was limited to restricted Atlantic epicontinental basins and that open marine settings were becoming increasingly ventilated (Figure 1.3; Thiede and van Andel, 1977; van Andel et al., 1977; Dean et al., 1984; Arthur et al., 1990; Ly and Kuhnt, 1994; Mello et al., 1995; Holbourn et al., 1999; Wagner and Pletsch, 1999; Davis et al., 1999; Erlich et al., 1999). For example, the organic matter-rich Turonian-Santonian lower La Luna Formation (and stratigraphic equivalents) of the Maracaibo and Barinas/Apure basins (western Venezuela) is thought to have been deposited under low-oxygen or anoxic bottom waters (Erlich et al. 1999). Recently, these black shales have been cored offshore at Demerara Rise representing the bathyal extension of oxygen stress into deeper waters (Myers et al., 2006).

However, Wagner *et al.* (2004) documented the expression of at least intermittent photic zone euxinia in equatorial Atlantic sediments (Deep Ivorian Basin, ODP Site 959)

suggesting open ocean anoxia was still occurring. The authors also concluded that the large concentrations of marine-derived organic matter deposited in the Deep Ivorian Basin were influenced by eccentricity and precessional orbital cyclicity. Using geochemical proxies of continental runoff (Ti/Al and K/Al), Beckmann *et al.* (2007) were able to directly link anoxia and black shale deposition in the Deep Ivorian Basin to cyclical changes in monsoon climate and increased river discharge. Deposition of organic matter during OAE 3 led to a broad positive $\delta^{13}C$ excursion seen in carbonates from around the globe (Jenkyns *et al.*, 1994; De Romero *et al.*, 2003).

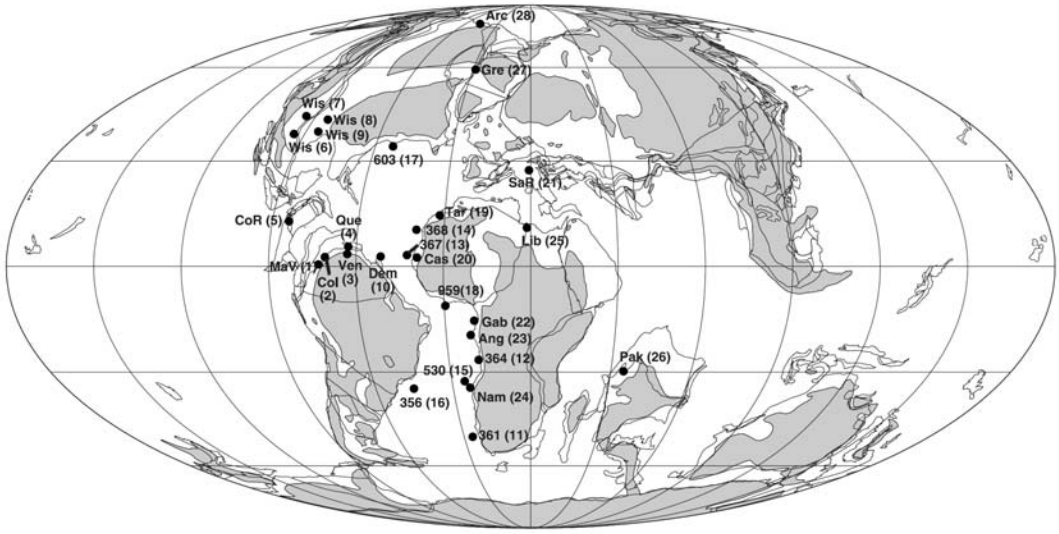

Figure 1.3 Locations of organic carbon-rich intervals associated with OAE 3 superimposed on the paleogeographic map of the mid-Cretaceous at 80 Ma (of Hay *et al.*, 1999; from Wagner *et al.*, 2004)

In the Western Interior Seaway, OAE 3 should be expressed in sediments of the Niobrara cyclothem particularly the Coniancian-Santonian Smoky Hill Member. A study of stable isotopic ratios of carbonate in bulk sediment as well as inoceramid bivale shells discovered a broad ^{13}C-enrichment in the shells of bivalves contained in the lower Smoky

Hill (Pratt *et al.*, 1985). An investigation by Dean and Arthur (1998) of organic matter through the Smoky Hill revealed the source as marine. However, HI values for their section ranged from less than 100 to greater than 300, more consistent with type III and II/III (terrestrial and paralic) kerogen. Additionally, these authors recognized many levels of depositional cyclicity in their studied section ranging in duration from orbital (precession 20-40 kyr) to tectonic (1-3 myr). This cyclicity modulated carbonate and organic carbon contents as well as detrital inputs suggesting deposition and preservation of organic matter in the WIS during OAE 3 were influenced by continental runoff. However, a detailed biomarker study of oxygen stress, ecology, and sediment diagenesis within this preexisting framework is still lacking.

1.2 High Global Sea Level and the Late-Cretaceous Western Interior Seaway

Elevated rates of sea floor spreading, emplacement of several Large Igneous Provinces, extremely high pCO_2-induced greenhouse conditions, and the presumed lack of large ice sheets led to high eustatic sea-level during the Mesozoic peaking in the late Cretaceous (Fig. 1.4). Superimposed on this first and second order eustatic signal are ten globally recognized major transgressive events in epicontinental basins during the Cretaceous (Fig 1.5a; T1 - T10; Kaufmann, 1977) reflecting the third-order eustatic variations of Haq et al. (1987). More specifically, in the Western Interior Seaway (WIS, Fig. 1.5b) major marine deposition was confined to the Cenomanian through the Campanian (99.6-70.6 Ma) coincident with peak eustatic sea-level, high rates of thrusting in the Sevier orogenic belt to the west, and rapid subsidence of the associated foreland basin (Kauffman, 1977; Kauffman, 1985; Elder, 1993; Kauffman and Caldwell, 1993). In

a zone termed the 'axial basin' by Kauffman et al. (1985), subsidence occurred faster than sediment delivery resulting in thick deposition of fine-grained clastic sediment, interbedded with pelagic carbonates, particularly in the southern and eastern reaches of the basin. This resulted in four Western Interior transgressive-regressive pulses of late Cenomanian to early Campanian age labeled T1-T4 by Molenaar (1983). Today, these mud-dominated sediments are exposed at numerous outcrops around the Colorado Plateau.

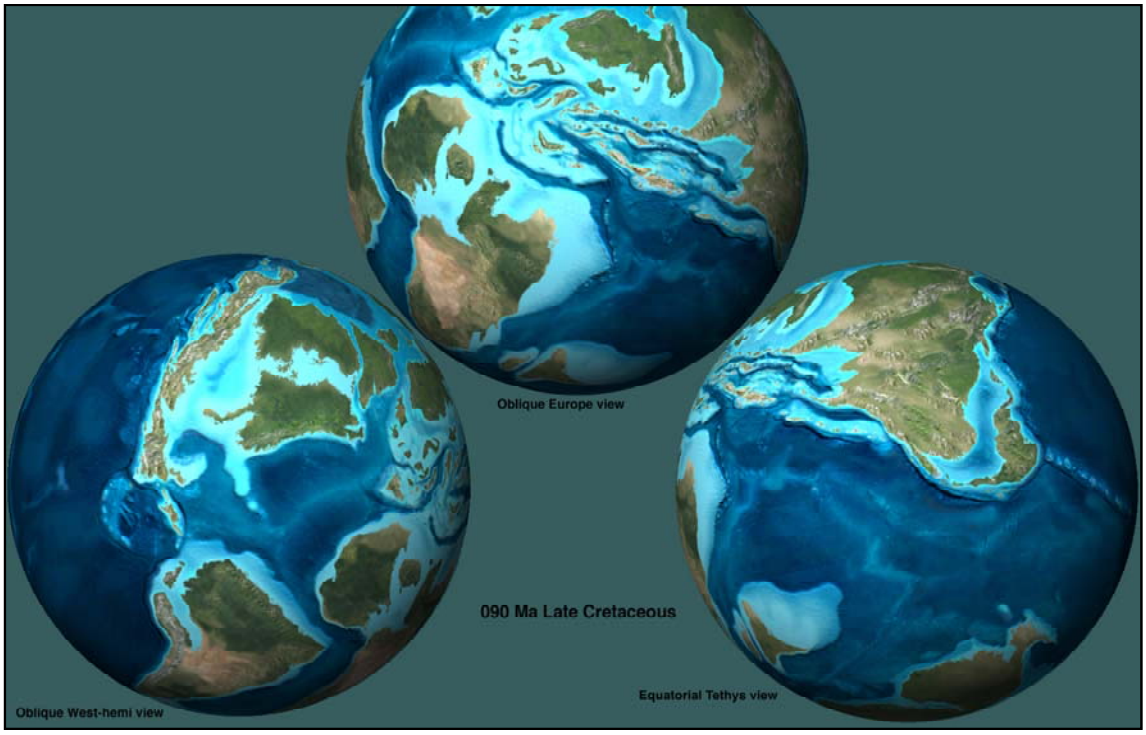

Figure 1.4 Global paleography of the Late Cretaceous showing marine inundation of the continents (light blue). http://jan.ucc.nau.edu/~rcb7/090_Cretaceous_3globes.jpg

Rising global sea level and regional subsidence led to the deposition of thick transgressive-regressive sequences of sediment, called cyclothems. One cyclothem records the transgression and regression of the seaway in either a symmetrical or asymmetrical stack of sediments transitioning from sands on the bottom to muds and carbonate in the middle to muds and eventually back to sands upon regression at the top

of the cyclothem. The two most widespread cyclothems preserved in the Cretaceous sediments of the Western Interior Seaway are the late Cenomanian–middle Turonian Greenhorn Cyclothem and the late Turonian-early Campanian Niobrara Cyclothem. These two cyclothems record the four third-order transgressive events of Molenaar (T1 – T4; Molenaar, 1983). The Greenhorn Cyclothem (T1), represents maximum flooding of the North American continent coincident with Oceanic Anoxic Event 2 (Arthur et al., 1987; Schlanger et al., 1987). The Niobrara Cyclothem (T2, T3, and T4) represents less extensive continental flooding than the Greenhorn, and is coincident with Ocean Anoxic Event 3 (Schlanger and Jenkyns, 1976, Arthur et al., 1990).

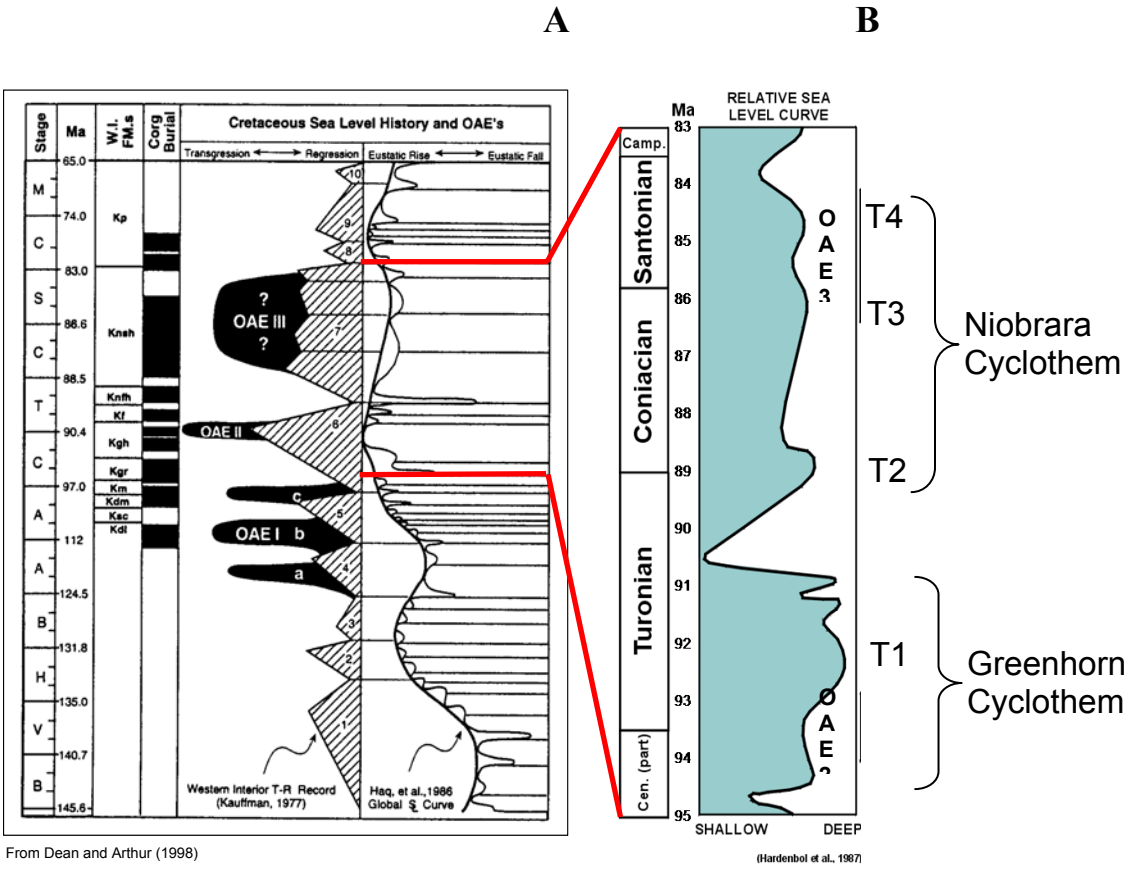

Figure 1.5 Cretaceous sea level (from Hardenbol et al., 1987) and OAEs relative to a) Kaufmann's T1-T10 and b) Molenaar's T1-T4 transgressive-regressive cycles. Left panel from Kaufmann and Caldwell (1993).

1.2.1 Depositional Patterns and Cyclicity in the KWIS

Previous sea level reconstructions and correlations in the Western Interior Seaway (Kaufmann, 1977; Molenaar, 1983; Elder, 1993; Kaufmann and Caldwell, 1993) have employed basin wide lithostratigraphy, biostratigraphy, and the presence of rhythmically-bedded laterally-continuous carbonate beds, such the Bridgecreek Limestone of the Greenhorn cyclothem (Fig. 1.6) and the Fort Hayes Limestone of the Niobrara cyclothem, as a "fingerprint" for specific units and times expressed in the basin. Many of these widespread beds were deposited throughout the basin (over 1000s of km) and therefore act as superb markers for visually correlating geographically separated outcrops. These limestone correlations are supported by molluscan biostratigraphy. Variations in lithology from carbonate-rich marls, chalks, and limestones to carbonate-poor organic matter-rich mudrocks and shales are believed to reflect changes in orbitally sensitive delivery of continental detritus and nutrients, fresh water runoff, water-column (Fischer, 1980; Arthur, 1984; Herbert and Fischer, 1986; Sageman et al., 1998, Dean and Arthur, 1998). Additionally, volcanic activity associated with the Sevier orogeny to the west produced episodic bentonites, which coupled with molluscan biostratigraphy allow correlation of units not associated with high carbonate deposition. stratification, and primary productivity during transgression and highstand of the seaway.

1.2.2 Paleoceanography of the KWIS

The Western Interior Seaway (WIS; Fig 1.7) at maximum Cenomanian-Turonian (T1; Greenhorn Cyclothem) transgression stretched meridionally from the subtropical Tethys (Gulf of Mexico) to the polar Boreal Oceans (over 45° of latitude) and zonally

Figure 1.6 The rhythmically bedded limestone and calcareous shale of the Bridge Creek Limestone Member of the Mancos Shale exposed at Pueblo, CO. The author for scale.

from Utah to Kansas. Creation and delivery of bottom water masses in the Cretaceous world ocean may have been controlled by strong evaporation and negative water balance at the equator resulting in the sinking of warm and saline waters (Chamberlain 1906; Arthur et al., 1985; Hay, 1993). This situation was much different that today's modern meridional circulation driven by formation of cold and salty deep water masses at the poles.

In the WIS, cool relatively fresh Boreal surface water masses met warm relatively saline Tethyan surface water masses. Hay *et al*. (1993) suggested that mixing of these two disparate water masses led to the creation of a third, more-dense, oxygen-depleted WIS water mass through the process of cabelling. This new mater mass would have been

exported to the north and/or south at intermediate depth to the Cretaceous world ocean. Such export would have required an increased inflow of surface water from the Tethyan and Boreal Oceans, thus the authors hypothesized that formation and sinking of a dense WIS water mass may have been more prominent during late transgression and highstand system tracts when communication with the world ocean was less restricted.

Surface waters in the basin are believed to have exhibited gyre-like rotation similar to modern subtropical analogues although the direction of circulation is not without contention. Most studies, including reconstructions based on models of ocean circulation (Ericksen and Slingerland, 1990; Jewell, 1996) foraminiferal assemblages (Kent, 1968, Leckie et al., 1998), marine fauna (Scott and Taylor, 1977), and the presence of cross-beds in lithologies of varying age (Spearing, 1976; Boyles and Scott, 1982) point to the presence of a cyclonic, or counter-clockwise, gyre in the seaway with Boreal water masses moving down the western margin and Tethyan water masses moving up the central and eastern side of the seaway. Depending on the strength and organization of this gyre, prevailing wind patterns, sea-level, and local bathymetry, this cyclonic motion could have resulted in the upwelling of deeper water masses at the center of the basin and the downwelling and possible export elsewhere in the basin, further complicating the reconstruction of ventilation and nutrient regeneration of the seaway.

Sea level change would result in dynamic spatial and temporal variations in water column oxygen, nutrient, salinity, and temperature profiles impacting macro- and micro-faunal diversity, trophic structure, primary productivity, water column processes, the delivery of organic matter to depth, and the preservation of sedimentary organic matter.

How or if these variations are then recorded in the geochemical record of the Western Interior Seaway remains largely unresolved.

Figure 1.7 Paleogeography of the Late Cretaceous Western Interior Seaway at ~ 85 ma. MV = Mesa Verde National Park, CO. Blue and red arrows show suggested paths of cool brackish northern and warm saline southern water masses (Kent, 1968; Scott and Taylor, 1977; Spearing, 1976; Boyles and Scott, 1982). Adapted from http://jan.ucc.nau.edu/~rcb7/namK100.jpg

1.2.3 The San Juan Basin: Late Cretaceous Depocenter

The sediments that are the focus of this study were deposited in a foreland basin in accommodation space produced by ongoing Sevier tectonics to the west (Elder, 1993;

Leckie et al., 1997). Superimposed on the elongate north-south trending foreland basin is the Paleogene San Juan Basin. The San Juan basin was created due to the intermittent Paleozoic and Mesozoic reactivation of earlier north-dipping normal faults. Between 73-30 Ma, this faulting resulted in the emplacement of shallow monoclines creating the accommodation space for later sediments (Kelly, 1951, 1955; Silver, 1957; Kelly and Clinton, 1960; Laubach and Tremain,1994; Fassett, 2000). The San Juan Basin is a 100-200 mile wide quasi-circular basin which led to the protection and preservation of Upper Cretaceous sediments. During the early Late Cretaceous, sediments were delivered into the region of San Juan Basin across an area of low-relief from the Sevier highlands to the west (Molenaar, 1977). Nearly all of the almost 2000 m of Cretaceous sedimentary rocks in the San Juan Basin were deposited during marine regression or progradation during late highstand. The Mancos Shale represents the bulk of marine deposition in quiet low energy environments. Molenaar (1977) suggested that during the Cretaceous, maximum water-depths in the more distal parts of the region now associated with the San Juan Basin were never more than 122 m. Our section at Mesa Verde National Park is centrally located at the north rim of the basin.

1.2.4 The Niobrara Cyclothem and Mesa Verde

The Mancos Shale at Mesa Verde National Park (MVNP) is a 682 m thick Upper Cretaceous formation characterized as dark-gray, moderately to well laminated, calcareous shale, calcareous mudstone, and medium-gray mudstone (Leckie et al., 1997; Fig 1.9). The unit is sparsely interbedded with limestone, calcarenite, dolomitic mudstone, and sandstone. Bentonites, limonites, and concretions are also prominent in

parts of the section and aid in the correlation of this section to others of the Colorado Plateau. At MVNP, the Mancos Shale represents the local expression of the Greenhorn and Niobrara cyclothems and exhibits geochemical evidence consistent with Oceanic Anoxic Events 2 and 3. Molluscan biostratigraphy provides age control through the section Fig 1.8).

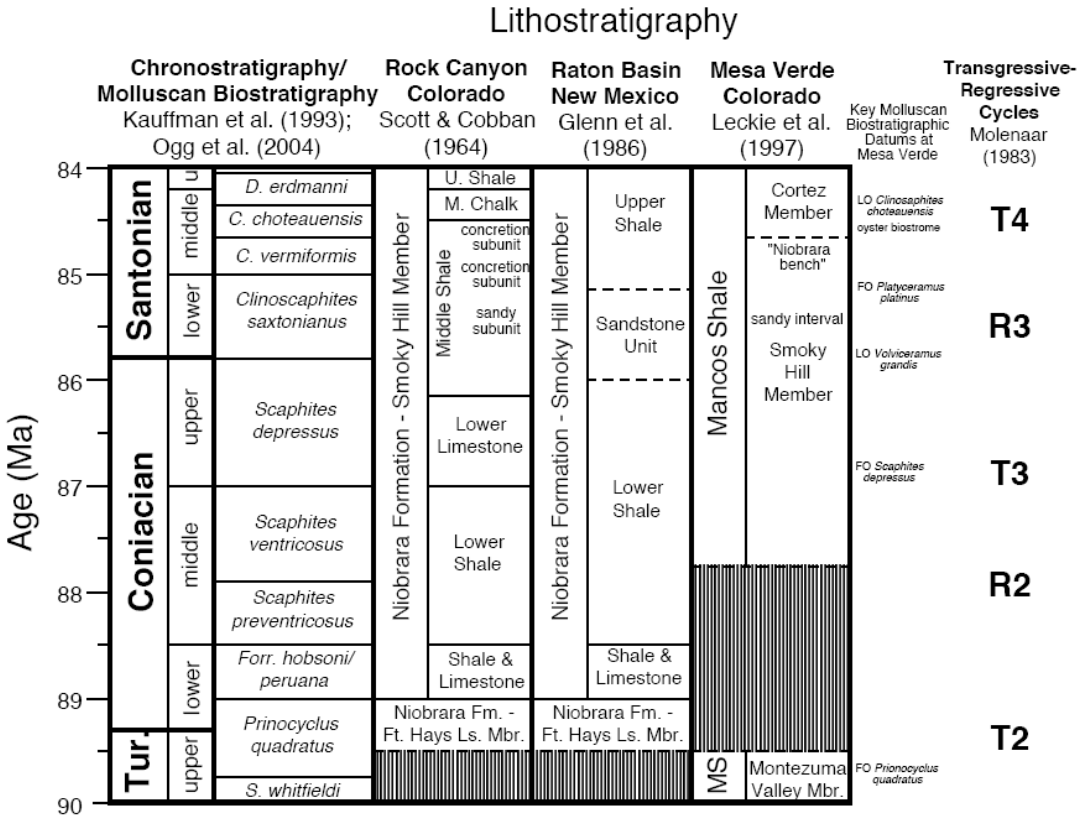

Figure 1.8) Chronostratigraphy of the Smoky Hill Member of the Mancos Shale at MVNP based on molluscan biostratigraphy and correlation with the Rock Canyon (Pueblo Reservoir), Colorado reference section and Raton Basin, New Mexico (based on Leckie et al., 1997). Transgressive-regressive (T-R) terminology from Molenaar (1983).

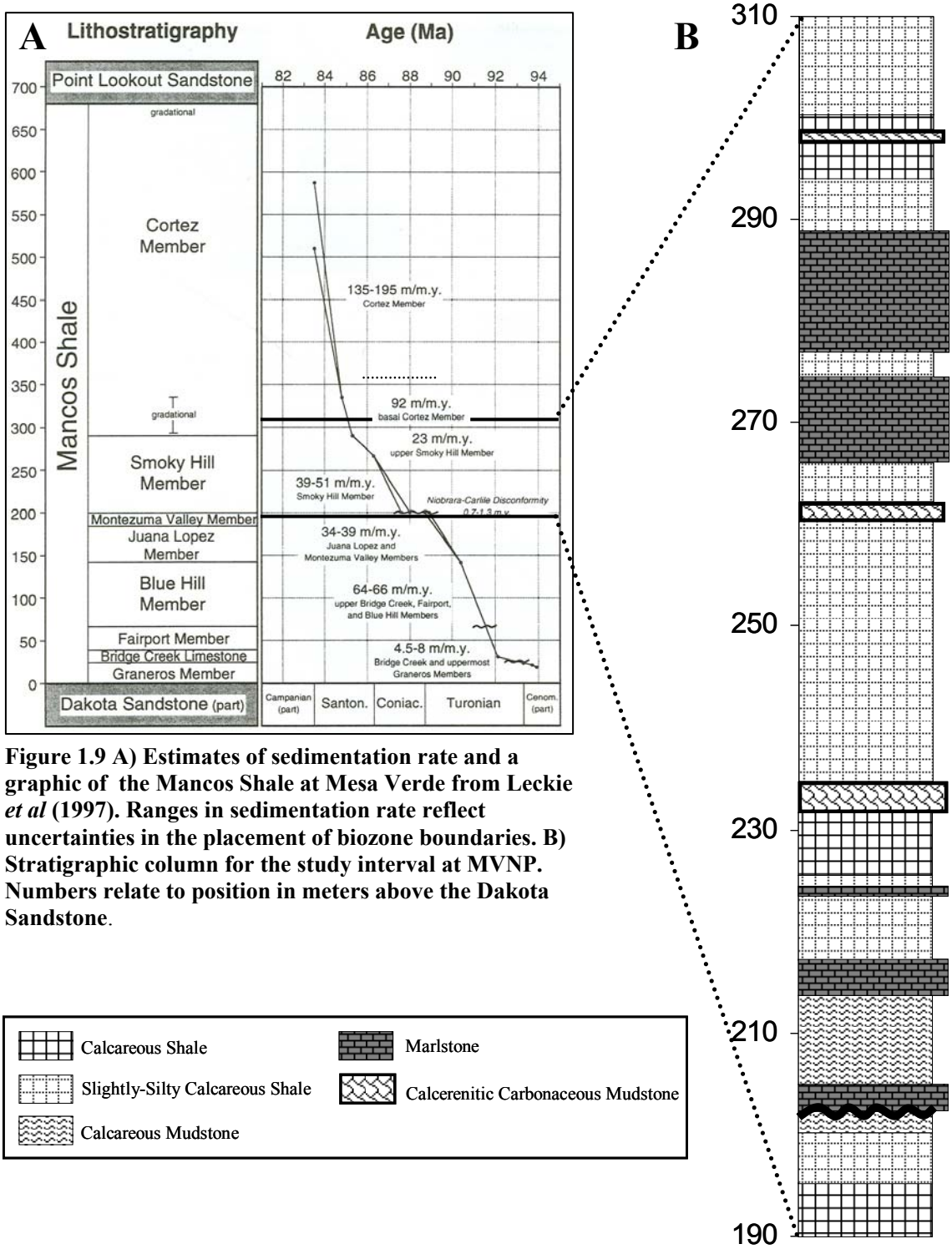

Figure 1.9 A) Estimates of sedimentation rate and a graphic of the Mancos Shale at Mesa Verde from Leckie *et al* (1997). Ranges in sedimentation rate reflect uncertainties in the placement of biozone boundaries. B) Stratigraphic column for the study interval at MVNP. Numbers relate to position in meters above the Dakota Sandstone.

The part of the Niobrara cyclothem at MVNP presented here and revisited in this study, includes the Juana Lopez, Montezuma Valley, Smoky Hill, and Cortez Members of the Mancos Shale (Fig 1.8 and 1.10; Leckie et al, 1997). The upper Montezuma Valley Member correlates to regressive facies across the San Juan Basin (Molenaar, 1977, 1983; Hook et al., 1983; Cobban and Hook, 1989; Dyman et al., 1993; Leckie et al., 1997) such as the Sage Breaks equivalent of the Carlile Shale (Fisher, 1985). These deposits probably represent early transgressive (T2) and regressive phases of the Niobrara Cyclothem. The Montezuma Valley Member at MVNP is punctuated by a hiatus lasting ~ 1.8 myr which separates it from the overlying Smoky Hill Member of the Mancos Shale (Fig 1.8-1.10). Rocks correlative to the Fort Hays Limestone Member of the Front Range Niobrara Formation are missing at Mesa Verde (Leckie et al. 1997).

At Mesa Verde, the Smoky Hill and lower Cortez Members have been correlated, from bottom to top, to the following informal units of the Smoky Hill Member of the Niobrara Formation (Scott and Cobban, 1964; Kaufmann et al., 1985): the upper part of the lower shale, lower limestone, middle shale, and middle chalk units (Fig 1.8 and 1.10). The lower Smoky Hill Member of the Mancos shale at MVNP correlates with other San Juan Basin transgressive facies such as Mulatto Tongue Member of the Mancos Shale which is thought to represent transgression (T3) through highstand (Molenaar 1983; Leckie et al., 1997). The upper Smoky Hill Member at MVNP is capped by a bench-forming marlstone representing transgression (T4) which culminates in chalky shale in the basal Cortez Member. The Dalton Sandstone Member of the Crevasse Canyon Formation, a regressive facies in the San Juan Basin, may be expressed as an increase in sand in the middle part of the Smoky Hill Member at MVNP. The overlying Cortez

Sandstone Member coarsens upwards and represents later terminal regression of the seaway. Our samples capture most if not all transgressive facies, and the beginning of regressive facies, deposited during the Niobrara Cyclothem at Mesa Verde.

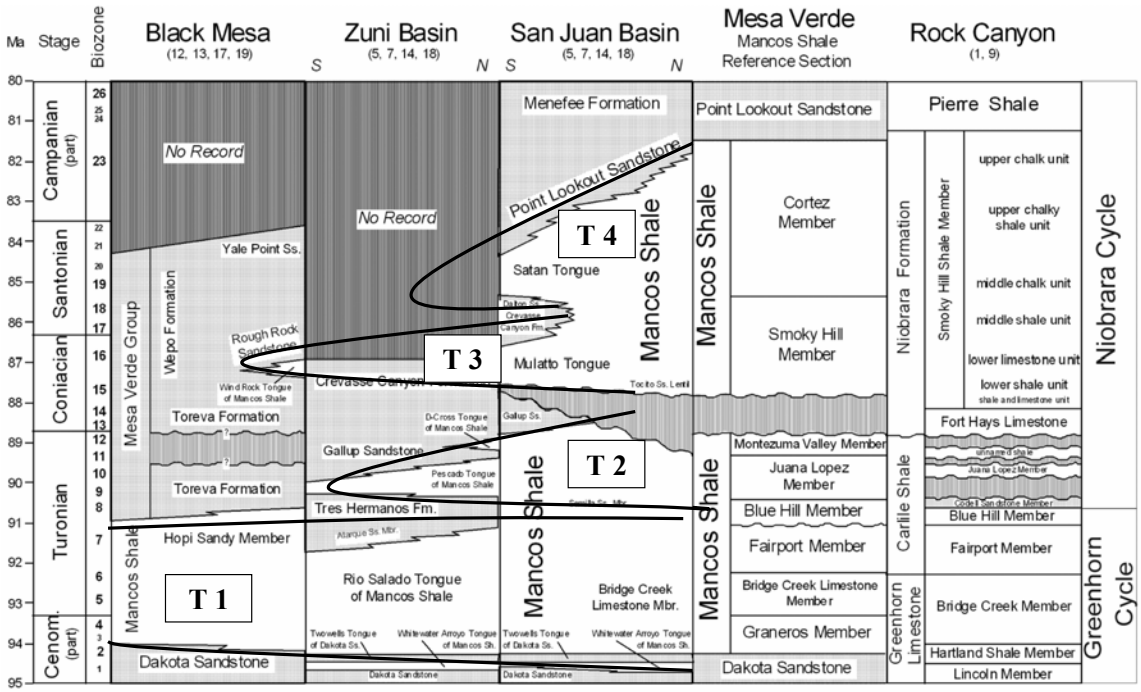

Figure 1.10 Correlation of Mancos Shale at MVNP with other locations of the Colorado Plateau illustrating Molenaar's (1983; T1-T4) transgressive-regressive cycles (adapted from Leckie et al., 1997)

CHAPTER 2

SEA LEVEL, OXYGEN STRESS, AND WATER COLUMN ECOLOGY DURING OCEANIC ANOXIC EVENT 3

The greenhouse world of the Cretaceous lacked significant amounts of continental ice, experienced high pCO_2 and sea-level, and experienced episodic Oceanic Anoxic Events (OAE's) characterized by widespread deposition of organic matter in open-marine, marginal, and epicontinental settings (Schlanger and Jenkyns, 1976, Jenkyns 1980). The Upper Cretaceous Niobrara cyclothem (upper Turonian-lower Campanian, 90.5 – 82 Ma) is a second-order transgressive-regressive cycle of the Cretaceous Western Interior Seaway (KWIS, USA) reflecting interactions among eustatic sea level change, regional tectonic events, climate, and sediment supply. These strata provide a unique window into Late Cretaceous sediment deposition and paleoceanographic conditions in an epicontinental seaway where the response of organic matter production, alteration, and burial to tectonic and climatic forcings remains less than fully resolved. Cretaceous sediments of the WIS are a valuable historical record with which to study possible future greenhouse conditions that may be dominated by different patterns of ocean and atmospheric circulation, carbon cycling, and ecological adaptation than are present today.

2.1 Hypothesis

Variations in bulk and molecular geochemical characteristics through the Niobrara Cyclothem reflect changes in both: 1) sea-level, sediment delivery, nutrient availability, and surface-water productivity, as well as, 2) the effects of these variables on water-column processes, ecology, dissolved oxygen profiles and the ultimate preservation of sedimentary organic matter.

2.1.1 Objectives

1) To re-assess sea-level changes through the Niobrara Cyclothem of the San Juan Basin at MVNP using a multi-proxy approach including higher-resolution bulk organic and inorganic carbon stratigraphy, molecular biomarkers, molluscan and foraminiferal biostratigraphy, and inorganic geochemistry.

2) To investigate geochemical evidence of variations in water column processes and ecology, oxygen stress, and organic matter preservation within the context of proposed sea-level change(s).

To this end, the upper Montezuma Valley, Smoky Hill, and basal Cortez members of the Mancos Shale (Principal Reference Section, Mesa Verde, CO) were investigated to ascertain local and global tectonic, eustatic, biotic, and chemical variability and its geochemical expression during second- and third-order transgressive-regressive cycles. Furthermore, the Smoky Hill Member of the Niobrara Cyclothem at Mesa Verde may contain the local expression of the spatially-restricted but temporally-extended Oceanic

Anoxic Event 3 of Coniacian to Santonian age (~87.3-84.6 Ma). New geochemical evidence of oxygen availability, water column ecology, and stable carbon isotopic records of organic and carbonate carbon in the Western Interior Seaway enhances our ability to decipher the last and least understood Cretaceous Oceanic Anoxic Event.

2.2 Methods

2.2.1 Sampling, Biostratigraphy, and Age

The Mancos Shale at MVNP was measured, trenched, described, and sampled during the summers of 1988 and 1989 (Fig 1.8 and 1.9; Leckie *et al.*, 1997). Due to the low relief associated with the bottom slopes of the mesa, bentonites, calcarenites, sandstones or other "marker beds" were vital in constructing a composite stratigraphic section based on geographically separated outcrops. Sampling for this study spanned seven outcrop segments labeled on Figures 2.1 and 2.2. More than 2 kg of whole rock were collected at one meter resolution from trenches dug into the shale to minimize weathering effects on geochemical properties. Samples are labeled in meters above the contact with the underlying Dakota Sandstone. The rock chunks and fragments have been stored in the University of Massachusetts-Amherst Geosciences Department since collection. Gamma Ray measurements were obtained in the field at roughly 1 m resolution using a GRS-101A portable gamma-ray scintillometer (Leckie *et al*., 1997). Estimates of sedimentation (Figure 1.8) rate are based on molluscan stratigraphy. Biozones and subzones were described by Cobban (1951,1984), Cobban and Reeside (1952), Gill and Cobban (1966), Kaufmann (1975), Hattin (1982), Scott *et al*. (1986),

Cobban *et al.* (1989) and Kirkland (1990,1991). The time scale is that of Kaufmann *et al*. (1993) and Obradovich (1993) (Leckie *et al.*, 1997).

Location	Interval Collected	Member(s)	Comments
16	187.4-194.0	lower-middle Montezuma Valley	in arroyo; south of aquaduct
17	193.9-196.3	middle Montezuma Valley	slope of knoll; east of arroyo and
			along aquaduct
18	196.3-231.2	upper Montezuma Valley	exposed gray slopes; south
		lower Smoky Hill	of aquaduct
19	231.2-248.2	middle Smoky Hill	lower third of slope
	261.0-273.5		upper fifth of slope
20	248.2-261.4	middle Smoky Hill	mid-slope section
21	273.2-299.5	upper Smoky Hill-basal Cortez	upper gray slopes and cliffs
			of Smoky Hill (Niobrara) Bench
22	297.5-383.2	lower Cortez	continuous shale slopes
			west side of N-S ridge

Figure 2.1 Aerial view of the study section at MVNP. Numbers correlate to sampling locations described in Leckie et al. (1997). North is at the top of the page. Image from googlemaps.com

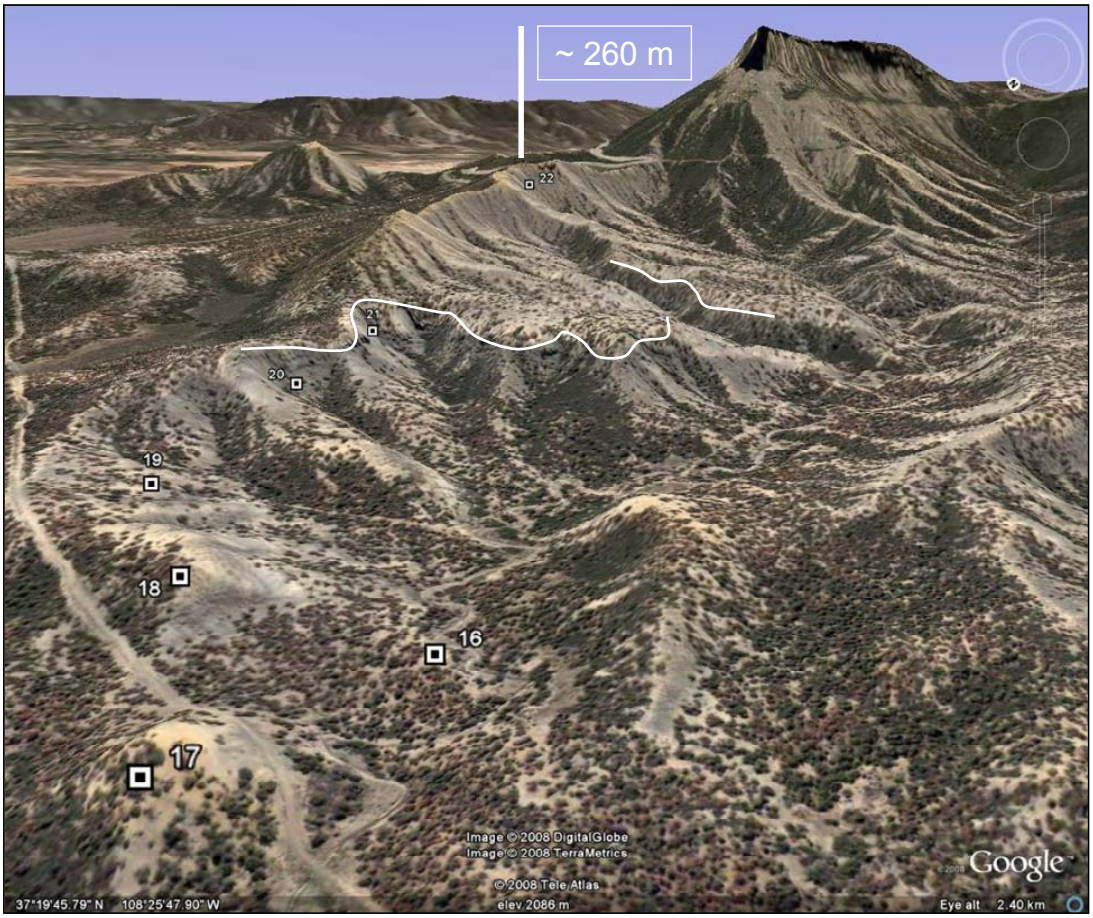

Figure 2.2 Oblique view of the study section. Numbers correlate to sampling locations described in Table 2.1 and Leckie (1997). The curving white line highlights the top of the prominent Niobrara Bench (289 m). Thick vertical white line included for scale. Image from googlemaps.com

2.2.2 Bulk analyses

Large chunks of whole rock samples stored in the UMass-Amherst Geosciences Department were selected to decrease the impact of environmental contamination and oxidation. These chunks were pulverized in a ball mill to ensure sample homogeneity and subsequently stored in combusted (450°C) ICHEM© jars capped with combusted foil.

Bulk geochemical analyses were performed on pulverized and homogenized whole rock samples (Figure 2.3). Total carbon (precision ± 2%) and N_t (precision ± 15%)

were obtained from whole rock samples on an Elemental Combustion System (Costech ECS4010, Valencia, CA). Organic carbon concentrations (precision ± 5%) were also analyzed on the Costech Elemental Combustion System after treatment of ~ 5-10 mg of powdered sediment with ~ 1N HCl in pressed silver boats. Samples were treated with HCl until reaction ceased and dried overnight (at 60°C) to remove all water. Inorganic carbon was calculated by difference. OM concentrations were computed on a carbonate-free basis to remove the effects of carbonate dilution.

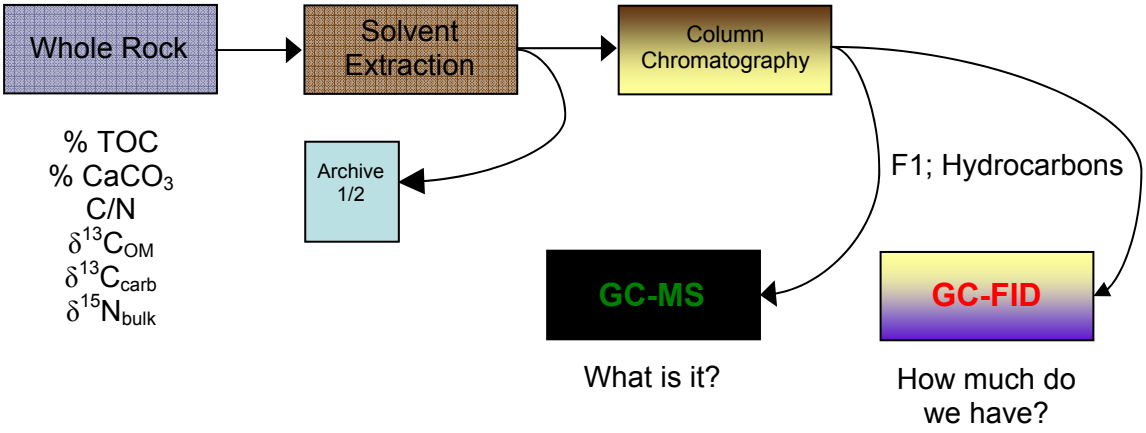

Figure 2.3 Idealized analytical flow chart for preparation of MVNP samples

The stable isotopic ratio of ^{12}C to ^{13}C in organic matter ($\delta^{13}C_{OM}$) was obtained (precision ± 1‰) after exhaustive treatment of ~10-20 g of powdered rock sample with ~ 1N HCl in glass 4 mL vials. Samples were treated with HCl until reaction ceased with overnight drying (at 60°C) of samples between treatments and to dryness before analyses. The stable isotopic ratio of nitrogen-14 to nitrogen-15 in ($\delta^{15}N$) was obtained (precision ± 0.3‰) on untreated powdered whole-rock samples. Both analyses were performed on the Costech Elemental Combustion System coupled to a Thermo-Finnegan Delta V isotope-

ratio mass-spectrometer (ir-MS, Waltham, MA). The stable isotopic ratio of ^{12}C to ^{13}C ($\delta^{13}C_{carb}$) of ~ 0.5 mg of powdered whole rock sample was obtained on a Kiel Carbonate Device III coupled to a Thermo-Finnegan Delta XL ir-MS (Waltham, MA). Data are expressed in traditional "δ" format relative to VPDB (Carbon) and air (Nitrogen). For example:

$$\delta^{13}C \text{ ‰} = [(R_{sample} / R_{VPDB}) - 1] \times 10^3$$

where R is the ratio of ^{13}C to ^{12}C.

2.2.3 Molecular analyses

Clean, pulverized, and homogenized whole rock samples (15 – 25 g) were extracted on a Dionex Automated Solvent Extractor with a 9:1 DCM:MeOH mixture at 100°C and 1200 psi. One half of the total lipid extract (TLE) was separated on pre-packed amino-propyl columns (Supelco, Bellefonte, PA) by elution of 5 mL of hexane and 15 mL of methanol to separate apolar (F1; saturated and unsaturated hydrocarbons) and polar (F2; N,S,O-bearing compounds) compounds respectively. An internal standard, 3-methyltricosane (2 μg/μL), was added to each apolar fraction after separation for quantification purposes (Injection concentration = 0.3 μg/μL).

Apolar compounds were quantified via gas chromatography (GC-FID, HP 6890, Andover, MA; equipped with an on-column injector and flame ionization detection) and identified via gas chromatography-mass spectrometry (GC-MS, HP 6890, Andover MA; with a mass range of *m/*z 50-550 and a cycle time of 1.53s) and comparison with retention times of reference compounds. For both analyses, the GC was equipped with a HP-5MS column (30m x .250mm) and samples were injected from an auto sampler at an

inlet temperature of 320°C. Helium was used as the carrier gas and initial oven temperature was 40°C held for 1.5 min; this was increased at 20°C/min to 130°C, and then at 4°C to 320°C where it was held for 10 min until the end of the run.

The concentration of aryl-isoprenoids was calculated by comparison of their peak area of their base ion (*m/z* 133) on the extracted ion chromatograph in the apolar fraction with the peak area of a compound of known concentration on a extracted ion chromatograph of its base ion (*n*-C_{17}; *m/z* 57). Due to non-linearities associated with this technique, concentrations of aryl-isoprenoids are considered relative, not absolute.

The apolar (F2) compounds were analyzed on a Dionex HPLC (P680, Valencia, CA) coupled to a MS (Thermo Surveyor MSQ, Waltham, MA) by Dr. Zhaohui Zhang (UMass-Amherst). Ratios of Thorium to Uranium (Th/U) and Rock-Eval were provided by Dr. Richard Yuretich (UMass-Amherst, unpublished data). Percent sand was provided by Hayden-Scott (UMass-Amherst, M.S. Thesis, % sand). Foraminiferal, pyrite, and quartz abundances were counted and calculated by Erica Sterzinar (UMass-Amherst, M.S Thesis).

2.2.4 Consideration of Maturity and Biodegradation

Molecular fossils, or biomarkers, are the chemical remains of deceased organisms which are preserved in ancient and modern sediments (Brocks, 2003). Therefore, biomarkers impart information regarding the identity of the organism responsible for its production and/or information regarding the environmental and ecological conditions at the time (Table 2.1). The integrity of any data inferred from biomarkers varies with the specificity of the biomarker in question to a given organism and the ecological range of

the organism being identified. Some biomarkers are produced by many organisms (eg. *n*-alkanes) and others are highly specific to a group of organisms (isorenieratene). Additionally, biomarkers are impacted by a host of post-production biotic and abiotic degradation processes occurring during transport, deposition, sedimentation, and lithification (Peters 2003 for a detailed summary). Therefore, maturity and biodegradation assessment is critical to the interpretation and utilization of any organic geochemical proxy.

Table 2.1 Biomarker Interpretation

Biomarkers	*Biological and environmental interpretation*	*References*
n-Alkanes		
n -C_{14} to *n* -C_{19}	Membrane lipids from marine and lacustrine algae	Collister *et al.* (1992)
> *n* -C_{27} with odd-over-even preference	Waxes derived from higher plants; terrestrial input; post-Silurian age	Hedberg (1968) and Tissot and Welte (1984)
Hopanes		
C_{30}-hopanes	Bacterial membrane lipids; few eukaryotic species	Rohmer *et al* .(1984)
Extended C_{31} to C_{36} hopanes	Diagnostic for Bacteria	Ourisson and Albrecht (1992) Rohmer *et al* . (1984)
28,30-Dinorhopane; 25,28,30-Trinorhopane	Often prominent in sediments from euxinic environments	Grantham *et al.* (1980) Peters and Moldowan (1993)
Steranes		
Cholestane	In aquatic sources probably almost exclusively derived from diverse eukaryotes; in terrestrial sources input from soil bacteria conceivable	Volkman (2003), Bode *et al.* (2003), Kohl *et al.* (1983)
Isoprenoids		
Pristane and Phytane	Most commonly considered transformation products of phytol from cyanobacterial and green-plant chlorophylls	Didyk *et al.* (1978)
Isorenieratane	One of many isorenieratene derivatives. Isorenieretene shown to be produced by Brown pigmented Chlorobiaceae	Bosch *et al.* (1998), Grice *et al.* (1996) Hartgers *ea al.* (1993), Koopmans *et al.* (1996), Pancost *et al.* (1998) Simons and Kenig (2001), Sinninghe Damste *et al.* (2001)
Glycerol di-alkyl glycerol tetra-ethers		
Isoprenoidal	Diagnostic for Crenarchaeota; used in the TEX 86 sea surface temperature reconstruction	DeRosa et al. (1988), Schouten et al. (2002)
Methyl-branched	In nearshore sediments probably from soil bacteria; used in CBT soil moisture and MBT mean annual air temperature reconstructions	Weijers et al. (2006, 2007)

2.2.4.1 Maturity

In the "biologic configuration", many biomarkers are: 1) functionalized (i.e. containing alcohol –OH, acidic –COOH, or ketone C=O functional groups), 2) chiral

(displaying "handedness" or the inability of mirror images of the molecule to be superimposed), and/or 3) stereospecific (i.e. α or β placement of hydrogen on specific carbon atoms within hopanes and steranes). This biological configuration changes in well-understood ways in response to post-depositional environmental impacts such as thermal stress and biodegradation (Peters, 2003).

For this study, well established biomarker indices constructed using the relative contributions of biologic and diagenetically altered hopanes, *n*-alkanes, and isoprenoids were employed to reveal post-production overprinting of authentic biomarker signals, constraining the integrity of other biomarker and non-biomarker proxies with respect to their use in paleoenvironmental reconstructions. This gives a sort of internal "alteration index" indicating the degree of alteration of the biomarkers used in a reconstruction.

Hopanes transform in predictable ways from a ββ configuration to either a more stable βα or αβ during increasing maturation. Therefore, the ratio of the βα to the sum of the βα and αβ hopanes decreases from 0.8 (immature) to 0.15 (late-immature/oil threshold) with increasing maturity. Minimum values reach 0.05 (Mackenzie *et al.*, 1980a; Seifert and Moldowan, 1980; Peters, 2003). Here, the ratio of these isomers in the C_{30}-hopane was used

Another useful ratio is based on the predictable isomerization of 17α-hoapnes at C-22 from S to R. In this ratio the S isomer is divided by the sum of the S and R isomers. Values increase from 0 to ~0.6 with maturation (Seifert and Moldowan, 1980). Here we apply this ratio to the C_{31}-hopanes.

2.2.4.2 Biodegradation

Two additional indices have been constructed to reflect the degree of biodegradation of a suite of samples.

- Pr/*n*-C_{17}
- Ph/*n*-C_{18}

These indices compare the relative concentrations of two acyclic isoprenoids (**Pr**istane and **Ph**ytane) to their *n*-alkane counterpart (*n*-C_{17} and *n*-C_{18} respectively) based on the assumption that *n*-alkanes will be consumed before acyclic isoprenoids during biodegradation (Peters, 2003). These indices are also sensitive to changes in source and maturity and so should be considered together with other qualitative signs of biodegradation to include:

1) An increase in the Unresolved Complex Mixture (UCM) and a growing chromatographic baseline hump with increasing degradation (Fig. 10)

2) Selective removal of short chain *n*-C_6 to *n*-C_{12} alkanes followed by degradation of longer chain *n*-alkanes. These short chain *n*-alkanes can also be removed during the sample workup procedures due to increased volatility of low molecular weight compounds.

3) Removal of alkylcyclohexanes and acyclic isoprenoids

4) Subsequent removal and alteration of saturated and aromatic biomarkers such as hopanes and steranes

2.2.5 Biomarker Utility in Environmental Reconstruction

Bulk geochemical analyses, including percent total organic carbon (TOC), percent carbonate (Carb), organic carbon to total nitrogen (C/N), bulk carbon stable-isotope ratios of both organic matter ($\delta^{13}C_{OM}$) and total carbonate ($\delta^{13}C_{IC}$), and stable-isotope ratios of

nitrogen ($\delta^{15}N_{bulk}$) provide a detailed record of broad variations in sea level, organic matter preservation, oxygen stress, detrital dilution, and water column processes over the cyclothem (Table 2.2). Lipid biomarkers such as *n*-alkanes, hopanes, steranes, and acyclic isoprenoids allows us to reconstruct environmental, depositional, and ecological shifts reflected in organic matter sources with respect to changes in sea level and water column oxygenation.

Table 2.2 Bulk Geochemical Interpretations

Bulk Analysis	*Biological and environmental interpretation*	*References*
% Calcuim Carbonate (IC)	Eukaryotic phytoplankton suggestive of normal or open marine settings	Kaufmann, 1977;Molenaar, 1983 Elder, 1993; Kaufmann, 1993; Leckie, 1997
% Total Organic Carbon	Fraction of primary product escaping remineralization via respiration and/or oxidation in the water column and sediments	Killops and Killops, 2005 and references therein Peters and Moldowan, 2003 and references therein
	Increases with increasing productivity and decreasing oxygen concentration	
Organic Carbon : Total Nitrogen	Moderately specific for organic matter source based on differneces in carbon and nitrogen concentrations between terrestrail and marine realms	Prahl *et al.* , 1980; Ishiwatari and Uzaki, 1980; Silliman et al., 1996; Meyers, 1997
	Complicated by post-production impacts such as water column and sediment denitrification	Thompson and Eglinton, 1978; 'Twichell et al., 2001 van Mooy *et al.* , 2002; Kuypers *et al.* , 2005; Meyers et al., 2006; Ohkouchi et al., 2006; and Junium and Arthur, 2007
Stable Isotope Ratios of Carbon	Inorganic carbon ratios are in equlibrium with sea-water and reflect changes in the global carbon cycle	Jarvis et al., 2006; Jenkyns et al 1994; De Romero et al, 2003
	Organic carbon ratios record kinetic isotope discrimination associated with primary prodution that is in equlibrium with sea water. Complicated by changes in ecology and organisms producing and consuming organic matter.	Ohkouchi et al., 2006; Junium and Arthur, 2007 Calvert et al., 1992; Meyers and Bernasconi, 2005; Jenkyns et al, 2001;'Calvert et al., 1996; Levman and von Bitter, 2002; 'Dean et al., 1986, Rau et al,. 1987; Meyers et al., 1989; (others see text)
Stable Isotope Ratios of Nitrogen	Still very little known. Thought to increase with increasing trophic structure as "light" nitrogen is preferentially consumed. Complicated by introduction of isotopically "light" nitrogen via N-fixation and preferential removal of "light" nitrogen via denitrification and anammox.	Ohkouchi et al., 2006; Junium and Arthur, 2007 Calvert et al., 1992; Meyers and Bernasconi, 2005; Jenkyns et al, 2001;Milder et al., 1999 Calvert et al., 1996; Levman and von Bitter, 2002

For example, the apolar (F1) fraction may contain biomarkers diagnostic of the presence of euxinic (anoxic and sulfidic) conditions in the photic zone. Isorenieratane, a C_{40} aryl-isoprenoid (carotenoid) is thought to be produced solely by the brown strain of green sulfur bacteria; obligate anaerobic chemoautotrophs requiring sulfide for their metabolism (Bosch et al., 1998; Grice et al., 1996; Hartgers et al., 1993; Koopmans et al. 1996; Pancost et al., 1998; Simons and Kenig, 2001; Sinninghe-Damste et al., 2001). The presence of isorenieratane and/or its derivatives has been used to imply the vertical

expansion of euxinia into the photic zone in modern (Bosch, 1998) and ancient (Summons, 1986) settings.

The **C**arbon **P**reference **I**ndex (CPI) and **O**dd over **E**ven **P**reference (OEP) utilize the relative concentrations of odd vs. even *n*-alkanes known to be produced almost exclusively by terrestrial higher plants as leaf waxes (Eglinton and Hamilton, 1967). Higher plants primarily produce *n*-alkanes of odd carbon number chain length and therefore values decrease to unity with decreasing terrestrial input and increasing maturity (Peters, 2003). They are calculated as such:

$$\mathbf{CPI} = [2(n\text{-}C_{23} + n\text{-}C_{25} + n\text{-}C_{27} + n\text{-}C_{29})] / [n\text{-}C_{22} + (2 \times (n\text{-}C_{24} + n\text{-}C_{26} + n\text{-}C_{28})) + n\text{-}C_{30}]$$

$$\mathbf{OEP_{31}} = [n\text{-}C_{29} + 6(n\text{-}C_{31}) + n\text{-}C_{33}] / [4(n\text{-}C_{30}) + 4(n\text{-}C_{32})]$$

The **T**errestrial vs. **A**lgal **R**atio (TAR) divides the relative contribution of terrestrial (n-$C_{27,29,31}$) by aquatic (n-$C_{15,17,19}$) *n*-alkanes in natural samples. Higher values of this index reflect the increasing contribution of terrestrial organic matter to the sediment. The ratio is highly sensitive toward terrestrial inputs because terrestrial primary production generates more n-alkanes than marine.

Synthesis of organic geochemical environmental and ecological reconstructions within the sequence- and biostratigraphic setting of the Mancos Shale at Mesa Verde allows us to further refine our understanding of sea level change as expressed in the Cretaceous Western Interior Seaway as well as the effects of this sea-level change, shedding light on the factors, both global and regional, responsible for the composition of

biogeochemical signals expressed in the sedimentary record. A better understanding of the processes affecting such signals is crucial in their use and application in paleoenvironmental and paleoceanographic reconstructions as well as in the identification and exploitation of fossil fuel reserves.

2.3 Results

2.3.1 Bulk Characteristics

The results of Rock-Eval pyrolysis in the section (Table 2.3) give hydrogen index (HI) values ranging from 85 to 264 with the lowest values at or near the disconformity at 200 m. TOC concentrations (Table 2.4; Fig 2.4) range from 0.58% to 7.61% with two maximum "zones" at approximately 214-220 m (avg ~4%) and 276-289 m (avg ~5.5%). Carbonate concentrations vary in similar fashion with most samples falling from 11.92% to 55.54% with maximum zones between 200 m-230 m and 290 m-300 m (Table 2.4; Fig 2.4). An extremely carbonate-rich calcarenitic zone between 230 m - 233 m is reflected in concentrations near 87% at 233 m. Plots of TOC and $CaCO_3$ exhibit a broad rise and fall over the cyclothem punctuated by two periods of more intense organic matter and carbonate deposition. In the lower zone, peak TOC concentrations are coincident with those of *high* carbonate concentrations. However peak TOC concentrations precede *peak* carbonate concetrations expressed in the calcarenite. Based on our chronology, in the upper zone, TOC concentrations lead those of carbonate by 10 m, or ~400 ky.

Ratios of TOC to total nitrogen (C/N; Table 2.4, Fig. 2.7) vary from 5.73 to 48.22 generally coincident with changes in TOC (Appendix 1; $r^2 = 0.62$, $n = 106$) and in agreement with values from other Cretaceous black shales (Meyers, 1997). The intercept

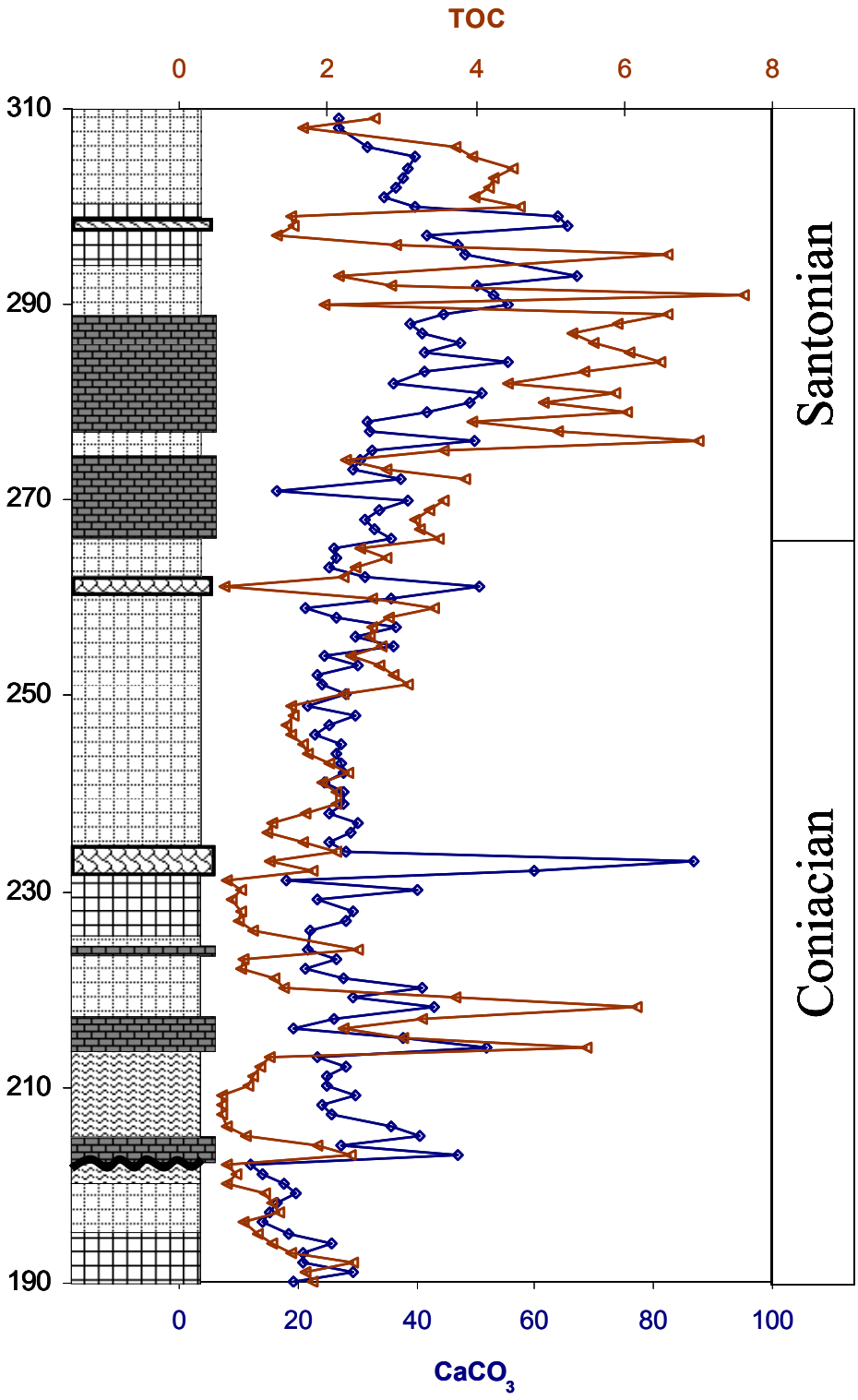

Figure 2.4 Plots of carbonate and total organic carbon. Note two broad maxima between 210 and 230 m and 270 and 300 m.

Table 2.3 Supporting Data (Sterzinar, 2005 and unpublished data)												
Sample (meters)	Total Foraminifera	% Planktic	% Biserial	% Infaunal Benthic	% Quartz	% Sand	% Silt	% Clay	% Pyrite	HI	OI	Th/U
310	18	44.4	37.5	0.0	14.3	0.0	64.8	35.2	58.6	182	59	
300	15	93.3	71.4	100.0	11.1	21.0	67.2	11.8	5.6			
295	307	99.0	83.2	33.3	0.0	8.7	69.5	21.8	1.0			
290	195	99.5	66.0	100.0	0.0	5.6	65.2	29.2	0.5	250	36	0.7
285	86	96.5	83.1	0.0	0.0	3.9	63.5	32.6	0.0			
280	143	86.7	50.0	94.7	0.0	6.2	81.7	12.1	4.0			
275	56	94.6	71.7	33.3	0.0	0.0	33.1	66.9	16.2			1.1
270	132	93.2	56.1	66.7	59.5	0.0	75.7	24.3	0.9			
260	321	95.3	55.2	33.3	11.1	0.0	71.1	28.9	1.3			
250	362	91.4	53.8	45.2	5.1	2.3	74.8	22.9	0.2	264	22	1.6
240	540	58.0	52.1	78.0	0.2	0.0	63.0	37.0	0.2			
235	314	72.3	30.8	86.2	1.1	0.0	60.4	39.6	0.8			1.8
230	224	92.0	46.1	66.7	0.0	5.3	77.1	17.6	0.3			
224	226	95.6	60.6	0.0	0.0	0.0	67.4	32.6	0.0			1.5
220	151	96.7	54.8	40.0	0.0	0.0	71.4	28.6	0.0			
210	312	60.3	58.5	45.2	0.0	0.0	52.6	47.4	0.0	133	77	2.8
205	273	95.2	46.2	0.0	0.0	0.0	71.1	28.9	1.9			
202	17	0.0	0.0	0.0	0.0				0.0			
201	75	4.0	0.0	9.7	96.0				0.0			
201	146	84.2	22.8	26.1	71.7				0.4			
200	51	0.0	0.0	19.6	37.6	0.0	69.8	30.2	0.0	85	76	
198	289	17.6	11.8	2.5	0.0				0.0			
195	244	75.0	53.6	36.1	17.1	0.0	73.2	26.8	5.9			
190	346	87.0	52.2	15.6	0.0	10.5	79.4	10.1	7.0	125	17	5.0

for this x/y plot is 0.11 suggesting most of the nitrogen is related to organic matter and not detrital sources. C/N values typical of marine phytoplankton, usually between 5-10, are encountered in only a few samples below the calcarenite from ~220 to 230 m and at the top of the record from 305 to 309 m. Higher C/N values in our record are more in agreement with those of terrestrially derived organic matter and may reflect either this or post-production alteration of marine organic matter via denitrification (Twichelle *et* al., 2002; see below).

Carbon stable-isotope analyses of bulk carbonate ($\delta^{13}C_{carb}$, Table 2.3, Fig 2.8) show a positive excursion from ~-0.5‰ in the middle Coniacian Montezuma Valley Member to a maximum of ~1.0‰ in the upper middle and lower upper Coniacian portion of the Smoky Hill. A negative excursion at sample 230 m of almost 3‰ punctuates the

Table 2.4: Bulk Geochemical Data

Age	Sample (meters)	Member	Gamma Ray	% $CaCO_3$	% TOC	C/N	$\delta^{13}C_{IC}$	$\delta^{13}C_{OM}$	$\delta^{15}N_{BULK}$
Upper Santonian	309	Cortez	69	27.02	2.63	21.5		-26.02	-0.05
	308		68	26.99	1.69	16.5		-25.84	-0.3
	306		74	31.61	3.74	26.9	0.02	-26.77	-0.93
	305		88	39.91	3.96	28.5		-26.87	
	304		89	38.64	4.51	30.5	0.17	-26.63	0.07
	303		76	37.88	4.25	29.9		-26.53	
	302		82	36.56	4.17	29.4	0.65	-26.78	-0.47
	301		84	34.40	3.99	22.5		-26.63	
? Middle Santonaian ?	300		80	39.65	4.61	29.3	0.41	-26.92	-1.49
	299		55	63.67	1.50	19.0		-24.97	
	298		88	65.66	1.53	14.2	0.53	-25.78	-2.62
	297		58	41.94	1.31	15.1		-25.65	
	296		60	46.87	2.92	23.2		-26.02	-0.63
	295		62	48.17	6.58	36.6	0.58	-27.26	-1.88
	293		68	67.19	2.14	18.2	-0.10	-25.95	-3.12
	292		49	50.08	2.86	25.1	0.45	-26.17	-0.83
	291		54	52.81	7.61	44.0		-26.70	-1.5
	290		59	55.54	1.97	20.9	0.78	-25.94	-3.35
Middle Santonian	289	Smoky Hill	53	44.69	6.58	32.6		-27.54	-2.55
Lower Santonian	288		68	38.87	5.93	28.4	0.35		-1.73
	287		61	41.06	5.29	28.2		-26.31	-1.95
	286		57	47.51	5.60	42.7	0.04	-27.30	-1.73
	285		56	41.46	6.06	48.1		-27.23	
	284		66	55.57	6.50	67.0	0.85	-26.84	-0.94
	283		69	41.40	5.45	45.8		-27.27	
	282		63	36.09	4.42	37.5	0.55	-27.12	-1.31
	281		61	50.92	5.88	62.6		-27.45	
	280		65	48.81	4.93	52.4	0.71	-27.46	-0.9
	279		60	41.93	6.04	38.0		-27.55	
	278		54	31.63	3.96	30.0	0.68	-27.14	-1.06
	277		55	32.15	5.12	30.6		-27.02	
	276		56	49.91	7.00	60.8	0.61	-27.26	-3.49
	275		58	32.47	3.57	27.3		-27.19	
	274		69	30.42	2.26	22.2	0.67	-26.48	0.3
	273		41	29.42	2.79	26.8		-27.07	
	272		48	37.17	3.87	29.1	0.50	-26.90	-0.69
	271		45	16.67				-26.58	
Lower Santonian	270		43	38.42	3.57	29.5	0.52	-27.12	-0.94
Upper Coniacian	269		42	33.67	3.36	23.7		-26.37	
	268		49	31.47	3.17	21.5	0.26	-26.68	-0.4
	267		40	32.79	3.25	18.9		-26.40	
	266		48	35.87	3.51	20.9	0.69	-26.45	-0.45
	265		45	26.01	2.45	16.5		-26.18	
	264		48	26.62	2.80	16.0	0.54	-26.03	-0.33
	263		40	25.35	2.38	13.2		-26.09	
	262		48	31.46	2.21	32.1	0.71	-26.18	-0.64
	261		43	50.56	0.60	23.9			
	260		48	35.64	2.61	20.9	0.47		-0.46
	259		52	21.35	3.43	21.3		-26.73	

Table 2.4: Bulk Geochemical Data (cont)

Age	Sample (meters)	Member		% $CaCO_3$	% TOC	C/N	$\delta^{13}C_{IC}$	$\delta^{13}C_{OM}$	$\delta^{15}N_{BULK}$
	258		55	26.37	2.83	20.6	0.24	-26.21	-1.29
	257		49	36.55	2.61	22.7		-26.32	
	256		52	29.79	2.58	18.7	0.67	-25.95	-1.3
	255		53	36.32	2.72	34.0		-26.27	
	254		51	24.69	2.31	27.5	0.88	-25.87	-0.92
	253		49	30.27	2.71	37.1		-25.85	
	252		59	23.47	2.91	27.2	0.61	-25.23	-1.08
	251		57	24.14	3.08	34.6		-25.35	
	250		61	28.02	2.21	12.2	0.50	-25.95	-0.36
	249		58	21.85	1.52	8.6		-25.57	
	248		62	29.52	1.54	9.5	-0.19	-25.46	-0.39
	247		57	25.46	1.43	8.1		-25.33	
	246		63	22.70	1.52	8.4	0.81	-25.12	-0.66
	245		60	27.44	1.66	6.6		-25.55	
	244		64	26.54	1.73	7.8	0.26	-25.64	-0.27
	243		68	27.20	2.03	6.2		-25.77	
	242		58	27.79	2.29	7.3	0.66	-26.00	-1.86
	241		59	24.44	1.92	14.5		-25.84	
	240		55	27.77	2.13	26.3	0.86	-25.63	-0.17
	239		65	27.69	2.13	30.0		-25.62	
	238		52	25.30	1.72	11.4	0.79	-25.31	-0.23
	237		61	30.14	1.24	11.5		-25.19	
	236		71	28.77	1.19	11.4	0.95	-25.07	-1.55
	235		65	25.33	1.68	14.0		-25.55	
	234		63	28.22	2.12	17.0	0.77		-1.74
	233		56	86.84	1.21	20.6		-25.77	2.44
	232		59	59.86	1.80	23.4	1.05	-25.73	0.53
	231		63	18.18	0.64	6.1		-24.34	
	230		63	40.06	0.82	10.3	-2.35	-25.01	0.02
	229		59	23.11	0.69	7.1		-25.31	
	228		55	29.22	0.83	8.6	0.36	-25.28	-0.41
	227		57	27.99	0.80	9.1		-25.39	
	226		58	22.01	1.01	9.6	0.67	-25.25	-0.17
Upper Coniacian	224		63	21.59	2.41	17.5	0.66	-25.84	-1.84
Middle Coniacian	223		60	26.66	0.86	9.0		-25.44	-2.26
	222		84	21.29	0.84	8.1	0.48	-25.36	-3.57
	221		76	27.85	1.28	12.5		-25.81	
	220		92	40.79	1.41	13.1	0.97	-25.89	
	219		77	29.17	3.71	24.4		-26.08	
	218		85	42.89	6.16	33.8	0.92	-25.89	-2.06
	217		85	26.08	3.29	20.1		-25.44	
	216		90	19.47	2.20	14.7	0.63	-25.93	
	215		72	37.78	3.02	27.2		-26.34	
	214		80	51.89	5.50	41.0	0.44		-3.14
	213		76	23.27	1.21	12.3		-26.23	
	212		65	28.12	1.11	12.7	0.39	-25.98	
	211		63	24.82	1.00	11.3		-25.57	
	210		70	24.97	0.93	10.6	0.08	-25.46	-1.28
	209		64	29.57	0.56	8.2		-25.26	

Table 2.4: Bulk Geochemical Data (cont.)

Age	Sample (meters)	Member		% $CaCO_3$	% TOC	C/N	$\delta^{13}C_{IC}$	$\delta^{13}C_{OM}$	$\delta^{15}N_{BULK}$
	208		64	24.07	0.58	8.4	0.25	-25.20	
	207		64	25.63	0.58	8.3		-24.94	
	206		72	35.55	0.63	10.7	-0.47	-25.21	
	205		54	40.59	0.90	15.3		-25.49	
	204		65	27.17	1.88	21.3	-0.16	-26.39	
	203		56	47.18	2.32	33.7		-26.23	
	202		72	11.92	0.64	7.9	0.02	-25.44	
Disconformity ~1.8 Ma	201		74	14.06	0.78	9.1		-26.15	
Upper Turonian	200	Montezuma	96	17.74	0.63	8.2	-0.14	-25.90	
	199	Valley	82	19.69	1.15	11.6		-24.63	
	198		84	16.37	1.26	11.3	-0.22	-26.29	
	197		75	15.37	1.35	13.4		-25.32	
	196		78	14.12	0.88	10.0	0.19	-23.58	
	195		84	18.42	1.05	10.4		-25.42	
	194		76	25.78	1.26	13.6	-0.27	-23.99	
	193		72	20.91	1.52	15.5		-25.20	
	192		76	21.01	2.33	18.8	-0.79	-25.78	
	191		76	29.33	1.72	16.5		-25.20	
	190		66	19.45	1.81	14.1	-0.14	-25.94	

period of highest isotope values. This excursion is coincident with the start of the calcarenitic zone but precedes peak carbonate concentrations. After the positive excursion reaches a maximum of ~1‰ at 232 m, values recover through the middle and upper Santonian to values close to those at the bottom of our record.

Carbon stable-isotope ratios of bulk organic matter ($\delta^{13}C_{OC}$, Table 2.4, Fig. 2.14) are quite different than those of carbonate. Coincident with increases in OC and high C/N, values of $\delta^{13}C_{OC}$ decrease twice through our record from ~ -26‰ to ~-27 and -28‰ during the first and second "maximum zones" respectively. Plots of TOC vs. $\delta^{13}C_{OC}$, TOC vs. C/N, and C/N vs. $\delta^{13}C_{OC}$ through the Smoky Hill member (Appendix 1) give r^2 values of 0.58, 0.72, and 0.50 respectively (n=106) suggesting these values may be controlled by related processes.

An incomplete record of nitrogen stable-isotope ratios of bulk sediment ($\delta^{15}N_{bulk}$; Table 2.3; Figure 2.13) is highly variable and quite depleted ranging from -3.6 to 2.4‰. Values increase from 210 m (the bottom of this record) to 233 m before a mutli-million

year decrease from 233 m to 290 m. From 290 m to 309 m values increase again with high variability. Again, long-term cycles are visible in the record, although lagging those of both TOC and carbonate.

2.3.2 Molecular Characteristics

2.3.2.1 Compound Distribution

The hydrocarbon fraction of each sample comprises n-alkanes (*n*-C_{15} to *n*-C_{35}), acyclic isoprenoids, hopanes, and steranes in order of decreasing relative concentration (Appendix 2 and 3). Additionally, small contributions of branched alkanes and poly-cyclic aromatic hydrocarbons (PAH's) are present throughout the record. Suspected diagenetic products of isorenieratene are found at the lower (190 – 234 m) and upper (300 – 309 m) bounds of our record. Bacterial and Archaeal tetra-ether membrane lipids were not detected in our samples.

2.3.2.2 Sample Maturity and Biodegradation

The results of maturity and biodegradation parameters discussed above are listed in Table 2.5. Values for 22S/(22S + 22R) of the C_{31}-hopane average 0.59 (sd = 0.01) very close to the upper value of 0.60 for this ratio and consistent with early hydrocarbon generation. However, values for αβ/(αβ+βα) of $_{C30}$-hopanes, applicable into higher levels of maturity, average 0.19 (sd = 0.03) suggesting these sediments have not yet reached maturity.

Ratios of Pr/*n*-C17 in the section range from 0.92 to 1.90 and average 1.39 (sd = .48) suggesting slight biodegradation (Wenger *et al.*, 2002; Peters, 2003). However, high

Table 2.5. Biomarker Resutls									
Sample	% Yield	CPI	OEP_{31}	Pr/*n*-C_{17}	Ph/*n*-C_{18}	22S/	βα/	TAR	Steranes/
(meters)	(g TLE/g dry sed) x 100					(22S+22R)	(βα+αβ)		Hopanes (x 10^8)
309	0.115	1.13	1.71	1.61	0.97	0.61	0.22	0.49	41.72
305	0.199	1.11	1.66	1.85	1.20	0.59	0.21	0.42	51.14
303	0.287	1.12	1.72	1.90	1.24	0.59	0.20	0.53	54.73
300	0.305	1.11	1.73	1.84	1.22	0.59	0.21	0.54	61.65
299	0.011	1.03	1.43	0.63	0.51			4.13	
295	0.458	1.02	1.56	1.89	1.26	0.60	0.20	0.57	97.27
293	0.030	1.00	1.36	1.52	1.04	0.60	0.21	2.38	77.34
291	0.254	0.96	1.46	1.56	1.20	0.60	0.18	0.38	102.62
290	0.065	1.01	1.41	1.29	0.80	0.61	0.19	1.53	66.25
289	0.312	1.00	1.51	1.88	1.16	0.59	0.19	0.45	84.80
285	0.291	0.95	1.64	1.51	1.06	0.60	0.17	0.33	77.00
280	0.394	1.05	1.40	1.29	0.88	0.60	0.18	0.50	61.76
276	0.296	1.02	1.47	1.58	1.03	0.60	0.19	0.47	62.54
275	0.200	0.97	1.53	1.24	0.85	0.60	0.17	0.50	51.24
274	0.078	1.01	1.36	1.08	0.63	0.60	0.20	0.46	50.75
270	0.105	1.02	1.16	1.37	0.92	0.60	0.18	0.41	70.72
265	0.081	0.98	1.19	1.33	0.81	0.57	0.17	0.31	50.29
261	0.051	0.98	1.13	1.01	0.70	0.61	0.17	0.33	64.03
260	0.055	1.04	1.31	1.28	0.87	0.58	0.17	0.55	62.45
259	0.166	0.97	1.47	1.42	1.06	0.59	0.18	0.44	69.64
255	0.065	1.02	1.52	1.37	0.86	0.59	0.16	0.46	52.93
251	0.099	1.03	1.25	1.41	1.01	0.59	0.16	0.42	38.86
250	0.064	1.08	1.52	1.25	0.75	0.58	0.18	0.48	43.86
248	0.074	1.05	1.43	0.88	0.66	0.61	0.17	0.43	31.94
240	0.082	1.10	1.58	1.42	0.72	0.60	0.19	0.48	35.61
234	0.056	1.03	1.37	1.10	0.79	0.59	0.15	0.54	47.78
233	0.026	0.98	1.17	0.89	0.91	0.56	0.13	0.35	42.94
230	0.013	1.03	1.27	0.70	1.21	0.60	0.18	4.21	28.57
224	0.059	1.07	1.42	1.09	0.78	0.59	0.17	0.51	46.58
221	0.042	1.04	1.26	0.68	0.58	0.60	0.17	0.89	31.53
218	0.267	1.00	1.41	1.19	0.64	0.59	0.17	0.23	50.29
216	0.062	1.04	1.31	1.05	0.60	0.59	0.18	0.37	35.93
214	0.180	1.05	1.69	1.40	0.82	0.57	0.17	0.25	43.40
210	0.029	1.03	1.26	1.08	0.89	0.58	0.22	0.36	13.27
208	0.019	1.00	1.29	1.08	1.71	0.57	0.26	0.42	6.78
203	0.063	1.06	1.39	1.36	0.68	0.60	0.17	0.28	23.25
200	0.014	1.01	1.18	0.92	1.65	0.59	0.23	0.59	
197	0.042	1.11	1.48	1.45	0.83	0.57	0.23	0.68	12.50
196	0.017	1.12	1.48	1.75	1.06	0.57	0.22	1.51	8.94
192	0.060	1.08	1.66	2.90	1.06	0.58	0.18	1.05	13.98
190	0.090	1.15	1.59	2.91	0.88	0.58	0.21	1.08	7.78
Average		1.04	1.43	1.39	0.94	0.59	0.19		
S.D.		0.05	0.17	0.48	0.26	0.01	0.03		

concentrations of C_{15} to C_{35} *n*-alkanes in these samples indicate very slight biodegradation. Additionally, the presence of cyclic and isoprenoidal hydrocarbons and lack of a pronounced UCM support very slight to slight biodegradation of these samples.

2.3.2.3 Saturated Hydrocarbons

n-alkane distributions vary between long-chain dominated (C_{27}-C_{35}), short-chain dominated (C_{15}-C_{19}), and bi-modal (displaying long and short chained) throughout our record (Fig. 2.5). They vary in concentration from 10^{-8} to 10^{-5} grams per gram of TOC

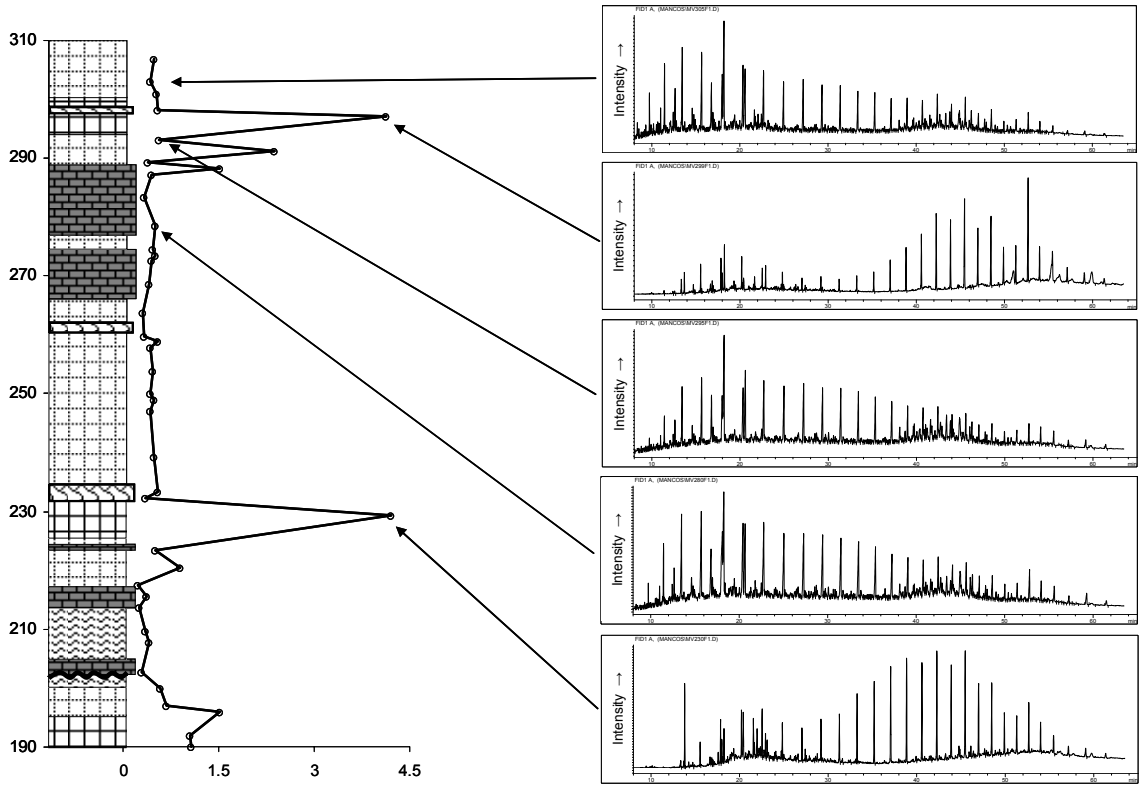

Figure 2.5 Illustration of changes in n-alkane distribution with respect to TAR

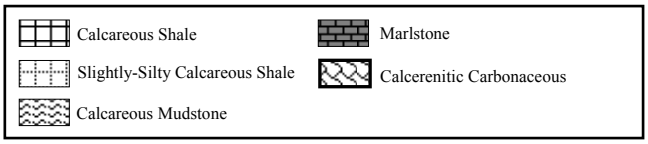

(Appendix 2). In order to illustrate changes in the distribution the terrestrial vs. aquatic ratio was employed (TAR; Bourbonniere and Meyers, 1996; Peters, 2003). This parameter measures the relative contribution of terrestrial (*n*-$C_{27,29,31}$) and aquatic (*n*-$C_{15,17,19}$) *n*-alkanes in natural samples. Higher values of this index reflect the increasing contribution of terrestrial organic matter to the sediment. The ratio is highly sensitive toward terrestrial inputs because terrestrial primary production generates more n-alkanes than marine. Thus, the ratio is especially helpful in reconstructing "down-core" variations in these two sources in a shallow marine setting such as the KWIS.

TAR values slowly decrease from 1.1 to 0.2 from 190 m to 218 m (Fig. 2.5). From 218 m to 230 m, TAR values increase from 0.2 to 4.2 and the gas chromatograph is dominated by long-chain n-alkanes. The chromatogram at 233 m is bi-modal in character and TAR values decrease before complete dominance of low values from 234 to 289 m. After this protracted signal, TAR values oscillate, in a progressively strengthening manner, between marine and terrestrial values from 290 to 299 m before once again returning to marine values from 300 to 309 m at the top of our section.

2.3.2.4 Aryl-isoprenoids

Suspected diagenetic products of carotenoid accessory pigments produced by green sulfur bacteria were found in our record (Appendix 2 and 3; Fig 2.7). Biosynthesis of these compounds results in molecules that are ~ 15‰ enriched with respect to bulk biomass indicative of their metabolism via the reverse TCA cycle, and discriminating them from ubiquitous β-carotene derivatives. We have not analyzed the ^{13}C content of the

molecules in our samples so their identity is not confirmed. The compounds disappear, or are present below analytical detection limits from 230 to 300 m.

2.4 Discussion

The goal of this investigation was to elucidate patterns of organic matter alteration and burial in the Late Cretaceous Western Interior Seaway associated with changes in basin-wide sea level. The first objective then is to properly define sea-level at our section at Mesa Verde followed with observations and interpretations of organic matter production, preservation and burial within the framework of proposed sea-level change.

2.4.1. Correlation of Coniacian-Santonian Sea Level Change at Mesa Verde

Sediment carbonate concentrations are routinely applied in the reconstruction of local sea level. This is predicated on the assumption that calcareous phytoplankton, the organisms responsible for the majority of carbonate production in surface waters, are associated with open or "normal" marine environments and that clastic dilution of these sediments decreases with distance from shore. Variations in carbonate stratigraphy through our section include changes in type (micritic, chalky, calcarenitic), thickness and concentration of various carbonate-rich facies. Additionally, the utility of sterane/hopane ratios in sea-level reconstructions has been demonstrated (Peters, 2003) as the relative contribution of steranes to the organic matter pool should increase with increasing eukaryotic activity. Cretaceous marine eukaryotes range in size and trophic level from tiny calcareous nanoplankton and dinoflagellate autotrophs, to small zooplankton such as foraminifera and copepod, to highly mobile predators such as ammonites; all of which

display higher success and better adaptation to saline open marine systems. In fact, the presence of normal marine "Tethyan" fauna, such as ammonites, in the WIS has been used as a measure of northward migration of southern water masses (Sohl, 1969; Kaufmann, 1984).

Variations in carbonate concentration are illustrated in Figure 2.6. A sixth order polynomial regression has been included and highlights two multi-million year cycles of increased carbonate deposition centered on ~220 m and 295 m respectively consistent with Niobrara cyclicity previously described by Dean and Arthur (1998). An x/y plot of carbonate vs. sterane/hopane ratio has a good correlation (Appendix 1; $r^2 = 0.46$ without the calcarenite at 233 m). Increased carbonate and sterane contributions are consistent with open marine influence; thus these two events have chemo-lithologically correlated with basin-wide third-order sea level fluctuations such as T3 and T4 along the Front Range, and the Mulatto and Satan Tongues in the San Juan Basin. This explanation is aided by the molluscan biostratigraphic correlations of Leckie *et al.* (1997). The lower transgressive pulse (Molenaar's T3) is accompanied by the incursion of marine biota, including ammonites and inoceramid bivalves (Leckie *et al.*, 1997), between 220 and 230 m. This incursion is probably associated with changes in water column habitability (temperature and salinity) as well as the advance of southern Tethyan water masses. In contrast, the upper pulse starting at ~276 m is coincident with many last occurrences and low molluscan diversity (Leckie *et al.*, 1997) suggesting conditions in the seaway, despite third-order transgression and the influence of open marine water masses, were generally not amenable to molluscan fauna. Carbonate facies during the start of these two intervals are dominated by foraminifera and mud-rich marls separated by calcareous and slightly-

silty calcareous shales suggesting that despite sea-level transgression our section was still impacted by siliciclastic sedimentation.

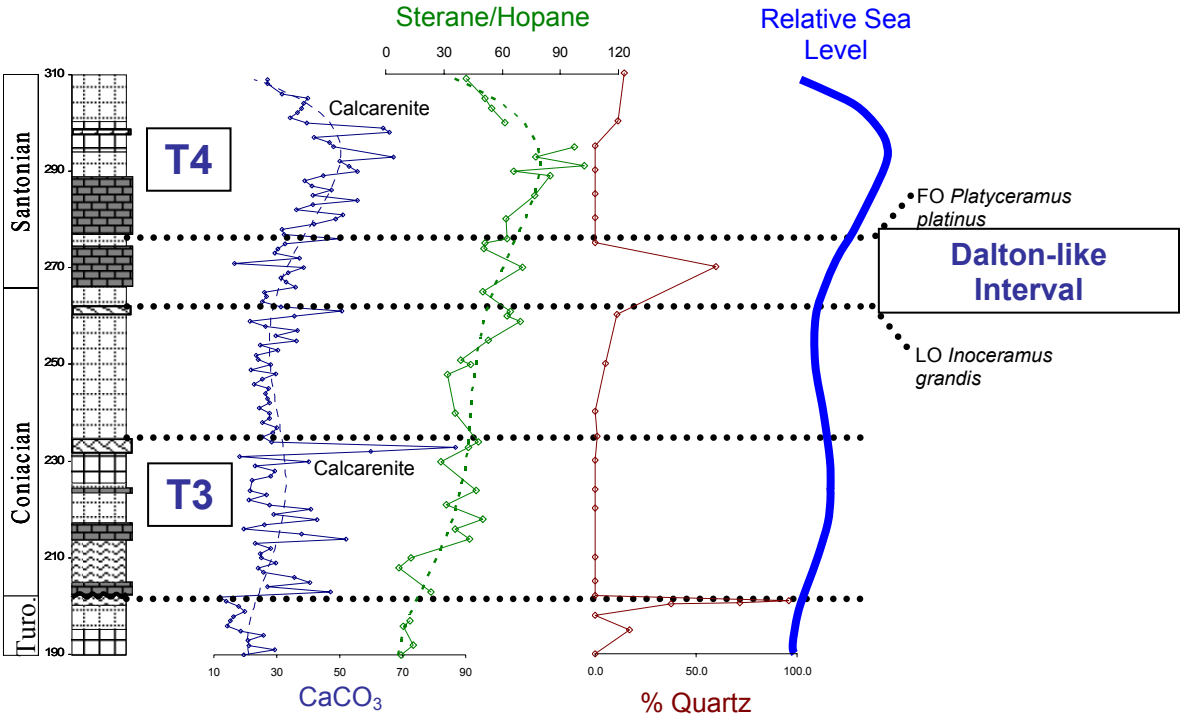

Figure 2.6 Plots illustrating relationships between carbonate concentration, sterane/hopanes (x 10^8), % Quartz, and sea level. Smoothed dashed lines are 6^{th}-order polynomial regressions.

An increase in quartz concentration associated with variable carbonate values and low gamma ray emission precedes the second third-order transgressive pulse. In the San Juan Basin, the Dalton Sandstone is a coarse grained regressive sand body. The timing of this event is constrained on the bottom by the last occurrence of *Inoceramus grandis* and on the top by the first occurrence of *Platyceramus platinus*. In the Smoky Hill at Mesa Verde, these occurrences have been documented and placed at 260 m and 274 m, respectively. This allows us to correlate the increase in quartz content to the Dalton Sandstone thereby extending the geographical influence of this feature northward. Lack of a coincident increase in grain size at this time may suggest a low energy depositional

setting due to suppressed current activity and associated winnowing and sediment bypass processes.

2.4.2 Terrestrial vs. Algal Ratio: Source Indicator or Diagenetic Imprint?

Co-varying with our sea-level reconstruction are parallel changes in the terrestrial vs. algal ratio (TAR) and % sand (Figure 2.7). During most of the record these two proxies suggest algal and sand-free conditions, respectively. However, late in both transgressive pulses are rapid and simultaneous shifts toward more terrestrial and sandy conditions probably taking place during highstand, stillstand, or early regression. One mechanism for this trend may be the progradation of coastal facies as sediment from the Sevier Highlands continued to fill the basin during decreased or stalled rates of sea level advance. This could have increased the delivery of both terrestrial organic matter and coarser grained continental material.

An increase in current activity in the basin may also help explain these results. During seaway highstand and early regression, connections to both the Tethys and Boreal Oceans would have been expanded; perhaps 700 km wide in the north and 1200 km wide in the south (Kauffman, 1975). As increasing volumes of warm saline Tethyan water and cool relatively fresh Boreal water mixed, current activity in the basin may have strengthened. Hay *et al.* (1993) suggested this mechanism may have led to the development of a third water mass more dense than the other two. Any increased current activity in the basin may have increased sediment bypass and winnowing leading to a relative increase the amount of sand without having to increase the amount of sand delivered. Additionally, stronger currents may have eroded, mobilized, and redistributed

terrestrially derived organic matter previously sequestered in now submerged coastal wetlands (Schlanger and Jenkyns, 1976; Montadert and Roberts, 1979) leading to the increase in TAR values seen in our results.

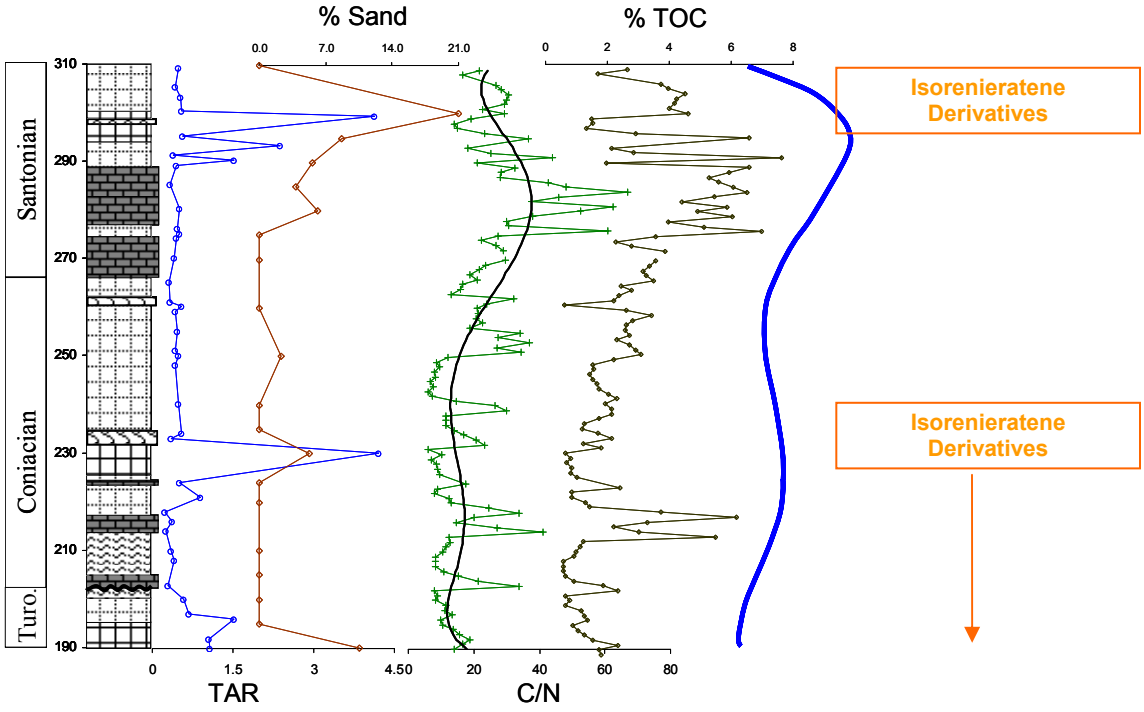

Figure 2.7 Plots illustrating relationships between the terrestrial vs. algal ratio, % sand, total organic carbon to total nitrogen (C/N), total organic carbon, photic zone euxinia, and sea level. Smoothed black line on C/N plot is a 6th-order polynomial regression.

Another possible mechanism for the apparent increased contribution of terrestrially derived organic may be an increased exposure time to oxic conditions under more ventilated conditions driven by increased current activity during highstand and early regression (Fig 2.8). Algal and terrestrial *n*-alkanes are diagenetically altered at different rates and this difference is magnified under oxic conditions (Sinninghe Damste, 2002). In the modern Arabian Sea this has led to the preferential preservation of terrestrial biomarkers during periods of increased water column oxicity. Indeed, in our record, times of higher TAR values coincide with some of the lowest organic and highest

inorganic carbon values; also a sign of increased oxicity associated with more open marine conditions.

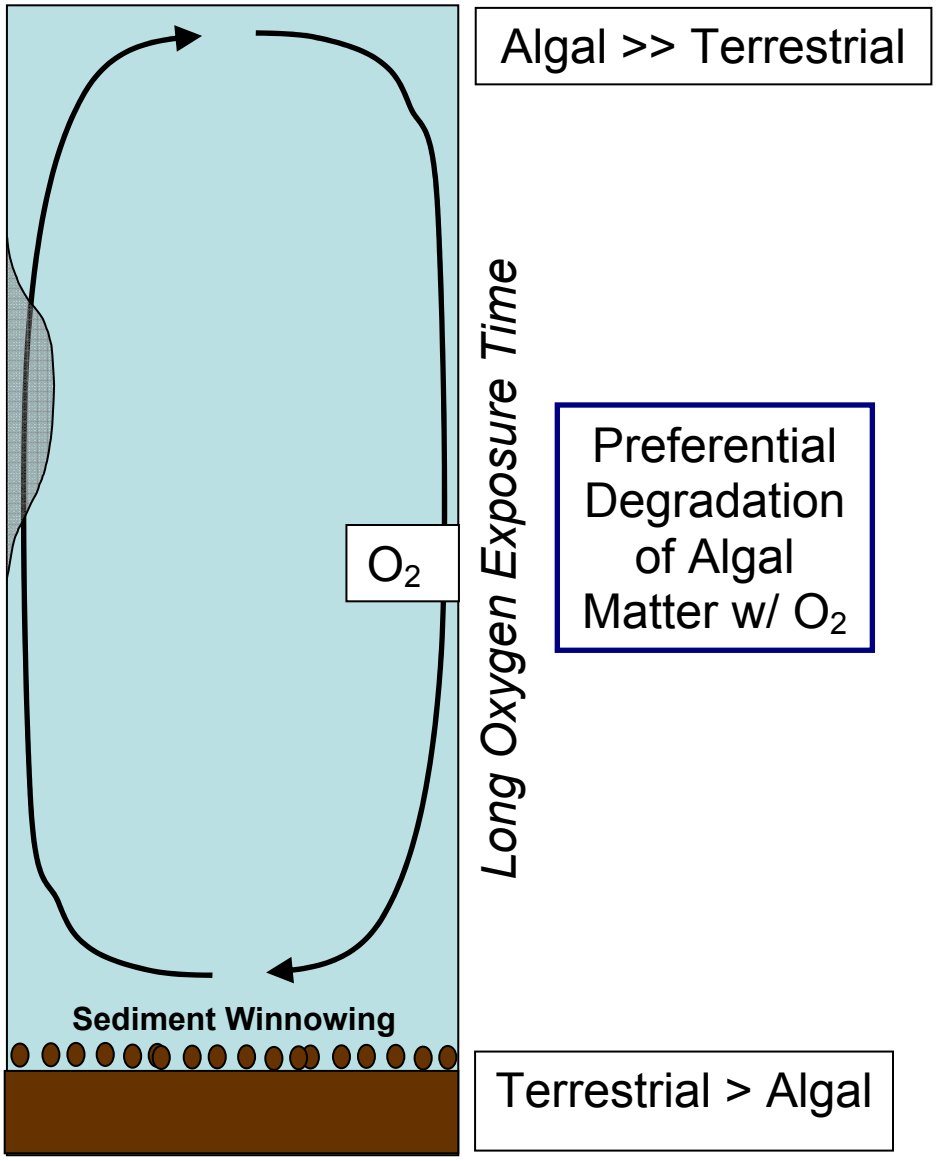

Figure 2.8 Water column schematic illustrating the effects of increasing current activity and oxygen exposure time on the terrestrial vs. algal ratio and grain size. Shaded gray area represents decreased oxygen minimum zone extent during periods of increased oxicity and current activity.

Between these two third-order transgressive events was a period of third-order regression or stillstand superimposed on the progressing second-order Niobrara transgression. Sediments deposited during this interval are characterized as slightly-silty calcareous shale after a switch from calcareous shale at ~231 m. This minor addition of

mud may be associated with regression or progradation. Carbonate values through this section remain steady at about 27% while sterane/hopane ratios continue to climb suggesting increasing eukaryotic/zooplanktonic abundance and/or a decreasing contribution from bacterial and archaeal biomass; both consistent with increased ventilation and open marine conditions suggested by increased foraminifera numbers.

During this period, TAR values are nearly constant at ~ 0.2 to 0.3 reflecting the absence of terrestrial depositional systems at MVNP. These low values also suggest that the preferential degradation of algal organic matter was not an important process at this time implying that although the upper water column was dominated by normal open marine conditions, an oxygen deficient deep water mass may have existed. Indeed, organic carbon values do increase over this interval without a coincident increase in carbonate productivity. These results, together with the marked absence of aryl-isoprenoids diagnostic of photic zone euxinia, support the onset and maintenance of more "marine-like" conditions in the upper water column and the presence of an oxygen minimum zone (OMZ) at depth during continued second-order sea level rise. This OMZ incursion may be the expression of OAE 3.

2.4.3 $\delta^{13}C_{carb}$: Timing of Oceanic Anoxic Event 3 at Mesa Verde

The stable carbon isotope ratios of bulk carbonate ($\delta^{13}C_{carb}$; Fig 2.9) through our section show little correlation with any of our other data. For example, and x/y plot of $\delta^{13}C_{carb}$ vs. %TOC gives an $r^2 = 0.07$ (Appendix 1). A recently published (Jarvis et al., 2006) composite $\delta^{13}C_{IC}$ reference curve compiled from chalks in England provides the opportunity for comparison of our record with global trends. In our record, there are

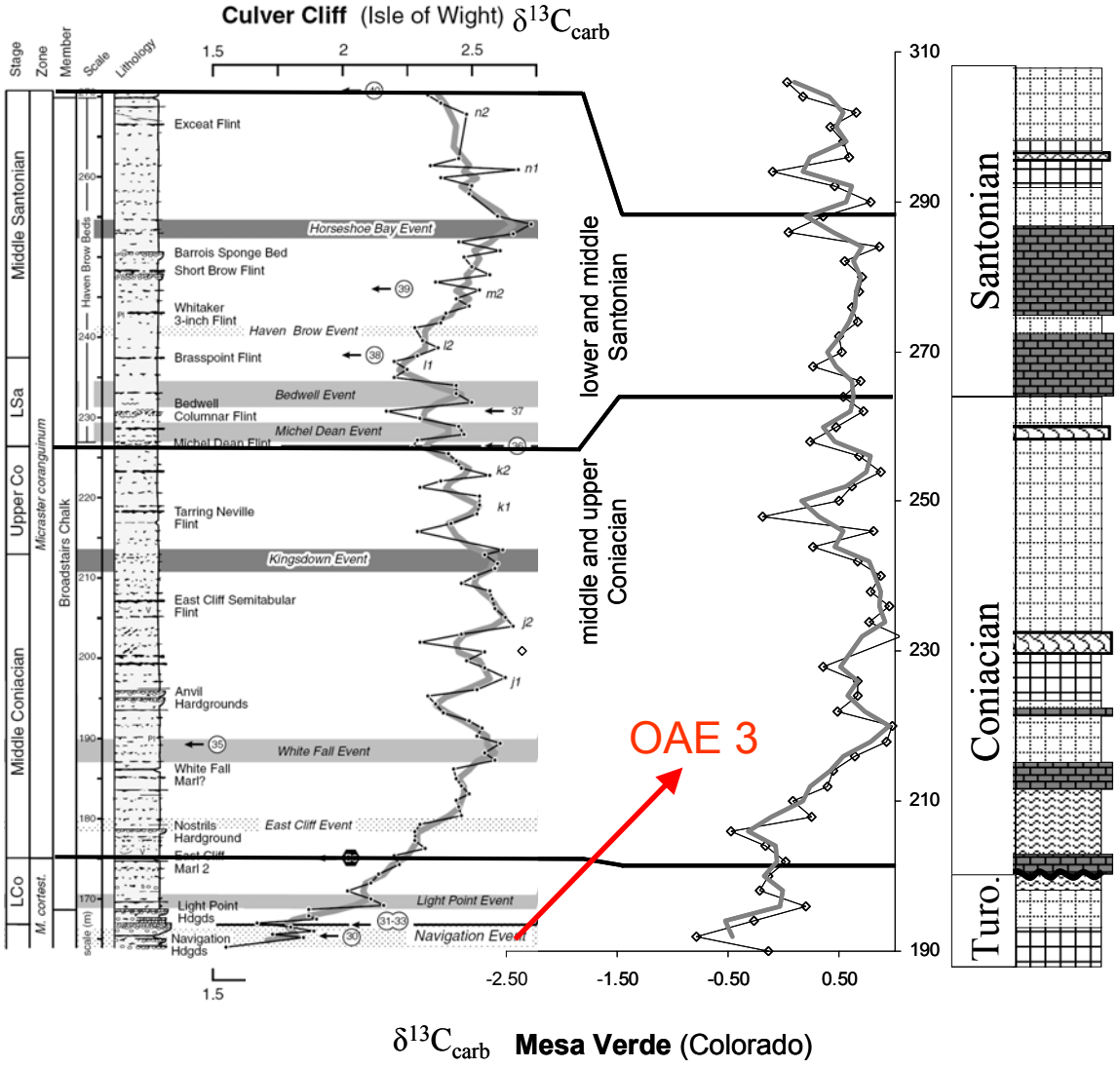

Figure 2.9 Comparison of the stable isotopic composition of carbonate at MVNP to those of the new reference section of Jarvis *et al.* (2006). ^{13}C-enrichment at the bottom of both records represents the global signal of OAE 3.

numerous rapid excursions of ~1‰, and long enrichment trend at the bottom of our record of ~2‰, and an excursion of ~3‰ at 230 m. Values through our section average ~0.4‰. Anomalously depleted values at 230 m may be the result of the introduction of

isotopically depleted carbon into the water column or the diagenetic alteration of the primary signal.

Broad first-order patterns of change in our record are like those seen in the Jarvis et al. (2006) record, especially at the bottom, although our record is still subject to much larger changes and more depleted values. The broad and long term enrichment encountered at the bottom of our record may be that which has been used previously in the Western Interior Seaway, the English Chalks, the Italian Scaglia (Jenkyns et al., 1994) as well as the Venezuelan La Luna Formation (De Romero et al., 2003) as the global expression of OAE 3. This general similarity suggests that the seaway, though restricted at times, was in good enough communication with the open global ocean to record broad scale variations in the global carbon cycle. Correlation of the MVNP section to the Jarvis English chalk section is based on age. A more precise and integrated correlation based on biostratigraphy and the new (Ogg, 2004) Cretaceous timescale is forthcoming.

2.4.4 Sediment Fabric

As stated earlier, sediments through the Smoky Hill comprise dark-gray, well laminated, calcareous shale, calcareous mudstone, and medium-gray mudstone. The unit is sparsely interbedded with marlstone and calcarenite. Bentonites are rare and limonites are prominent through most of the section. The laminated character of much of the section as well as the prominence of undisturbed limonites and, to a lesser extent, bentonites suggests bottom water anoxia may have been an important environmental control on organic matter accumulation and benthic community structure. Indeed, periods

of maximum organic carbon burial are accompanied by higher occurrences of intact limonite beds implying a lack of burrowing benthic macro-fauna. The paucity of benthic foraminifers through most of the Smoky Hill Member (Table 2.3) suggests excessive oxygen stress on the seafloor. Additionally, the presence of limonite beds themselves may relate information on the depositional setting. Limonite is an amorphous mixture of iron (III) oxides and hydroxides which can form from the oxidation of iron-sulfides such as pyrite. Leckie *et al.* (1997) proposed that these limonites were the diagenetic products of thin remnants of volcanic ash. Alternatively, their common occurrence in organic matter rich horizons may indicate a pyrite precursor formed during the mobilization of reduced iron and sulfur species during periods of bottom water anoxia.

2.4.5 Gamma Ray and Th/U Ratios

Gamma ray spectrometry allows for the field measurement of radiogenic nuclides of potassium (K), uranium (U), and thorium (Th) in sedimentary rocks. Its utility as a bottom water redox indicator is based on the differing behavior of uranium and thorium under oxidizing conditions (Rogers and Adams, 1976; Wedepohl *et al*., 1978; Liu et al., 1984, Wignall and Myers, 1988; and Postma and ten Veen, 1999). Thorium as Th^{4+} is insoluble regardless of sediment redox state; however under oxidizing conditions uranium as U^{6+} is soluble resulting in the relative depletion of uranium in oxidizing sediments and Th/U values > 3.8. Alternatively, in reducing environments uranium is reduced to insoluble U^{4+} resulting in the incorporation and enrichment of "authigenic" uranium and Th/U values between 2 and 0 (Wignall and Twichette, 1996). The increased contribution of authigenic uranium in anoxic environments leads to higher count per

second during gamma ray measurement independent of detrital U, K, and Th (and therefore Th/U) inputs which typically co-vary (Wignall and Myers, 1988).

Over the timescale of this study (~2.7 to 3.1 myr) changes in lithology, organic matter type, sedimentation rate, and migration of the redox boundary impact authigenic uranium concentrations and gamma ray values in ways that are difficult to constrain (Myers and Wignall, 1987; Van de Weijden, 1993). For example, Myers and Wignall (1987) found that changing lithology results in the "anoxic value" of the Th/U ratio being <3 and <1 in detrital and carbonate sediments respectively (instead of between 0 and 2 as discussed above). For these reasons, changes in these proxies are considered in a relative sense with respect to patterns expressed in other proxies such as TOC and C/N.

As expected, Th/U ratios through the Smoky Hill (Table 2.3) are low ranging from 2.8 to 0.7 (average 1.5) implying persistent bottom water anoxia. Gamma ray emission (Table 2.4; Fig 2.10) is relatively high during both third-order transgressive events suggesting that organic matter accumulation was aided by anoxia. Extremely high values during the first transgressive event and late in the second transgressive event (after ~300 m) probably result from highly reducing conditions supported by the presence of isorenieratane derivatives.

The period between the two events is characterized by falling gamma ray values reaching a low coincident with the expression of the Dalton Sandstone. This implies increasingly more oxidizing conditions at the sediment water interface. However, this conclusion is contradicted by coincident high and increasing TOC and C/N ratios (see below). Additionally, we would expect TAR values and grain size to increase as they do during more oxygenated periods of our record. Decreased emission may be the result of

decreasing sedimentation rate and delivery of these insoluble ions to the basin during continued second-order sea level rise. The development and growth of thick coastal wetland deposits during stillstand or third-order regression may have led to sediment starvation and sequestration of detrital radiogenic nuclides. Alternatively, perhaps the sediment water interface did become better ventilated and the increasing TOC and C/N are due to increases in primary production and the extent of a water column oxygen minimum zone.

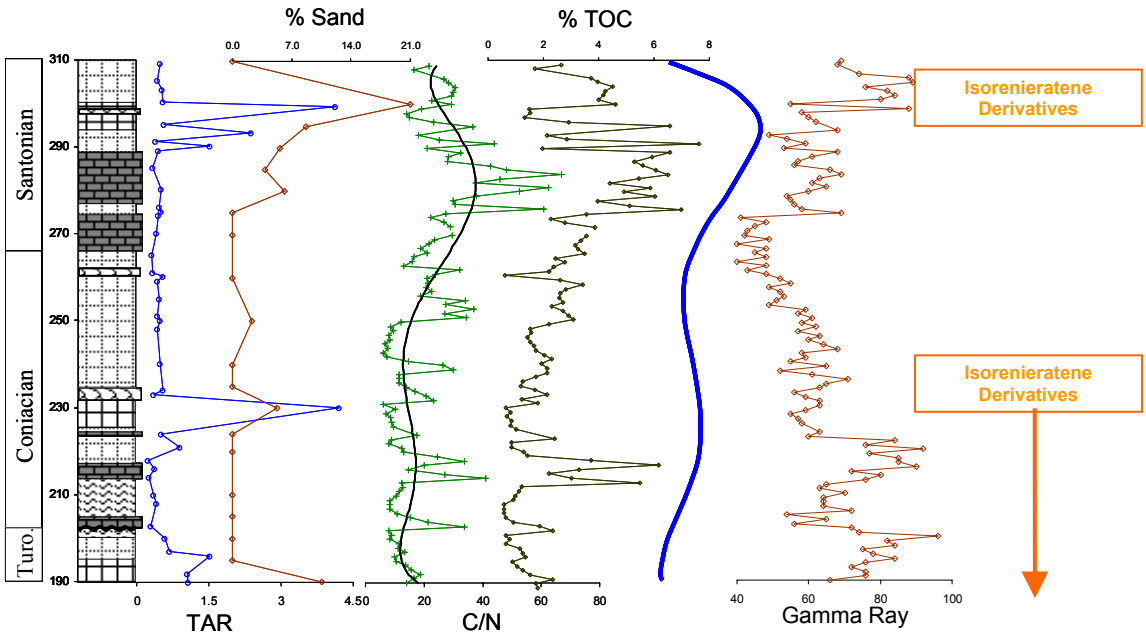

Figure 2.10 Plots illustrating relationships between the terrestrial vs. algal ratio, % sand (grain size), total organic carbon to total nitrogen (C/N), total organic carbon, gamma ray emission, photic zone euxinia, and sea level.

2.4.6 C/N Ratios and Denitrification

The ratio of total organic carbon to total nitrogen (C/N) has been commonly used in the reconstruction of organic matter sources to sediments (Prahl *et al.*, 1980; Ishiwatari and Uzaki, 1980; Silliman *et al.*, 1996; Meyers, 1997). The carbon-rich cellulosic material of terrestrial higher plants has C/N ratios >20 while nitrogen-rich proteinaceous

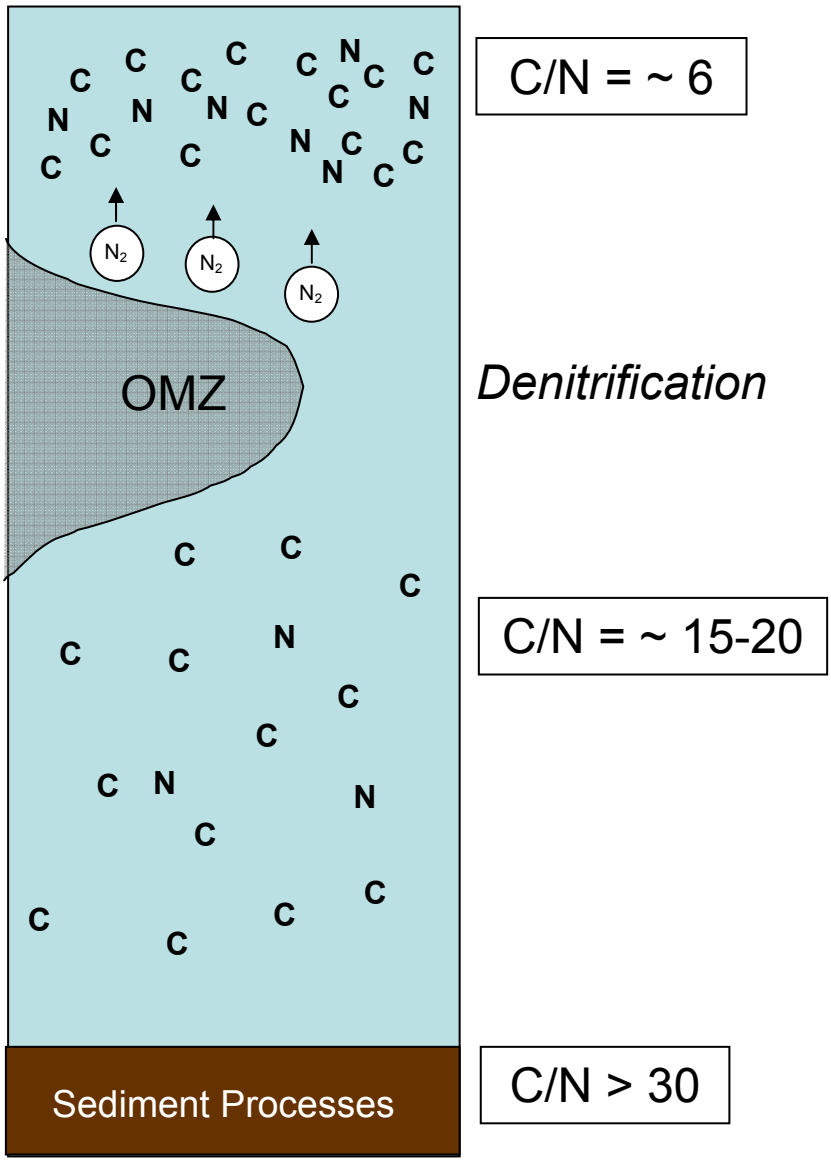

Figure 2.11 Water column schematic illustrating the impact of oxygen minimum zones and denitrification on C/N ratios.

material from algae has C/N ratios between 4 and 10 (Myers, 1994). Unfortunately, water-column alteration of primary product and mineral association often complicates this ratio. Mineral association effects are dominated by grain size; larger grain size sediment typically has higher C/N ratios and smaller grain size has lower (Thompson and Eglinton, 1978).

Water-column and sediment diagenetic processes also alter the C/N ratios of primary product (Twichell *et al.*, 2001; van Mooy *et al.*, 2002; Kuypers *et al.*, 2005; Meyers *et al.*, 2006; Ohkouchi *et al.*, 2006; and Junium and Arthur, 2007). For example, C/N ratios of organic matter-rich mudrocks and marls deposited during mid-Cretaceous Oceanic Anoxic Events are usually elevated with respect to the non-organic matter rich horizons above and below them (Meyers, 1997). In a study of modern processes, van Mooy *et al.* (2002) conducting sediment trap experiments in oxic and suboxic settings found that microbial denitrification operating under suboxic conditions preferentially degraded nitrogen-rich amino acids (Fig 2.11). Recently, Kuypers *et al.* (2005) linked loss of water column nitrogen in suboxic open-ocean settings to anaerobic ammonium oxidation (Anammox). Under modern day upwelling systems, C/N ratios may rise to 10-15 perhaps as the result of preferential utilization of N-rich organic matter in these settings (Twichell *et al*., 2002). In ancient sediments, high C/N ratios in sequences dominated by marine organic matter may record enhanced productivity and the presence of an oxygen minimum zone (Twichell *et al.*, 2002; Meyers *et al.*, 2006). In all cases, post-production increases in C/N ratios should be the result of the release of large amounts of organic nitrogen as N_2 during times of oxygen stress. A mixing model (Figure 2.12) produced by Junium *et al*. (2007) was assembled to clarify the effect the preferential utilization of N-rich amino and nucleic acids would have on sedimentary C/N ratios. They found that even complete removal of the N-rich fraction of available organic matter only increased C/N ratios to 10-15. These results are consistent with those of modern oxygen stressed water columns but far from values reported for the Cretaceous.

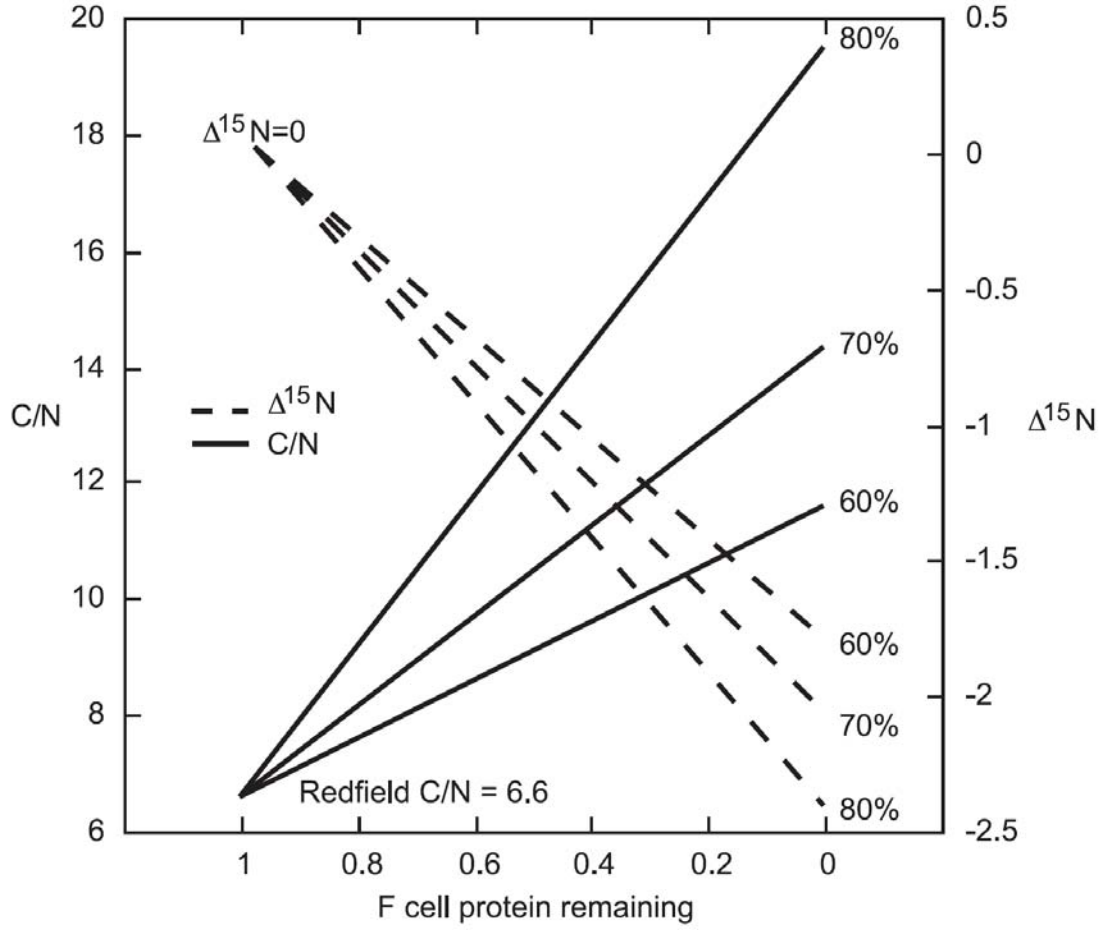

Figure 2.12 A hypothetical model demonstrating depletion of nitrogen isotope values and increases in C/N during N-rich-exclusive degradation assuming the protein fraction of prokaryotic biomass is enriched in ^{15}N relative to the whole cell by 3‰ (Macko *et al*., 1986). Percentages represent the percent mass of the degradaing cells that are "N-rich" based on the averages for prokaryotic cells (Neidhardt *et al*., 1996). Kinetic isotope fractionations are ignored for this estimation (from Junium *et al*., 2007).

2.4.7 $\delta^{15}N_{bulk}$ and Nitrogen Fixation

Values of $\delta^{15}N$ in this record are highly variable and do not obviously correlate with another proxy. However, long-term (myr) first-order changes in C/N ratios and $\delta^{15}N$ through our section appear anti-correlated such as those reported by Junium and Arthur (2007). This is illustrated by the gradual depletion of $\delta^{15}N$ values as C/N ratios increase from 230 – 289 m (Fig 2.13). Second-order exceptions to this trend exist below 230 m

and above 289 m during periods of increased water-column ventilation implied by sand concentration, organic matter concentrations, and TAR values. Here relationships between these proxies are less clear.

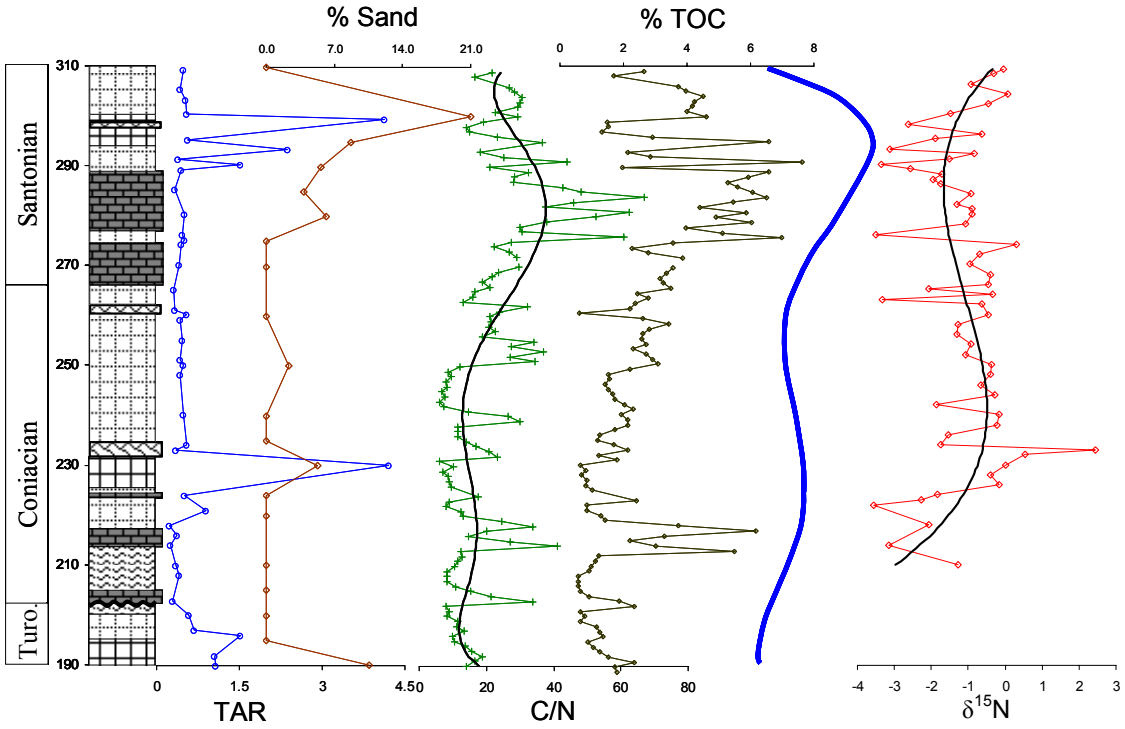

Figure 2.13 Comparison of ^{15}N values with those of other proxies. A weak negative correlation can be seen between ^{15}N and C/N ratios.

Low $\delta^{15}N$ values and high C/N ratios have been reported in other organic matter-rich horizons from the Aptian and Cenomanian-Santonian (Ohkouchi et al., 2006; Junium and Arthur, 2007), Devonian (Calvert et al., 1996; Levman and von Bitter, 2002), Toarcian (Jenkyns et al, 2001), and Mediterranean Quaternary Sapropels (Calvert et al., 1992; Milder et al., 1999; Meyers and Bernasconi, 2005). Such low $\delta^{15}N$ values are thought to represent the increased importance of cyanobacteria and diazotrophy (nitrogen fixation) during periods of nutrient cycling which differ greatly from those of today. The isotopic fractionation associated with the cleavage of the nitrogen-nitrogen triple bond in

N_2 is small relative to that associated with uptake of dissolved nitrate, nitrite, and ammonium (Wada and Hattori, 1991) and results in $\delta^{15}N$ values between 0 and -2‰ (Minagawa and Wada, 1986). Persistent and widespread oxygen stress during these times may have led to the removal of nitrogen via denitrification and the anaerobic oxidation of ammonia (anammox) and the liberation of reduced sedimentary mineral and organic phosphorus (Sachs and Rapeta, 1999; Kuypers et al., 2004). This would result in a switch from P-based to N-based nutrient limitation making nitrogen fixation an energetically favorable process. Additionally, preferential utilization of N-rich organic matter during times of water column oxygen stree (see above) can affect sedimentary $\delta^{15}N$ signatures. Nucleic and amino acids are enriched in ^{15}N by 3.6 ± 0.5‰ relative to bulk biomass (Macko, 1986) and their preferential uptake can modulate $\delta^{15}N$ values by 1-2‰ (Junium *et al.,* 2007).

Another source of isotopically depleted nitrogen is ammonium produced by the degradation of organic matter in a euxinic water column (Velinsky and Fogel, 1999). Nitrogen from such sources is typically 2-4 ‰ depleted relative to organic matter source (Silfer et al., 1992). High C/N and low $\delta^{15}N$ support the presence of persistent oxygen stress in the Coniacian-Santonian Western Interior Seaway at MVNP.

2.4.8 Photic Zone Euxinia

As stated earlier, biomarkers diagnostic of the presence of euxinic (anoxic and sulfidic) conditions in the photic zone were found in parts of this record (Fig. 2.10). Isorenieratane, a C_{40} aryl-isoprenoid (carotenoid) is thought to be produced solely by the brown strain of green sulfur bacteria; obligate anaerobic chemoautotrophs requiring

sulfide for their metabolism (Bosch et al., 1998; Grice et al., 1996; Hartgers et al., 1993; Koopmans et al. 1996; Pancost et al., 1998; Simons and Kenig, 2001; Sinninghe-Damste et al., 2001). The presence of isorenieratane and/or its derivatives has been used to imply the vertical expansion of euxinia into the photic zone in modern (Bosch, 1998) and ancient (Summons, 1986) settings. Their presence is illustrated by the vertical black bars on Figure 2.10. The compounds are present below 230 m and above 300 m suggesting third-order sea level cycles were not a main driver of their production or preservation. Instead, the occurrence of these compounds appears to setup a lower and upper bound to the record between which conditions were unfavorable to their production. Perhaps a strong oxygen minimum zone (and associated sulfidic waters) was only overlapping the photic zone during second-order relative low-stands on either end of the Niobrara cyclothem, a "relative" upward excursion of euxinia into the photic zone caused by sea level fall. During second- and third-order sea level transgressions, the seaway may have been too deep to allow the large vertical expansion of such oxygen-depleted sulfide-rich waters. Indeed, the presence of pyrite and diagenetically altered pyrite pseudomorphs (limonites) suggest that bottom waters held sulfide through much of this record.

2.4.9 Organic Matter

Stable carbon isotope ratios of carbonate in our section (Fig 2.14) suggest the global expression of OAE 3 begins near the bottom of our Smoky Hill record and high C/N and gamma ray values (Figs 2.10, 14) support the existence of bottom water anoxia through most of our study interval. Total organic matter values through our record (Fig. 2.14) are generally high ranging from 0.5% to almost 8%. Hydrogen Index values (Table

2.3) for this organic matter range from 85 to 264 suggesting type III and II/III kerogen. Type III organic matter is usually composed of terrestrial material and is only found at the disconformity at 200 m. Type II/III organic matter is a mixture of terrestrial and marine sources consistent with marine settings that are impacted by freshwater sources (paralic) such as those probably experienced in the KWIS.

Two rapid and dramatic increases in TOC are recorded above 214 m, 218 m, and 276 m. These events coincide with similar large shifts in C/N ratios and gamma ray emission (Fig 2.10). Additionally, both intervals are characterized by low molluscan diversity (Leckie et al., 1997) which rebounds and increases coincident with the end of the locally high TOC values. Coupled with increasing (terrestrial or better ventilated) TAR values (Fig 2.10) this suggests conditions in the water column were inhospitable during times of maximum organic matter burial probably as a result of expanded water-column anoxia. Conditions improved as the water-column became more ventilated. In fact, the upper organic matter-rich interval is characterized by the widespread occurrence of hypothesized chemosymbiotic *Platyceramus platinus* (Kaufmann et al., 2007). This large epifaunal inoceramid bivalve is commonly associated with moderately deep, pyritic, organic matter-rich, biotically deprived, calcareous shale facies of the Niobrara cyclothem (Kaufmann et al., 2007).

2.4.10 $\delta^{13}C_{OM}$: A Mixing Model

Stable carbon isotope ratios of bulk organic matter in our section ($\delta^{13}C_{OM}$; Fig 2.14) are depleted, typical of marine-derived organic matter-rich Cretaceous shales (Dean et al., 1986, Rau et al,. 1987; Meyers et al., 1989; Menegetti et al., 1998; Hofmann et al.,

2000; Kuypers et al., 2002; Tsikos et al., 2004; Kolonic et al., 2005; Meyers et al., 2006). Such depleted values (often between -30 and -25‰ for the Cretaceous) for marine derived organic matter are unlike those of modern day values

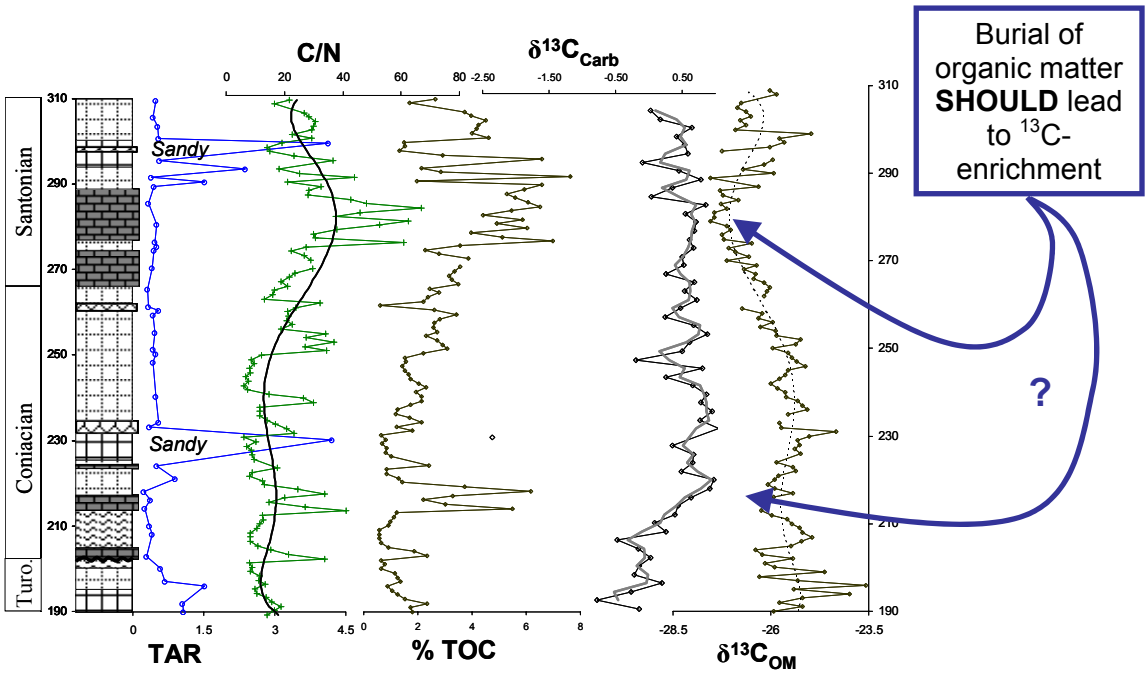

Figure 2.14 Plots illustrating the relationships between the stable carbon isotopes of organic matter and other proxies.

which range from -22 to -18‰ (Emerson and Hedges, 1988). Previous work on the widespread deposition and burial of organic matter rich horizons during Oceanic Anoxic Events has illustrated the progressive ^{13}C-enrichment of these sediments with increasing organic matter burial (Schlanger and Jenkyns, 1976; Arthur and Schlanger, 1979; Jenkyns, 1980; Arthur et al., 1987,1990; Bralower et al., 1993). However, values in our section become progressively depleted during these intervals. The kinetic isotope discrimination associated with the uptake of dissolved inorganic carbon results in the burial of isotopically depleted organic matter. Over time, the continued burial of more

and more organic material results in ^{13}C-enrichment of the reservoir. This process should be expressed by ever increasing $\delta^{13}C$ values of organic matter and carbonate.

Instead, perhaps $\delta^{13}C_{OM}$ is being controlled (like C/N, $\delta^{15}N$, and TOC) by water-column and sediment microbial processes during an extended period of oxygen stress. If, as van Mooy et al. found (2002), nitrogen-rich organic matter is being preferentially utilized during this time, differences in the $\delta^{13}C$ of varying compound classes associated with their synthesis may explain our results. Indeed plots of $\delta^{13}C_{OM}$ vs. TOC, $\delta^{13}C_{OM}$ vs. C/N, and C/N vs. TOC through the Smoky Hill have r^2 of 0.58, 0.50, and 0.62 (*n*=106) suggesting they are being controlled by a similar process (Appendix 1). A simple two end member mixing model was constructed to clarify the effects on $\delta^{13}C_{OM}$ of the preferential utilization of nitrogen rich organic matter.

EQ 1) $\delta^{13}C_{OM}^{sed} = (\delta^{13}C_{lipids} \times f_{lipids}) + (\delta^{13}C_{amino} \times f_{amino})$

Where:

$\delta^{13}C_{OM}^{sed}$ is the stable isotopic ratio of carbon in the sediment

$\delta^{13}C_{lipids}$ is the stable isotopic ratio of carbon in the relatively ^{13}C-depleted lipid portion of settling primary product

f_{lipids} is the fraction of settling primary product that is "lipid-like"

$\delta^{13}C_{amino}$ is the stable isotopic ratio of carbon in the relatively ^{13}C-enriched amino acid portion of settling primary product

f_{amino} is the fraction of settling primary product that is "amino acid-like"

If $\delta^{13}C_{OM}$ is being driven by these processes, then when C/N and TOC are lowest $\delta^{13}C_{OM}$ should reflect an "undegraded" signal. Plots of both TOC and C/N vs. $\delta^{13}C_{OM}$ give an intercept value of ~ 25 ‰ when TOC and C/N are at their lowest or most-algal

respectively. We will consider this our initial value ($\boldsymbol{\delta^{13}C_{OM}^{undegraded}}$). During times of strongest ^{13}C-depletion, and highest TOC and C/N values, $\delta^{13}C_{OM}$ nears – 28 ‰. This will be our "degraded" signal ($\boldsymbol{\delta^{13}C_{OM}^{degraded}}$). Assuming that hydrogen-rich lipids are ~ 5 ‰ depleted in ^{13}C relative to bulk biomass (Dai and Sun, 2006) and that nitrogen-rich amino acids are ~ 7 ‰ enriched (Macko *et al*., 1987) we have an initial "undegraded" condition of:

$\boldsymbol{\delta^{13}C_{lipids}}$ = - 30 ‰

$\boldsymbol{\delta^{13}C_{amino}}$ = - 18 ‰

and,

$$\textbf{EQ 2) } \boldsymbol{\delta^{13}C_{OM}^{undegraded}} = -25 \text{ ‰} = [-30 \text{ ‰} \times (1-x)] + [-18 \text{ ‰} \times (x)]$$

$$\text{and } \mathbf{f_{amino} = .42}$$

and a "degraded" condition of:

$$\textbf{EQ 3) } \boldsymbol{\delta^{13}C_{OM}^{degraded}} = -28 \text{ ‰} = [-30 \text{ ‰} \times (1-x)] + [-18 \text{ ‰} \times (x)]$$

$$\text{and } \mathbf{f_{amino} = .17}$$

Van Mooy et al. (2002) found that amino acids accounted for 37% of the *in situ* particulate organic matter "falling" from the euphotic zone (75 m), but that after *in vitro* suboxic degradation they only accounted for 16%. *In situ* contributions of amino acids at 500 m, after passage through an "oxygen deficient zone", were 10%. These values agree well with those from our model which suggest unaffected organic matter leaving the euphotic zone in the Western Interior Seaway would be 42% amino acids and subsequent suboxic degradation would decrease this fraction to 17%. These findings suggest that the

preferential utilization of N-rich compounds during denitrification may have been an important water-column process at our site during the late Cretaceous.

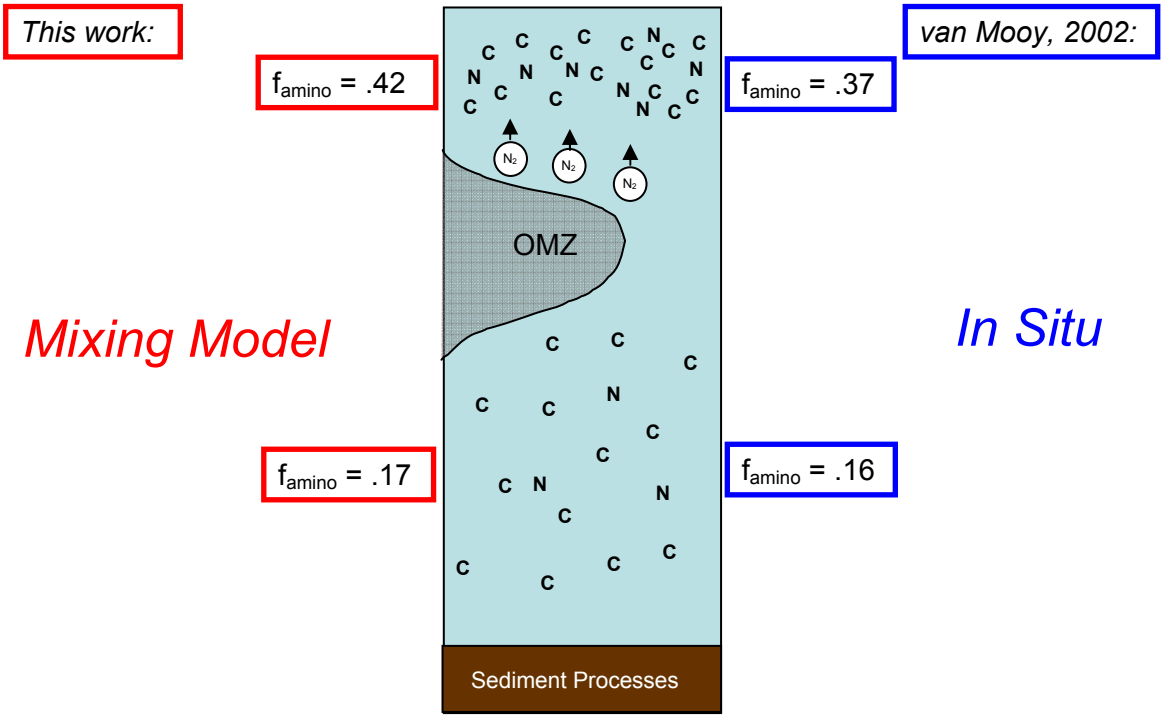

Figure 2.15 A water column schematic comparing the results of our simple two-end member mixing model with those of the in situ study of van Mooy (2002)

2.5 Conclusions

New high-resolution investigation of Late Cretaceous sea level change associated with the second-order Niobrara cyclothem at MVNP supports prior work by Leckie *et al.* (1998). Two multi-million year third-order transgressive pulses correlate with other well established transgressive facies such as Molenaar's (1983) T3 and T4 and the depositional cyclicity of Dean and Arthur (1998). A broad ^{13}C-enrichemnt in bulk carbonates at the bottom of our record signals the onset of Oceanic Anoxic Event 3 and suggests that while the basin may have been restricted in nature it was well enough connected to record this global signal.

The highest concentrations of organic matter are confined to transgressive facies of the Smoky Hill and basal Cortez Members of the Mancos Shale and lesser amounts are associated with highstand and regressive facies. This may be due in part to increased ventilation of the seaway during highstand and early regression reconstructed here by terrestrial vs. algal ratios (TAR). Intensified water ventilation may have resulted from the emplacement of bottom water currents implied by increased grain size associated with these intervals. Additionally, the meeting and mixing of Tethyan and Boreal water masses during two peaks in third-order transgressions may have led to cabeling and production of a more-dense, oxygen-depleted, WIS derived water mass as suggested by Hay et al. (1993).

Despite occasional increases in water column ventilation, sediment fabric, gamma ray, Th/U, and C/N analyses suggest not only the sediments but also the water column of the Coniacian-Santonian Western Interior Seaway was oxygen stressed more often than not. The numerous limonite seams encountered in the section may be the oxidized remnants of sedimentary pyrite. During relative sea level low-stand on the lower and upper bounds of our record, the presence of isorenieratane derivatives is consistent with a "relative" upward excursion of the oxygen minimum zone.

Periods of intensified denitrification in the presence of a water column oxygen minimum zone is supported by high C/N and depleted $\delta^{13}C_{OM}$ values. A mixing model constructed to measure the impact of the preferential utilization of N-rich organic matter during these periods agrees well with values obtained in other *in situ* and culture studies (van Mooy, 2002). Denitrification, coupled with the long-term emplacement of bottom and water column anoxia may have led to the regeneration of nutrient phosphorus levels

and the development of nitrogen-limited surface waters. Under these circumstances, nitrogen fixation, implied by low and decreasing $\delta^{15}N_{bulk}$ values, may have become an energetically favorable process. The later degradation of nitrogen fixing cyanobacterial biomass would be important in the maintenance of surface water nutrient levels.

CHAPTER 3

FURTHER WORK

Many opportunities for further work at this location exist. In the section described here, higher-resolution biomarker investigation would be of primary interest and would allow us to better constrain the effects of oxygenation on biomarker distributions, such as in the TAR. Equipped with a better understanding of the sources of variation in the TAR, further investigation into the processes responsible for organic matter deposition would be critical in expanding our current understanding of the carbon cycle during the perturbed states represented by Oceanic Anoxic Events. Additionally, higher-resolution biomarker analyses may shed light on the effect of oxygenation on water column ecology and the sedimentary record.

The application of compound specific carbon and hydrogen isotopes to this record is another area deserving attention. To date, little is known regarding the differences in the stable isotopic ratios of carbon in marine and terrestrial realms during the Cretaceous. How did extremely high carbon dioxide concentrations get expressed in the molecular components making up plant and algal tissue? Analyses of the stable isotopic ratios of hydrogen in marine-derived biomarkers in these samples could hold information regarding the changing influence of Tethyan and Boreal water masses at MVNP improving future modeling studies of paleoceanography of the Western Interior Seaway. Coupling the analyses of the stable isotopic ratios of hydrogen in marine-derived biomarkers to those of terrestrial biomarkers could provide information regarding changes in local precipitation and evaporation schemes and their effect on the marine

realm. This would be critical in expanding our understanding of triggers for Oceanic Anoxic Events in the Western Interior Seaway. Was water column anoxia caused or maintained by a so-called “fresh water lid”?

In addition to the new analyses proposed here, the application of these same high-resolution analyses to the more than 700 m of sample stored at UMass-Amherst could greatly expand our current understanding of the behavior of the Western Interior Seaway in response to numerous sea level fluctuations during the Late-Cretaceous.

APPENDIX 1

CORRELATIVE X/Y PLOTS DISCUSSED IN THE TEXT

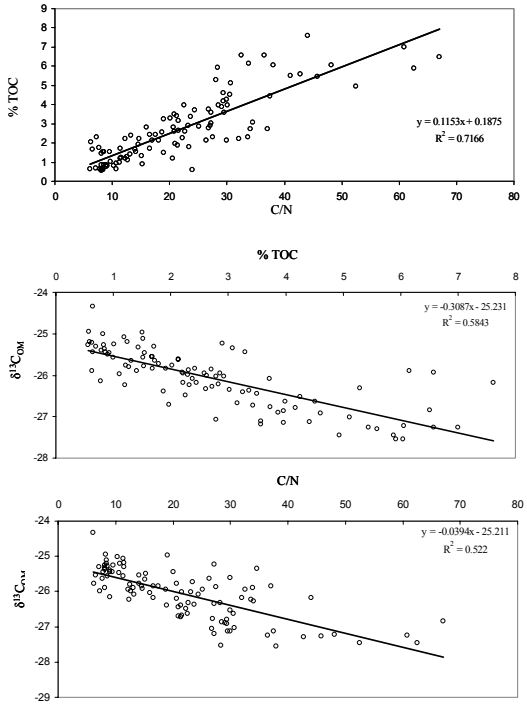

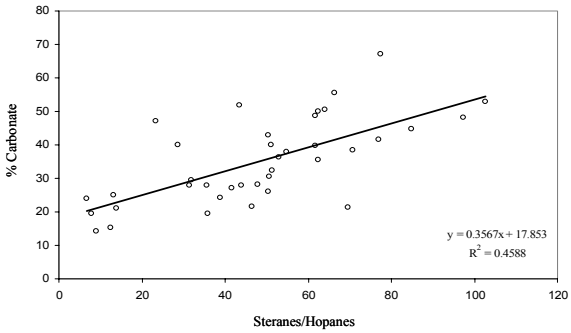

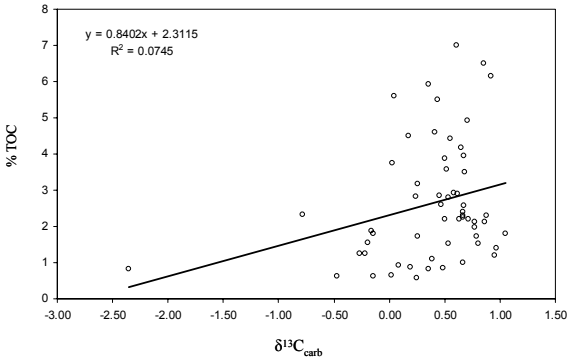

APPENDIX 2

BIOMARKER CONCENTRATIONS

Sample (m)	Concentration (ng/g TOC)												
	n-C_{14}	*n*-C_{15}	*n*-C_{16}	*n*-C_{17}	*n*-C_{18}	*n*-C_{19}	*n*-C_{20}	*n*-C_{21}	*n*-C_{22}	*n*-C_{23}	*n*-C_{24}	*n*-C_{25}	*n*-C_{26}
309	52.8	101.9	111.2	115.2	93.4	89.0	73.2	76.5	66.0	66.8	63.4	53.1	42.0
305	178.9	320.2	332.0	328.8	283.8	273.8	216.3	221.5	185.2	190.9	166.0	154.7	124.8
303	114.1	256.0	294.1	298.0	262.4	252.9	187.6	198.7	171.2	181.3	163.4	160.5	135.3
300	183.7	388.7	417.8	432.6	388.0	358.2	277.9	301.0	267.6	272.4	260.5	240.9	199.9
299	0.0	23.3	52.0	68.2	72.3	47.7	41.3	30.2	33.9	32.6	61.3	49.4	78.2
295	80.6	233.3	295.9	349.0	348.2	327.7	327.8	338.6	306.0	290.0	266.7	237.5	214.6
293	0.0	0.0	108.8	139.8	135.5	134.1	132.6	142.1	139.6	141.6	158.6	136.9	149.5
291	132.9	281.6	333.0	365.0	323.7	293.2	271.4	296.0	240.2	230.6	232.0	204.0	179.1
290	0.0	0.0	129.6	318.6	436.7	455.6	433.0	464.4	408.5	383.6	365.9	313.9	312.0
289	134.0	333.6	374.5	401.0	376.7	369.1	348.6	346.0	307.2	279.7	272.9	231.4	214.9
285	68.6	195.3	260.0	286.4	267.0	233.3	195.1	201.5	175.3	169.9	167.2	137.4	122.4
280	313.8	747.1	866.5	944.4	919.4	804.8	715.2	723.8	681.8	702.1	640.2	550.7	472.4
276	175.2	346.9	382.5	412.2	389.5	347.8	314.6	324.5	304.1	307.4	296.2	262.4	219.6
275	33.6	104.8	156.0	197.7	186.7	174.8	147.3	157.2	138.5	137.2	132.0	112.1	95.0
274	0.0	90.3	161.7	209.0	199.5	168.1	141.7	137.9	123.6	121.4	120.0	96.7	83.1
270	52.8	123.6	146.3	156.3	144.2	122.3	101.5	116.3	96.9	97.8	99.8	90.2	79.3
265	47.6	97.5	115.5	126.1	118.0	102.3	93.3	93.1	78.6	78.7	78.8	63.4	52.9
261	102.0	365.4	621.1	809.4	792.2	657.3	624.7	502.2	442.9	424.4	427.3	335.8	299.9
260	0.0	63.8	124.9	161.8	164.7	140.2	144.6	130.4	117.7	120.5	122.0	101.5	94.7
259	72.1	200.7	274.6	330.8	296.3	260.6	234.0	220.7	194.8	189.1	187.2	158.9	152.6
255	31.1	160.3	252.4	301.5	285.7	252.3	243.7	225.6	194.3	195.1	186.8	157.8	142.4
251	53.2	104.8	119.1	128.7	122.8	103.9	104.9	103.6	84.0	83.2	81.4	65.9	54.7
250	35.9	151.8	227.5	273.6	259.9	231.1	208.5	195.1	166.9	172.1	161.9	141.1	122.6
248	0.0	303.0	646.4	927.4	867.6	722.2	557.5	533.6	421.5	449.8	411.1	344.0	299.0
240	59.8	175.4	234.4	244.3	224.1	196.2	164.2	170.5	139.2	142.6	134.3	122.1	102.3
234	35.2	162.5	238.0	276.2	248.5	216.5	192.8	191.5	165.9	170.2	171.9	151.3	138.1
233	0.0	233.6	651.5	1133.4	1277.7	1326.3	923.0	810.5	727.5	676.1	691.1	534.7	453.3
230	0.0	0.0	63.4	122.2	130.8	161.6	118.2	105.1	125.2	169.0	271.6	290.2	344.2
224	29.2	115.6	184.6	231.5	227.0	197.1	176.7	157.4	138.9	138.2	139.0	122.3	106.2
221	0.0	98.8	200.0	265.4	229.0	203.1	163.4	128.4	117.5	131.9	161.2	163.3	173.4
218	152.6	337.1	404.4	458.9	453.6	381.1	344.6	317.0	252.3	235.9	211.1	179.5	147.0
216	46.1	125.7	160.6	177.9	154.7	148.4	120.7	129.1	103.0	99.9	98.2	83.2	68.2
214	201.4	426.0	487.1	526.6	506.1	459.2	393.7	360.9	306.5	295.8	257.9	226.4	170.4
210	0.0	62.1	168.3	264.3	248.7	293.6	193.9	209.6	159.0	148.8	150.7	106.6	82.2
208	0.0	24.9	78.4	137.7	148.4	222.1	130.3	137.0	111.9	109.0	121.8	81.3	64.4
203	65.5	242.3	338.9	403.4	341.6	304.3	246.4	252.4	208.7	209.8	192.9	166.4	129.1
200	0.0	39.1	97.5	145.3	129.6	174.4	97.3	92.8	85.5	94.0	121.4	95.4	86.5
197	23.0	116.6	199.0	254.4	197.4	210.5	137.2	123.9	118.3	124.2	128.6	119.1	111.1
196	0.0	47.0	98.4	149.9	138.8	156.1	109.0	100.9	104.0	120.9	143.8	140.0	138.7
192	50.3	139.7	183.9	199.3	170.4	174.4	134.4	128.1	120.8	129.4	140.0	130.0	129.5
190	78.3	187.2	248.5	233.0	190.2	193.7	152.1	143.8	139.7	151.6	161.5	150.9	144.9

Sample (m)						Concentration (ng/g TOC)						Iso
	n-C_{27}	*n*-C_{28}	*n*-C_{29}	*n*-C_{30}	*n*-C_{31}	*n*-C_{32}	*n*-C_{33}	*n*-C_{34}	*n*-C_{35}	Ph	Pr	Derivatives
309	42.2	37.2	54.9	33.1	53.5	28.5	44.5	20.1	24.3	90.5	185.5	0.2
305	112.3	126.5	152.8	80.6	122.3	63.8	73.4	34.1	49.4	341.5	608.3	2.0
303	126.5	131.7	158.5	90.3	140.9	68.3	88.6	36.0	44.2	325.3	564.7	1.8
300	207.0	193.6	228.2	128.8	206.1	102.5	139.2	55.6	65.2	474.0	795.9	10.7
299	111.3	138.5	204.9	183.4	258.0	158.1	194.4	101.4	97.7	36.9	42.9	n/d
295	169.9	182.5	199.9	118.0	146.2	69.6	96.7	53.9	60.9	437.1	660.7	n/d
293	144.0	160.5	219.2	205.9	288.1	196.9	244.7	152.4	182.9	141.2	212.4	n/d
291	117.5	138.6	133.5	85.7	110.1	62.1	71.9	44.4	43.4	386.9	568.7	n/d
290	285.9	324.5	417.7	356.8	478.8	290.7	351.9	209.8	243.1	351.0	409.4	n/d
289	177.6	175.5	184.2	113.6	138.2	67.7	79.2	41.3	57.3	437.7	754.8	n/d
285	82.5	94.9	83.7	50.7	70.5	32.9	41.0	23.9	25.8	281.9	431.9	n/d
280	419.0	405.2	441.4	314.5	387.6	221.0	229.1	0.0	166.0	808.9	1216.9	n/d
276	173.8	172.1	179.7	126.3	161.4	86.2	97.3	52.3	60.1	402.8	650.2	n/d
275	69.8	96.0	90.7	58.2	78.5	42.5	52.4	28.0	32.4	158.5	245.5	n/d
274	70.0	62.7	72.5	55.2	71.2	47.1	56.5	31.8	33.6	125.5	225.6	n/d
270	64.2	54.1	56.9	45.0	43.1	30.2	33.5	18.3	21.3	133.1	214.1	n/d
265	40.5	38.6	35.9	26.4	25.5	17.5	19.2	11.0	11.4	95.5	167.7	n/d
261	230.6	197.2	214.4	168.2	157.2	117.5	130.6	78.2	85.9	553.7	814.6	n/d
260	69.4	58.1	79.4	48.8	51.4	31.9	34.6	17.7	22.2	143.3	207.8	n/d
259	103.6	123.6	132.8	79.8	109.2	64.1	57.4	29.5	34.0	313.4	470.4	n/d
255	107.6	110.3	125.8	75.2	98.6	51.8	56.9	30.4	32.6	246.7	414.4	n/d
251	49.8	47.2	50.9	35.2	41.1	30.6	30.8	18.1	18.5	124.7	181.2	n/d
250	103.0	87.5	113.7	73.9	98.9	52.1	56.8	30.9	31.4	196.1	341.1	n/d
248	260.2	258.1	296.4	219.1	285.6	165.5	182.7	113.8	100.2	576.4	818.6	n/d
240	98.1	84.4	102.4	68.7	94.6	45.9	52.6	29.2	29.7	162.4	347.0	n/d
234	116.9	105.8	120.4	92.2	114.6	70.0	78.5	45.8	47.6	196.5	303.8	1.1
233	378.4	333.0	336.8	235.1	235.0	176.5	179.7	123.4	115.9	1160.6	1006.2	13.0
230	367.3	356.0	417.6	344.6	409.3	274.2	270.2	158.4	146.6	158.1	85.1	0.3
224	98.0	82.5	97.7	60.1	81.1	52.2	54.9	32.6	32.3	177.0	251.3	0.9
221	170.0	155.8	174.1	135.0	159.9	114.3	123.8	77.1	76.4	132.5	181.0	1.5
218	102.4	98.4	97.6	59.8	70.1	39.6	40.6	30.2	24.9	291.2	547.3	1.0
216	59.9	55.8	61.5	36.7	45.1	33.3	35.9	22.2	22.0	93.4	186.3	1.1
214	120.8	126.8	139.8	69.1	98.9	47.2	53.7	31.6	34.9	413.9	736.1	2.8
210	84.4	73.8	85.7	51.7	52.9	35.2	35.1	24.4	22.2	221.2	286.4	3.6
208	62.6	51.8	58.9	36.9	38.7	24.3	25.0	0.0	0.0	254.1	148.0	8.1
203	109.1	90.6	91.7	54.5	69.3	46.2	53.5	28.9	30.4	233.0	547.2	0.9
200	88.3	75.8	76.8	51.6	46.4	29.2	24.7	0.0	0.0	214.2	133.4	6.1
197	125.8	116.1	144.4	97.3	122.4	62.2	62.8	28.0	24.0	164.8	369.2	3.7
196	166.6	156.6	196.7	135.3	169.7	84.9	83.8	37.8	31.2	147.7	262.1	2.6
192	143.4	147.3	186.0	136.9	211.3	99.2	113.1	50.7	46.6	181.0	578.9	1.5
190	183.5	167.5	235.9	172.5	242.1	112.9	122.0	52.6	51.8	168.2	678.1	1.4

APPENDIX 3

REPRESENTATIVE CHROMATOGRAMS (A) AND MASS FRAGMENTATION PATTERS (B) OF OF *N*-ALKANES (M/Z 57), HOPANES (M/Z 191), AND STERANES (M/Z 217)

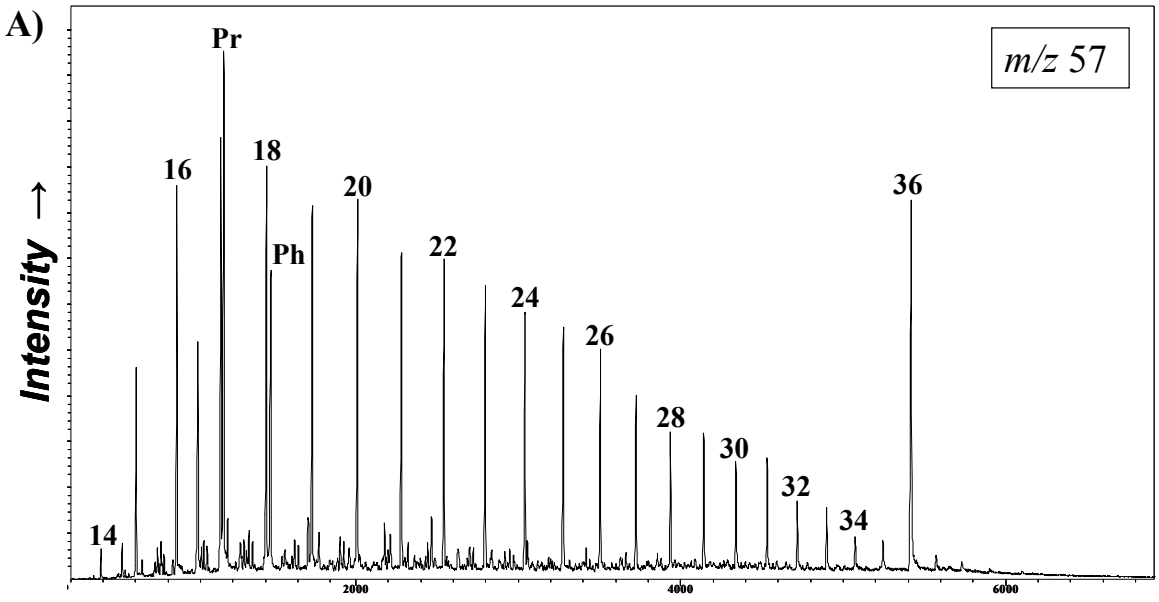

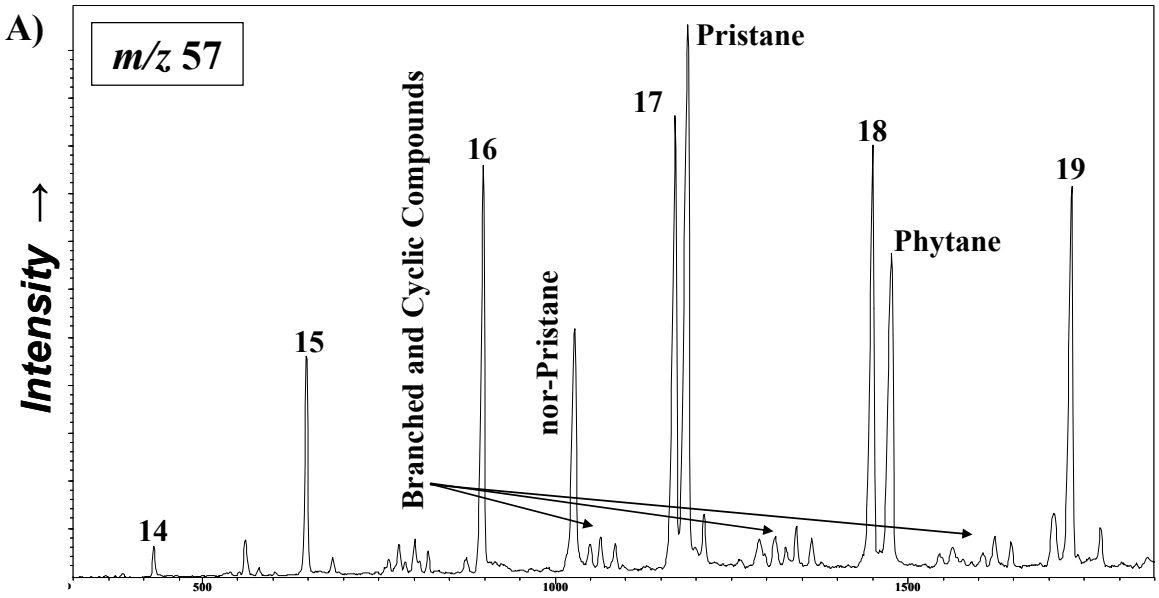

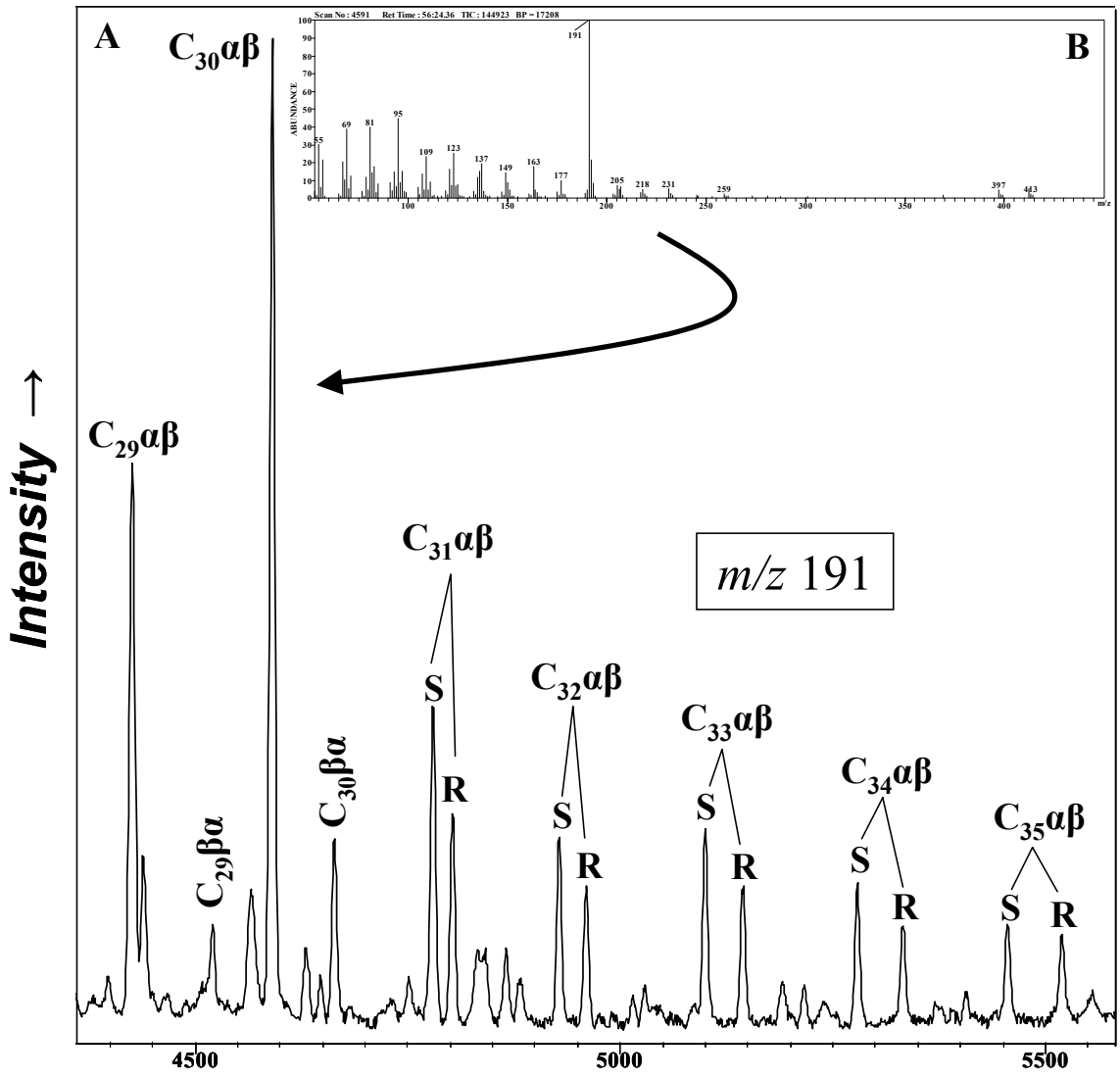
A
B
Scan No : 4591 Ret Time : 56:24.36 TIC : 144923 BP = 17208
ABUNDANCE
m/z
Intensity →
m/z 191
C29αβ
C29βα
C30αβ
C30βα
C31αβ
S
R
C32αβ
S
R
C33αβ
S
R
C34αβ
S
R
C35αβ
S
R
4500
5000
5500

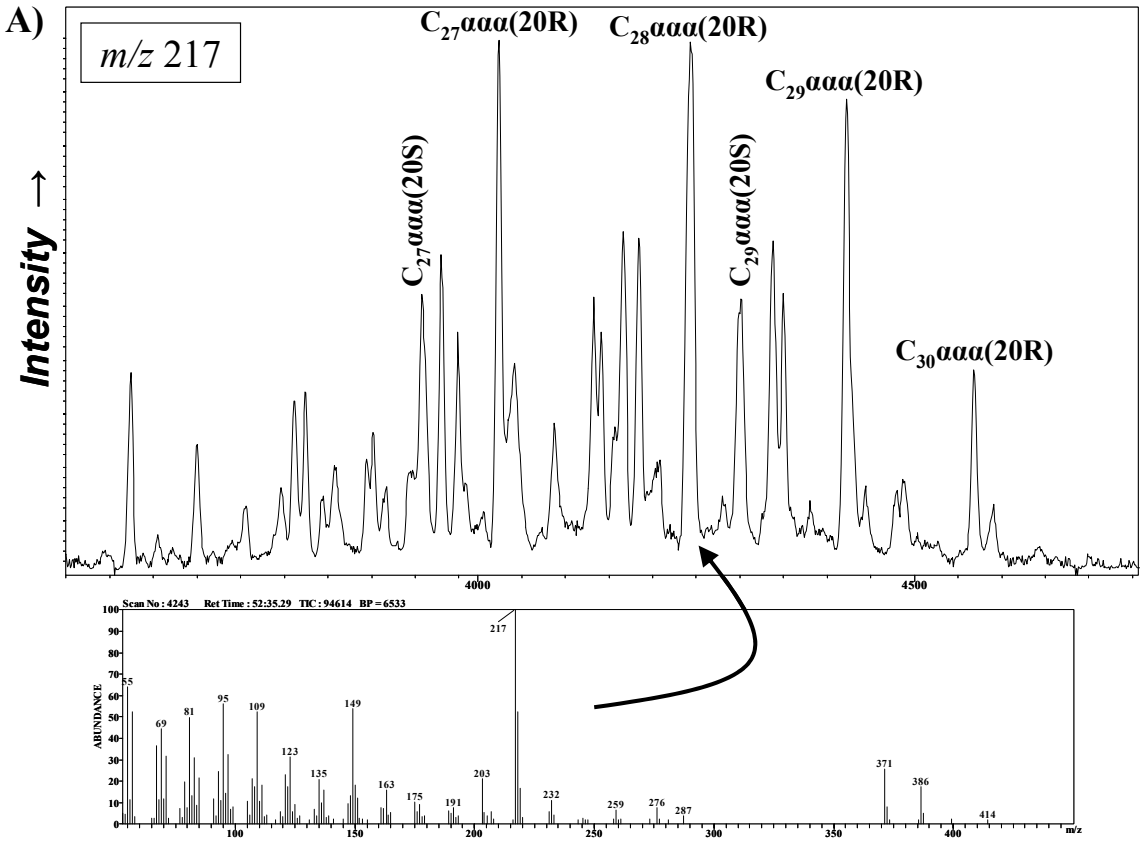
A)
m/z 217
Intensity →
C27αααα(20R)
C28αααα(20R)
C29αααα(20R)
C27αααα(20S)
C29αααα(20S)
C30αααα(20R)
4000
4500
Scan No : 4243 Ret Time : 52:35.29 TIC : 94614 BP = 6533
ABUNDANCE
m/z
55
69
81
95
109
123
135
149
163
175
191
203
217
232
259
276
287
371
386
414

References

Arthur, M.A., Natland, J.H., 1979. Carbonaceous sediments in the north and south Atlantic: The role of salinity in stable stratification of Early Cretaceous basins. In: Talwani, M., Hay, W.W., Ryan, W.B.F. (Eds.) Deep Drilling Results in the Atlantic Ocean: Continental Margins and Paleoenvironment. AGU, Washington D.C., pp. 375–401

Arthur, M. A., and Premoli Silva, I. 1982. Development of widespread organic carbon-rich strata in the Mediterranean Tethys. In: Schlanger, S.O. and Cita, M.B., (Eds.) Nature of Cretaceous Carbon-Rich Facies. Academic Press, San Diego, Calif pp. 7–54

Arthur, M. A., Dean, W.E., Bottjer, D.J., and Scholle, P.A., 1984. Rhythmic bedding in Mesozoic-Cenozoic pelagic carbonate sequences: The primary and diagenetic origin of Milankovitch-like cycles. In: Berger, A. (Eds.) Milankovitch and Climate. D. Riedel, Norwell, Mass, pp. 191–222

Arthur, M. A., Dean, W.E., and Schlanger, S.O., 1985. Variations in the global carbon cycle during the Cretaceous related to climate, volcanism, and changes in atmospheric CO2. In: Sundquist, E.T., and Broecker, W.S. (Eds.) The Carbon Cycle and Atmospheric CO2: Natural Variations Archean to Present. Geophys. Monogr. Ser., vol. 32, AGU, Washington, D. C., pp. 504– 529

Arthur, M. A., Schlanger, S.O., and Jenkyns, H.C., 1987. The Cenomanian-Turonian oceanic anoxic event II, paleoceanographic controls on organic matter production and preservation, In: Brooks, J. and Fleet, A. (Eds) Marine Petroleum Source Rocks. Geol. Soc. Spec. Publ., 24, pp. 399– 418

Arthur, M. A., Dean, W. E., Pratt, L. M., 1988. Geochemical and Climatic Effects of Increased Marine Organic-Carbon Burial at the Cenomanian Turonian Boundary. Nature, 335, 714-717

Arthur, M. A., Brumsack, H.J., Jenkyns, H.C., and Schlanger, S.O., 1990. Stratigraphy, geochemistry, and paleoceanography of organic carbon rich Cretaceous sequences, In: Ginsburg, R.N. and Beaudoin, B. (Eds) Cretaceous Resources, Events, and Rhythms. Kluwer Acad., Norwell, Mass., pp. 75 – 119

Bode H. B., Zeggel B., Silakowski B., Wenzel S. C., Hans R., and Müller R., 2003. Steroid biosynthesis in prokaryotes: identification of myxobacterial steroids and cloning of the first bacterial 2,3(S)-oxidosqualene cyclase from the myxobacterium Stigmatella aurantiaca. Molecular Microbiology, 47, 471–481.

Bosch H.-J., Sinninghe Damste´ J. S., and de Leeuw J. W., 1998. Molecular palaeontology of eastern Mediterranean sapropels: evidence for photic zone euxinia. Proceedings of the Ocean Drilling Program, Sci. Res., 160, 285–295.

Bourbonniere, R.A., Meyers, P.A., 1996. Sedimentary geolipid records of historical changes in the watersheds and productivities of Lakes Ontario and Erie. Limnology and Oceanography, 41, 352-359

Boyles, J.M., Scott, A.J., 1982. A model for migrating shelfbar sandstone in upper Mancos Shale (Campanian) northwestern Colorado. American Association of Petroleum Geologists, Bulletin, v.66, 491-508

Bralower, T. J., Sliter, W.V., Arthur, M.A., Leckie, R.M., Allard, D., and Schlanger, S.O., 1993. Dysoxic/anoxic episodes in the Aptian-Albian (Early Cretaceous), In: Pringle, M.S. (Eds) The Mesozoic Pacific: Geology, Tectonics and Volcanism. Geophys. Monogr. Ser., AGU, Washington, D. C., vol. 77, pp. 5 – 37

Bralower, T. J., Arthur, M.A., Leckie, R.M., Sliter, W.V., Allard, D, and Schlanger, S.O., 1994. Timing and paleoceanography of oceanic dysoxia/anoxia in the late Barremian to early Aptian. Palaios, 9, 335– 369

Bralower, T. J., Fullagar, P.D., Paull, C.K., Dwyer, G.S., and Leckie, R.M., 1997. Mid-Cretaceous strontium-isotope stratigraphy of deep-sea sections. Geol. Soc. Am. Bull., 109, 1421–1442

Bralower, T. J., CoBabe, E., Clement, B. Sliter, W.V., Osburn, C.L., Longoria, J., 1999. The record of global change in mid-Cretaceous (Barremian- Albian) sections from the Sierra Madre, northeastern Mexico. J. Foraminiferal Res., 29, 418–437

Bréhéret, J.-G., Caron, M., and Delamette, M., 1986. Niveaux riches en matie`re organique dans l'Albien vocontien; quelques caracte`res du pale´oenvironnement essai d'interpre´tation ge´ne´tique, In: J.-G. Bréhéret (Eds) Les Couches Riches en Matie`re Organique et leurs Conditions de Dépôt, Documents B.R.G.M., 110, 141– 191

Bréhéret, J.-G., and Delamette, M., 1989. Faunal fluctuations related to oceanographical changes in the Vocontian basin (SE France) during Aptian- Albian time. Geobios Mem. Spec., 11, 267–277

Bréhéret, J.-G., 1994. The mid-Cretaceous organic-rich sediments from the Vocontian zone of the French Southeast Basin, In: Mascle, A. (Eds) Hydrocarbon and Petroleum Geology of France, Springer-Verlag, New York, pp. 295–320

Brocks, J.J., Summons, R.E., 2003. Sedimentary Hydrocarbons, Biomarkers for Early Life, In: Treatise on Geochemistry, Vol. 8, pp. 63-115

Calvert, S. E., 1992. Evidence from nitrogen isotope ratios for enhanced productivity during formation of eastern Mediterranean sapropels. Nature, 359, 223–225.

Calvert, S. E., 1996. Influence of water column anoxia and sediment supply on the burial and preservation of organic carbon in marine shales. Geochimica et Cosmochimica Acta, 60, 1577–1593.

Chamberlin, T. C., 1906. On a possible reversal of deep sea circulation and its influence on geologic climate. Journal of Geology, 14, 363– 373

Cobban, W.A., 1951. Scaphitoid cephalopods of the Colorado Group. U.S. Geological Survey, Professional Paper 239, 42 p.

Cobban, W.A., 1984. Mid-Cretaceous ammonite zones, Western Interior United States, Bulletin, Geological Society of Denmark, 33, p.71-89

Cobban, W.A., and Hook, S.C., 1989. Mid-Cretaceous molluscan record from west-central New Mexico. New Mexico Geological Society, Guidebook 40, p. 247-264

Coccioni, R., and Galeotti, S., 1993. Orbitally induced cycles in benthonic foraminiferal morphogroups and trophic structure distribution patterns from the late Albian ‘‘Amadeus Segment’’ (central Italy), J. Micropaleontol., 12, 227 – 239

Collister J. W., Summons R. E., Lichtfouse E., and Hayes J. M., 1992. An isotopic biogeochemical study of the Green River oil shale. Organic Geochemistry, 19, 265–276

Cool, T. E., 1982. Sedimentological evidence concerning the paleoceanography of the Cretaceous western North Atlantic Ocean. Palaeogeogr. Palaeoclimatol. Palaeoecol., 39, 1– 35

Cowie, G.L., Hedges, J.I., Prahl, F.G., de Lange, G.J., 1995. Elemental and biochemical changes across an oxidation front in a relict turbidite: An oxygen effect. Geochimica et Cosmochimica Acta, 59, 33-46

Cowie, G., Calvert, S., de Lange, G., Keil, R., Hedges, J., 1998. Extents and implications of organic matter alteration at oxidation fronts in turbidites from the Medeira abyssal plain. Proceedings of the Ocean Drilling Program, Scientific Results, 157, 581-589

Curaile, J.A., 1994. High-resolution organic record of Bridge Creek deposition, northwest New Mexico. Organic Geochemistry, 21, 489-507

Davis, C., Pratt, L., Sliter, W., Mompart, L., and Murat, B., 1999. Factors influencing organic carbon and trace metal accumulation in the upper Cretaceous La Luna Formation of the western Maracaibo Basin, Venezuela. In: Barrera, E., and Johnson, C. (Eds) The Evolution of Cretaceous Ocean/Climate Systems. Geol. Soc. of Am., Boulder, Colo, vol. 332, pp. 203– 230,

Dean, W. E., Arthur, M.A., and Stow, D.A.V., 1984. Origin and geochemistry of Cretaceous deep-sea black shales and multicolored claystones, with emphasis on Deep Sea Drilling Project Site 530, southern Angola Basin. Initial Rep. Deep Sea Drill. Project, 75, 819– 844

Dean, W.E., Arthur, M.A., Claypool, G.E., 1986. Depletion of ^{13}C in Cretaceous marine organic matter: Source, diagenetic, or environmental signal? Marine Geology 70, 119–157

De Romero, L. M., Truskowski, I.M., Bralower, T.J., Bergen, J.A., Odreman, O., J. Zachos, J.C., and Galea-Alvarez, F.A., 2003. An integrated calcareous microfossil biostratigraphic and carbon-isotope stratigraphic framework for the La Luna formation, western Venezuela, Palaios, 18, 349– 366.

DeRosa, M., and Gambacorta, A., 1988. The lipids of Archaebacteria, Progress in Lipid Research, 27, 153–175

Didyk B. M., Simoneit B. R. T., Brassell S. C., and Eglinton G., 1978. Organic geochemical indicators of palaeoenvironmental conditions of sedimentation. Nature 272, 216–222

Dumitrescu M, Brassell SC., 2005. Biogeochemical assessment of sources of organic matter and paleoproductivity during the early Aptian Oceanic Anoxic Event at Shatsky Rise, ODP Leg 198, Organic Geochemistry, 36, 1002-1022

Dyman, T.S., Merewether, E.A., Molenaar, C.M., Cobban, W.A., Obradovich, J.D., Weimer, R.J., and Bryant, W.A., 1993. Stratigraphic transects for Cretaceous rocks, Rocky Mountains and Great Plains region. In: Caputo, M.V., Peterson, J.A., and Franczyk, K.J., (Eds) Mesozoic Systems of the Rocky region, USA. Rocky Mountain Association of Geologists, p. 365-392

Eglinton, G. and Hamilton, R.J., 1967. Leaf epicuticular waxes, Science, 156, 1322-1335

Elder, W.P., and Kirkland, J.I., 1993. Cretaceous paleogeography of the Colorado Plateau and adjacent areas, In: Morales, M. (Eds) Aspects of Mesozoic geology and paleontology of the Colorado Plateau. Museum of Northern Arizona Bulletin 59, p. 129-151

Emerson, S., Hedges, J.I., 1988. Processes controlling the organic carbon content of open ocean sediments. Paleoceanography 3, 621–634.

Erba, E., 1994. Nannofossils and superplumes: The early Aptian ‘‘nannoconid crisis’’, Paleoceanography, 9, 483– 501

Erbacher, J., Thurow, J., and Littke, R., 1996. Evolution patterns of radiolaria and organic matter variations: A new approach to identify sea level changes in mid-Cretaceous pelagic environments, Geology, 24, 499– 502, 1996.

Erbacher, J., Friedrich, O., Wilson, P.A., Birch, H., and Mutterlose, J., 2005. Stable organic carbon isotope stratigraphy across Oceanic Anoxic Event 2 of Demerara Rise, western tropical Atlantic. Geochem. Geophys. Geosyst., 6, Q06010, doi:10.1029/2004GC000850.

Ericksen, M.C., Slingerland, R., 1990, Numerical Simulations of Tidal and Wind-Driven Circulation in the Cretaceous Interior Seaway of North-America. Geological Society of America Bulletin, 102, 1499-1516

Erlich, R. N., SPalmer-Koleman, S.E., and Antonieta Lorente, M., 1999. Geochemical characterization of oceanographic and climatic changes recorded in upper Albian to lower Maastrichtian strata, western Venezuela. Cretaceous Res., 20, 547– 581

Fischer, A.G., 1980. Gilbert-bedding rhythms and geochronology In: Yochelson, E.I. (Eds) The Scientific Ideas of G.K. Gilbert. Geological Society of America Special Paper 183. p. 93-104

Fassett, J. E., 2000, Geology and coal resources of the Upper Cretaceous Fruitland Formation, San Juan Basin, New Mexico and Colorado. In: M. A. Kirschbaum, Roberts, L.N.R., and Biewick, L.R.H. (Eds) Geologic assessment of coal in the Colorado Plateau: Arizona, Colorado, New Mexico, and Utah. U.S. Geological Survey Professional Paper 1625-B, p. Q1–Q131

Fisher, C.G., Kaufmann, E.G., and von Holdt, W.L., 1985. The Niobrara transgressive hemicyclothem in central and eastern Colorado: the anatomy of a multiple disconformity. In: Pratt, L., Kaufmann, E.G., and Zelt, F. (Eds) Fine-Grained Deposits and Biofacies of the Cretaceous Western Interior Seaway-Evidence of Cyclic Sedimentary Processes. Society of Economic Paleontologists and Mineralogists Field Trip Guidebook, No. 4, 1985 Midyear Meeting, Golden Colorado, p. 184-198

Föllmi, K. B., Weissert, H., Bisping, M., and Funk, H., 1994. Phosphogenesis, carbon-isotope stratigraphy, and carbonate platform evolution along the Lower Cretaceous northern Tethyan margin, AAPG Bull., 106, 729–746

Gale, A. S., Jenkyns, H.C., Kennedy, W.J., and Corfield, R.M., 1993. Chemostratigraphy versus biostratigraphy: Data from around the Cenomanian- Turonian boundary, J. Geol. Soc. London, 150, 29– 32

Gill, J.R., and Cobban, W.A., 1966. The Red Birst Section of the Upper Cretaceous Pierre Shale in Wyoming. U.S. Geological Survey, Professional Paper 393-A, 73p.

Grantham P. J. and Douglas A. G., 1980. The nature and origin of sesquiterpenoids in some tertiary fossil resins. Geochimica et Cosmochimica Acta, 44, 1801–1810

Grice K., Schaeffer P., Schwark L., and Maxwell J. R., 1996. Molecular indicators of palaeoenvironmental conditions in an immature Permian shale (Kuperschiefer, Lower Rhine Basin, north-west Germany) from free and S-bound lipids. Organic Geochemistry, 25, 131–147.

Haig, D. W., and Lynch, D.A., 1993. A late early Albian marine transgressive pulse over northeastern Australia, precursor to epeiric basin anoxia: Foraminiferal evidence. Mar. Micropaleontol., 22, 311 – 362, 1993.

Hartgers W. A., Sinninghe Damste´ J. S., Requejo A. G., Allan J., Hayes J. M., Ling Y., Tiang- Min X., Primack J., and de Leeuw J. W., 1993. A molecular and carbon isotopic study towards the origin and diagenetic fate of diaromatic carotenoids. Organic Geochemistry, 22, 703–725

Hartnett H. E., Keil R. G., Hedges J. I., and Devol A. H., 1998. Influence of oxygen exposure time on organic carbon preservation in continental margin sediments. Nature 391, 572–574

Haq. B.U., Hardenbol, J. and Vail, P.R., 1987. Chronology of fluctuating sealevels since the Triassic, Science, v. 235, p.1156-1167

Hattin, D.E., 1982. Stratigraphy and depositional environmental environment of Smoky Hill Chalk Member, Niobrara Chalk (Upper Cretaceous) of the type area, western Kansas. Kansas Geological Survey, Bulletin 225, 108 p.

Hay, W.W., Eicher, D.L., and Diner, R., 1993. Physical Oceanography and Water Masses in the Cretaceous Western Interior Seaway, In: Caldwell, W.G.E., Kauffman, E.G. (Eds) Evolution of the Western Interior Basin. Geological Association of Canada, Special Paper 39, p.297-318

Hay, W. W., 1995. Cretaceous paleoceanography, Geology Carpathica, 46, 257– 266

Hayes, J.M., Popp, B.N., Takigiku, R., and Johnson, M.W., 1989. An isotopic study of biogeochemical relationships between carbonates and organic carbon in the Greenhorn Formation. Geochimica et Cosmochimica Acta, 53, 2961-2972

Hedberg H. D., 1968. Significance of high-wax oils with respect to genesis of petroleum. American Association of Petroleum. Geologists, Bull. 52, 736–750

Hedges J. I., Hu F. S., Devol A. H., Hartnett H. E., Tsamakis E., and Keil R. G., 1999. Sedimentary organic matter preservation: A test for selective degradation under oxic conditions. Am. J. Sci. 299**,** 529–555

Herbert, T. D., and Fischer, A.G., 1986. Milankovitch climate origin of mid-Cretaceous black shale rhythms, central Italy, Nature, 321, 739– 743, 1986.

Hilbrecht, H., Hubberten, H.W., and Öberhänsli, H., 1992. Biogeography of planktonic foraminifera and regional carbon isotope variations: Productivity and water masses in Late Cretaceous Europe. Palaeogeogr. Palaeoclimatol. Palaeoecol., 92, 407–421

Hoefs, M.J.L., Sinninghe Damste, J.S., de Lange, G., de Leeuw, J.W., 1998. Changes in kerogen composition across an oxidation front in Madeira abyssal plain turbidites as revealed by pyrolysis GC-MS. Proceedings of the Ocean Drilling Program Scientific Results, 157, 591-607

Hofmann, P., Ricken, W., Schwark, L., Leythaeuser, D., 2000. Carbon–sulfur–iron relationships and d13C of organic matter for late Albian sedimentary rocks from the North Atlantic Ocean: paleoceanographic implications. Palaeogeography, Palaeoclimatology, Palaeoecology 163, 97–113.

Holbourn, A., Kuhnt, W., Abderrazzak, E.A., Pletsch, T., Luderer, F., and Wagner, T., 1999. Upper Cretaceous paleoenvironments and benthic foraminiferal assemblages of potential source rocks from the western African margin, central Atlantic. In: Cameron, N., Bate, R., Clure, V. (Eds) The Oil and Gas Habitat of the South Atlantic, Geol. Soc., London vol. 153, pp. 195– 222

Hook, S.C., Molenaar, C.M., Cobban, W.A., 1983. Stratigraphy and revision of upper Cenomanian to Turonian (Upper Cretaceous) rocks of west-central New Mexico: New Mexico Bureau of Mines and Mineral Resources, Circular 185, p.7-28

Ishiwatari R., 1987. Diagenetic changes of lignin compounds in a more than 0.6 million-year-old lacustrine sediment (LAKE BIWA, Japan) Geochimica et Cosmochimica Acta 51, p.321

Jarvis, I., GCarson, G.A., Cooper, M.K.E., Hart, M.B., Leary, P.N., Tocher, B.A., Horne, D., and Rosenfeld, A., 1988. Microfossil assemblages and the Cenomanian-Turonian (Late Cretaceous) oceanic anoxic event. Cretaceous Res., 9, 3 –103

Jarvis, I., Gale, A.S., Jenkyns, H.C., Pearce, M.A., 2006. Secular variation in Late Cretaceous isotopes: a new $\delta^{13}C$ carbonate reference curve for the Cenomanian-Campanian (99.6-70.6 Ma), Geology Magazine, 143, p.561-608

Jenkyns, H. C., 1980. Cretaceous anoxic events: From continents to oceans, J. Geol. Soc. London, 137, 171– 188

Jenkyns, H. C., Gale, A.S., and Corfield, R.M., 1994. Carbon- and oxygen-isotope stratigraphy of the English Chalk and Italian Scaglia and its palaeoclimatic significance, Geol. Mag., 131, 1 –34

Jenkyns, H. C., 2001. Nitrogen isotope evidence for water mass denitrification during the early Toarcian (Jurassic) oceanic anoxic event, Paleoceanography, 16, 593–603.

Jewell P.W., 1996. Circulation, salinity, and dissolved oxygen in the cretaceous North American seaway, American Journal of Science, 296, 1093-1125

Jones, C. E., and Jenkyns, H.C., 2001. Seawater strontium isotopes, oceanic anoxic events, and seafloor hydrothermal activity in the Jurassic and Cretaceous, Am. J. Sci., 301, 112–149

Junium, C.K., Arthur, M.A., 2007. Nitrogen cycling during the Cretaceous, Cenomanian-Turonian Oceanic Anoxic Event II, Geochemistry, Geophysics, Geosystems, 8, p. 1-18

Kauffman, E.G., 1975. Dispersal and biostratigraphic potential of Cretaceous benthonic Bivalvia in the Western Interior, In: Caldwell, W.G.E. (Eds) The Cretaceous System in the Western Interior of North America. Geological Association of Canada, Special Paper 13, p. 163-194

Kaufmann, E.G., 1977. Geological and Biological Overview: Western Interior Cretaceous Basin. In: Kaufmann, W.G.E. (Eds) Cretaceous Facies, Faunas, and Paleoenvironments across the Western Interior Basin, Field Guide, North American Paleontological Convention II. The Mountain Geologist 13, p. 75-99

Kaufmann, E.G., 1984. Paleobiogeography and evolutionary response dynamic in the Cretaceous Western Interior Seaway of North America, In: Westermann, G.E.G., (Eds) Jurassic-Cretaceous Biochronology and Paleogeography of North America. Geological Association of Canada, Special Paper 27, p. 273-306

Kaufmann, E.G., 1985. Cretaceous Evolution of the Western Interior Basin of the United States. In: Pratt, L., Kaufmann, E.G., and Zelt, F. (Eds) Fine-Grained Deposits and Biofacies of the Cretaceous Western Interior Seaway-Evidence of Cyclic Sedimentary Processes. Society of Economic Paleontologists and Mineralogists Field Trip Guidebook, No. 4, 1985 Midyear Meeting, Golden Colorado, IV-XII

Kaufmann, E.G., 1993. The Western Interior in Space and Time. In: Caldwell, W.G.E., and Kaufmann, E.G. (Eds) Evolution of the Western Interior Basin. Geological Association of Canada Special Paper 39, p. 1-30

Kaufmann, E.G., 2007. Paleoecology of the Giant Inoceramidae (*Platyceramus*) on a Santonian (Cretaceous) Seafloor in Colorado, Journal of Paleontology, 81, p. 64-81

Kelly, V. C., 1951, Tectonics of the San Juan Basin, In: Guidebook of the south and west sides of the San Juan Basin, New Mexico and Arizona: New Mexico Geological Society, Guidebook to the 2nd Field Conference, p. 124– 131.

Kelly, V. C., 1955, Regional tectonics of the Colorado Plateau and relationship to the origin and distribution of uranium. University of New Mexico Publications in Geology, no. 5, 120 p.

Kelly, V. C., and Clinton, N.J., 1960. Fracture systems and tectonic elements of the Colorado Plateau. University of New Mexico Publications in Geology, no. 6, 104 p.

Kent, H.C., 1968. Biostratigraphy of Niobrara-equivalent part of Mancos Shale (Cretaceous) in Northwestern Colorado. American Association of Petroleum Geologists, Bulletin, v.52, p.2098-2115

Kerr, A. C., 1998. Oceanic plateau formation: A cause of mass extinction and black shale deposition around the Cenomanian-Turonian boundary, J. Geol. Soc. London, 155, 619–626

Killops, S. and Killops, V. (2005) Introduction to Organic Geochemistry 2nd ed. Blackwell Publishing, Malden, MA, USA

Kirkland, J.I., 1990. The paleontology and paleoenvironments of the middle Cretaceous (late-Cenomanian-middle Turonian) Greenhorn Cyclothem at Black Mesa , northeastern Arizona [PhD Dissertation], Boulder, University of Colorado, 1320p.

Kirkland, J.I., 1991. Lithostratigraphic and biostratigraphic framework for the Mancos shale (late-Cenomanian –middle-Turonian) at Black Mesa, northeastern Arizona. Geological society of America, Special Paper 260, p.85-111

Kohl W., Gloe A., and Reichenbach H., 1983. Steroids from the myxobacterium Nannocystis exedens. J. Gen. Microbiol. 129, 1629–1635

Kolonic, S., Wagner, T., Forster, A., Sinninghe-Damste´, J.S., Walsworth-Bell, B., Erba, E., Turgeon, S., Brumsack, H.-J., Chellai, E.H., Tsikos, H., Kuhnt, W., Kuypers, M.M.M., 2005. Black shale deposition on the northwest African shelf during the Cenomanian/Turonian oceanic anoxic event: Climate coupling and global organic carbon burial. Paleoceanography 20.

Koopmans M. P., Koster J., van Kaam-Peters H. M. E., Kenig F., Schouten S., Hartgers W. A., de Leeuw J. W., and Sinninghe Damste´ J. S., 1996. Diagenetic and catagenetic products of isorenieratene: molecular indicators for photic zone anoxia. Geochimica et Cosmochimica Acta, 60, 4467–4496

Kuypers, M.M.M., Pancost, R.D., Nijenhuis, I.A., Sinninghe Damste´, J.S., 2002. Enhanced productivity led to increased organic carbon burial in the euxinic North Atlantic basin during the late Cenomanian oceanic anoxic event. Paleoceanography, 17, 1051

Kuypers, M. M. M., 2004. N2-fixing cyanobacteria supplied nutrient N for Cretaceous oceanic anoxic events, Geology, 32, 853–856

Larson, R. L., 1991a. Geological consequences of superplume, Geology, 19, 963– 966

Larson, R. L.,1991b, Latest pulse of Earth: Evidence for a mid-Cretaceous superplume, Geology, 19, 547– 550

Larson, R. L., and Erba, E., 1999. Onset of the mid-Cretaceous greenhouse in the Barremian-Aptian: Igneous events and the biological, sedimentary, and geochemical responses. Paleoceanography, 14, 663– 678

Laubach, S. E., and Tremain, C.M., 1994. Tectonic setting of the San Juan Basin, In: Ayers, Jr. W.B., and Kaiser, W.R. (Eds) Coalbed methane in the Upper Cretaceous Fruitland Formation, San Juan Basin, New Mexico and Colorado. NewMexico Bureau of Mines and Mineral Resources Bulletin, v. 146, p. 9–11.

Leckie, R.M., Kirkland, J.I., and Elder, W., 1997. Stratigraphic Framework and Correlation of a Principal Reference Section of the Mancos Shale (Upper Cretaceous), Mesa Verde, Colorado. New Mexico Geological Society Guidebook, 48th Field Conference, Mesozoic Geology and Paleontology of the four Corners Region, p. 163-216

Leckie, R. M., Yuretich, R.F., West, O.L.O., Finkelstein, D., and Schmidt, M., 1998. Paleoceanography of the southwestern Western Interior Sea during the time of the Cenomanian-Turonian boundary (Late Cretaceous). In: Dean, W.E., and Arthur, M.A., (Eds) Stratigraphy and Paleoenvironments of the Cretaceous Western Interior Seaway, USA, Concepts in Sedimentol. Paleontol., Soc. Sediment. Geol., Tulsa, Okla., vol. 6, pp. 101 – 126

Leckie, R. M., Bralower, T. J., and Cashman, R. 2002. Oceanic anoxic events and plankton evolution: Biotic response to tectonic forcing during the mid-Cretaceous. Paleoceanography, 17

Levman, B. G., and von Bitter P.H., 2002. The Frasnian-Famennian (mid-Late Devonian) boundary in the type section of the Long Rapids Formation, James Bay Lowlands, northern Ontario, Canada. Can. J. Earth Sci., 39, 1795–1818.

Liu,Y., Chao, L., Li, Z., Wang, H., Chu, T., Zhang, J., 1984. Trace Elements Geochemistry. Science Press, Beijing, pp. 1–548

Ly, A., and Kuhnt W., 1994. Late Cretaceous benthic foraminiferal assemblages of the Casamance shelf (Senegal, NW Africa): Indication of a Late Cretaceous oxygen minimum zone. Rev. Micropaleontol., 37, 49– 74

Mackenzie, A.S., Leythaeuser, D., Altebaumer, F.J., Disko, U., and Rullkotter, J., 1988. Molecular measurements of maturity for Lias δ shales in N.W. Germany, Geochimica et Cosmochimica Acta, 52, 1145-1154

Macko, S. A., 1986. Kinetic fractionation of stable nitrogen isotopes during amino-acid transamination. Geochimica et Cosmochimica Acta, 50, 2143–2146

Mello, M. R., Telnaes, N., and Maxwell, J.R., 1995. The hydrocarbon source potential in the Brazilian marginal basins: A geochemical and paleoenvironmental assessment, In: Paleogeography, Paleoclimate, and Source Rocks

Menegetti, A.P., Weissert, H., Brown, R.S., Tyson, R.V., Farrimond, P., Strasser, A., Caron, M., 1998. High-resolution d13C stratigraphy through the early Aptian ‘‘Livello Selli’’ of the Alpine Tethys. Paleoceanography 13, 530–545

Meyers, P.A., 1989. Sources and deposition of organic matter in Cretaceous passive margin deep-sea sediments: a synthesis of organic geochemical studies from Deep Sea Drilling Project Site 603, outer Hatteras Rise. Marine and Petroleum Geology 6, 182–189.

Meyers, PA, 1997. Organic geochemical proxies of paleoceanographic, paleolimnologic, and paleoclimatic processes Organic Geochemistry 27, 213-250

Meyers PA, 1994. Preservation of elemental and isotopic source identification of sedimentary organic-matter Chemical Geology 114: 289

Meyers, P. A., and Bernasconi, S.M., 2005. Carbon and nitrogen isotope excursions in mid-Pleistocene sapropels from the Tyrrhenian Basin: Evidence for climate-induced increases in microbial primary production. Mar. Geol., 220, 41–58.

Meyers, P.A., Bernasconi, S.M., Forster, A., 2006. Origins and accumulation of organic matter in expanded Albanian to Santonian black shale sequences on the Demarara Rise, South American Margin. Organic Geochemistry, 37, p. 1816-1830

Milder, J. C., 1999. Carbon and nitrogen stable isotope ratios at sites 969 and 974; interpreting spatial gradients in sapropel properties. Proceedings Ocean Drill. Program Sci. Results, 161, 401–411

Minagawa, M. and Wada, E., 1986. Nitrogen isotope ratios of red tide organisms in the East China Sea: a characterization of biological nitrogen fixation. Mar. Chem., 19, 245–259

Molenaar, C.M., 1977. Stratigraphy and Depositional History of Upper Cretaceous Rocks of the San Juan Basin Area, New Mexico and Colorado, with a Note on Economic Resources, New Mexico Geological Society Guidebook, 28th Field Conference, San Juan Basin III, p. 159-167

Molenaar, C. M., 1983. Major Depositional Cycles and Regional Correlation of Upper Cretaceous Rocks, Southern Colorado Plateau and Adjacent Areas. In: Reynolds, W.M. and Dolley, E.D. (Eds) Mesozoic Paleogeography of the West-Central United States. Society of Economic Paleontologists and Mineralogists, Rocky Mountain section, Rocky Mountain Paleogeography Symposium 2, 201-224

Montadert, L. & Roberts, D.G., 1979. Initial Reports Deep Sea Drilling Project, 48, U.S. Government Printing Office, Washington D.C., 1183 pp.

Myers, K.J. and Wignall, P.B., 1987. Understanding Jurassic organic-rich mudrocks - new concepts using gamma-ray spectrometry and palaeoecology: examples from the Kimmeridge clay of Dorset and the Jet Rock of Yorkshire. In: Leggett, J.K., Zuffa, G.G. (Eds.), Marine Clastic Sedimentology. Graham and Trotman, London, pp. 172–189.

Ohkouchi, N., Kashiyama, Y., Kuroda, J., Ogawa, N.O., Kitazato, H., 2006. The importance of diazotrophic cyanobacteria as primary producers during Cretaceous Ocean Anoxic Event 2, Biogeosciences, 3, p. 467-478

Ourisson G. and Albrecht P., 1992. Hopanoids: 1. Geohopanoids: the most abundant natural products on Earth? Acc. Chem. Res. 25, 398–402

Pancost R. D., Freeman K. H., Patzkowsky E., Wavrek D. A., and Collister J. W., 1998a. Molecular indicators of redox and marine photoautotroph composition in the late Middle Ordovician of Iowa USA. Organic Geochemistry, 29, 1649–1662

Pancost, R.D., Freeman, K.H., and Arthur, M.A., 1998b. The Organic Geochemistry of the Cretaceous Western Interior Seaway: A Trans-Basinal Evaluation. In: Dean, W.E., and Arthur, M.A. (Eds) SEPM Concepts in Sedimentology and Paleontology No. 6

Peters, K.E., Moldowan, J.M., 2003. The Biomarker Guide, Prentice Hall, Englewood Cliffs, NJ

Postma, G., ten Veen, J.H., 1999. Astronomically and tectonically linked variations in gamma-ray intensity in Late Miocene hemipelagic successions of the Eastern Mediterranean Basin. Sedimentary Geology 128, 1– 12.

Poulsen, C. J., Barron, E.J., Arthur, M.A., and Peterson, W.H., 2001. Response of the mid-Cretaceous global ocean circulation to tectonic and CO_2 forcings, Paleoceanography, 16, 576 –592

Prahl, F.G., 1980. The early diagenesis of aliphatic-hydrocarbons and organic-matter in sedimentary particulates from Dabob Bay, Washington. Geochimica et Cosmochimica Acta, 44, 1967-1976

Pratt, L. M., and Threlkeld, C.N., 1984. Stratigraphic significance of 13C/12C ratios in mid-Cretaceous rocks of the Western Interior, U.S.A. In: Stott, D.F., and Glass, D.J. (Eds) The Mesozoic of Middle North America, Mem. Can. Soc. Pet. Geol., 9, 305– 312

Pratt, L. M., and King, J.D., 1986. Low marine productivity and high eolian input recorded by rhythmic black shales in mid-Cretaceous pelagic deposits from central Italy. Paleoceanography, 1, 507–522, 1986

Premoli Silva, I., Erba, E., and Tornaghi, M.E., 1989. Paleoenvironmental signals and changes in surface fertility in mid-Cretaceous Corg-rich pelagic facies of the fucoid marls (central Italy). Geobios Mem. Spec., 11, 225 – 236

Rau, G.H., Arthur, M.A., Dean, W.E., 1987. 15N/14N variations in Cretaceous Atlantic sedimentary sequences; implication for past changes in marine nitrogen biogeochemistry. Earth and Planetary Science Letters 82, 269–279.

Rogers, J.J.W. and Adams, J.A.S., 1976. Handbook of Thorium and Uranium Geochemistry

Rohmer M., Bouvier-Nave´ P., and Ourisson G., 1984. Distribution of hopanoid triterpenes in prokaryotes. J. Gen. Microbiol. 130, 1137–1150

Sachs, J. P., and Repeta, D.J., 1999. Oligotrophy and nitrogen fixation during eastern Mediterranean sapropel events, Science, 286, 2485–2488.

Sageman, B. B., Rich, J., Arthur, M.A., Dean, W.E., Savrda, C.E., and Bralower, T.J., 1998. Multiple Milankovitch cycles in the Bridge Creek Limestone (Cenomanian-Turonian), Western Interior Basin. In: Dean, W.E., and Arthur, M.A. (Eds) Stratigraphy and Paleoenvironments of the Cretaceous Western Interior Seaway, USA, Concepts in Sedimentol. Paleontol., Soc. Sed. Geol., Tulsa, Okla vol. 6, pp. 153– 171

Scholle, P. A., and Arthur, M.A., 1980. Carbon isotope fluctuations in Cretaceous pelagic limestones: Potential stratigraphic and petroleum exploration tools, AAPGeol. Bull., 64, 67– 87

Schlanger, S.O. and Jenkyns, H.C., 1976. Cretaceous oceanic anoxic events: causes and consequences, Geol. Mijnbouw, 55, 179-184

Schlanger, S. O., Arthur, M.A., Jenkyns, H.C., and Scholle, P.A., 1987. The Cenomanian-Turonian oceanic anoxic event, Stratigraphy and distribution of organic carbon-rich beds and the marine C excursion. In: Brooks, J., and Fleet, A.J. (Eds) Marine Petroleum Source Rocks, Geol. Soc. Spec. Publ., 26, 371 – 399

Schouten, S., E., Hopmans, E.C., Schefuss, E., and Sinninghe Damste´, J.S., 2002. Distributional variations in marine crenarchaeotal membrane lipids: A new tool for reconstructing ancient sea water temperatures? Earth and Planetary Science Letters, 204, 265– 274

Scott, G.R., and Cobban, W.A., 1964. Stratigraphy of the Niobrara Formation at Pueblo, Colorado: U.S. Geological Survery, Professional Paper 454-L, p.L1-L30

Scott, R.W., and Taylor, A.M., 1977. Upper Cretaceous environments and paleocommunities in the southern Western Interior, In: Kaufmann, E.G. (Eds) Cretaceous Facies, Faunas, and Paleoenvironments across the Western Interior Basin: The Mountain Geologist, v.14, p.155-173

Scott, G.R., Cobban, W.A., Merewether, E.A., 1986. Stratigraphy of the Upper Cretaceous Niobrara Formation in the Raton Basin, New Mexico, New Mexico Bureau of Mines and Mineral resources , Bulletin 115, 34 p.

Seifert, W.K., and Moldowan, J.M., 1980. The effect of thermal stress on source-rock quality as measured by hopanes stereochemistry, Physics and chemistry of the Earth, 12, 229-237

Silliman J.E., 1996. Record of postglacial organic matter delivery and burial in sediments of Lake Ontario, Organic Geochemistry, 24, 463

Silver, C., 1957. Relation of coastal and submarine topography to Cretaceous stratigraphy (New Mexico): Four Corners Geological Society Guidebook, Geology of southwestern San Juan Basin, Second Field Conference, p. 128–137.

Simoneit, B.R.T., 1986. Biomarker Geochemistry of Black Shales from Cretaceous Oceans - An Overview, Marine Geology, 70, 9-41

Simons, D.-J. H. and Kenig, F., 2001. Molecular fossil constraints on the water column structure of the Cenomanian-Turonian Western Interior Seaway, USA. Palaeogeography Palaeoclimatology Palaeoecology 169, 129-152

Sinninghe Damste´ J. S., Schouten S., and van Duin A. C. T., 2001. Isorenieratene derivatives in sediments: possible controls on their distribution. Geochimica et Cosmochimica Acta, 65, 1557–1571

Sinninghe Damsté, J.S., Rijpstra, W.I.C., and Reichart, G.-J., 2002. The influence of oxic degradation on the sedimentary biomarker record II. Evidence from Arabian Sea sediments. Geochimica et Cosmochimica Acta, 66, 2737–2754

Sinton, C. W., and Duncan, R.A., 1997. Potential links between ocean plateau volcanism and global ocean anoxia at the Cenomanian-Turonian boundary, Econ. Geol., 92, 836– 842

Sliter, W. V., 1989. Aptian anoxia in the Pacific basin, Geology, 17, 909–912

Snow, L. J., and Duncan, R.A., 2001. Hydrothermal links between ocean plateau formation and global anoxia, Eos Trans. AGU, 82(47), Fall Meet. Suppl., abstract OS41A-0437, 2001

Sohl, N.F., 1969. North American biotic provinces delineated by gastropods: Proceedings, North American Paleontological Convention, pt. 1, p.1610-1638

Spearing, D.R., 1976. Upper Cretaceous Shannon Sandstone, and offshore shallow marine sand body: Wyoming Geological Association, 28th Annual Conference Guidebook, p.65-72

Sugarman, P. J., Miller, K.G., Olsson, R.K., Browning, J.V., Wright, J.D., De Romero, L.M., White, T.S., Muller, F.L., and Uptegrove, J., 1999. The Cenomanian/Turonian carbon burial event, Bass River, NJ, USA: Geochemical, paleoecological, and sea-level changes. J. Foraminiferal Res., 29, 438– 452

Summerhayes, C. P., 1981. Organic facies of middle Cretaceous black shales in the deep North Atlantic. AAPG Bull., 65, 2364–2380

Summerhayes, C. P., 1987. Organic-rich Cretaceous sediments from the North Atlantic. In: Brooks, J. and Fleet, A.J. (Eds) Marine Petroleum Source Rocks. Geol. Soc. Spec. Publ., 26, 301– 316

Summons, R.E., Powell, T.G., 1986. Chlorobiaceae in Paleozoic seas revealed by biological markers, isotopes, and geology, Nature, 319, 763-765

Tarduno, J. A., Sliter, W.V., Kroenke, L., Leckie, M., Mayer, H., Mahoney, J.J., Musgrave, R., Storey, M., and Winterer, E.L., 1991. Rapid formation of Ontong Java Plateau by Aptian Mantle Plume Volcanism, Science, 254, 399– 403

Thiede, J., and van Andel, T.H., 1977. The deposition of anaerobic sediments in the late Mesozoic Atlantic Ocean, Earth Planet. Sci. Lett., 33, 301–309

Thompson, S. and Eglinton, G., 1978, Fractionation of a recent sediment for organic geochemical analysis. Geochimica et Cosmochimica Acta, 42, 199-221

Thurow, J., Brumsack, H.J., Rullkötter, J., Littke, R., and Meyers, P., 1992. The Cenomanian/Turonian boundary event in the Indian Ocean—A key to understand the global picture. In: Synthesis of Results From Scientific Drilling in the Indian Ocean, Geophys. Monogr. Ser., vol. 70, pp. 253–273, AGU, Washington, D.C., 1992

Tissot B. P. and Welte D. H., 1984. Petroleum Formation and Occurrence. Springer, Berlin, Germany

Tsikos, H., Jenkyns, H.C., Walsworth-Bell, B., Petrizzo, M.R., Forster, A., Kolonic, S., Erba, E., Premoli-Silva, I., Baas, M., Wagner, T., Sinninghe-Damste´, J.S., 2004. Carbon-isotope stratigraphy recorded by the Cenomanian–Turonian oceanic anoxic event: correlation and implication based on three localities. Journal of the Geological Society 161, 711–719

Tucholke, B.E., and Vogt, P.R., 1979. Western North Atlantic: Sedimentary evolution and aspects of tectonic history, Initial Rep. Deep Sea Drill. Proj., 43, 791– 825

van Andel, T.H., Thiede, J., Sclater, J.G., and Hay, W.W., 1977. Depositional history of the South Atlantic Ocean during the last 125 million years, J. Geol., 85, 651– 698

Van der Weijden, C.H., Middelburg, J.J., De Lange, G.J., Van der Sloot, H.A., Hoede, D., Woittiez, J.R.W., 1993. Profiles of the redox-sensitive trace elements As, Sb, V, Mo and U in the Tyro and Bannock Basins (eastern Mediterranean). Mar. Chem. 31, 171–186

Van Mooy, B.A.S., 2002. Impact of suboxia on sinking particulate organic carbon: Enhanced carbon flux and preferential degradation of amino acids via denitrification, Geochimica et Cosmochimica Acta, 66, 457–465.

Velinsky, D.J., and Fogel, M.L., 1999. Cycling of dissolved and particulate nitrogen and carbon in the Framvaren Fjord, Norway: Stable isotopic variations. Mar. Chem., 67, 161–180.

Volkman J. K., 2003. Sterols in microorganisms. Appl. Microbiol. Biotechnol. 60, 496–506

Wada, E. and Hattori, A., 1991. Nitrogen in the Sea: Forms, Abundances, and Rate Processes, CRC Press, Boca Raton, FL, USA

Wagner, T., and Pletsch, T., 1999. Tectonosedimentary controls on Cretaceous black shale deposition along the opening equatorial Atlantic gateway (ODP Leg 159). In: Cameron, N., Bate, R., and Clure, V. (Eds) The Oil and Gas Habitat of the South Atlantic, Geol. Soc., London, vol. 153, pp. 241– 265

Wagner, T, Herrle, JO, Damste, JSS, Schouten, S, Stusser, I, Hofmann, P, (2008) Rapid warming and salinity changes of Cretaceous surface waters in the subtropical North Atlantic, *Geology*, **36**, 203-206

Wedepohl, K.H., Correns, C.W., Shaw, D.W., Turekian, K.K., Zemann, J., 1978. Handbook of Geochemistry, vol.1-11(1–5).Springer-Verlag, New York.

Weijers, J.W.H., Schouten, S., Hopmans, E.C., Geenevasen, J.A.J., David, O.R.P., Coleman, J.M., Pancost, R.D., Sinninghe Damste´, J.S., 2006. Membrane lipids of mesophilic anaerobic bacteria thriving in peats have typical archaeal traits. Environmental Microbiology, 8, 648–657

Weijers, J.W.H., Schouten, S., van den Donker, J.C., Hopmans, E.C., Sinninghe Damste´, J.S.S., 2007. Environmental controls on bacterial tetraether membrane lipid distribution in soils, Geochimica et Cosmochimica Acta, 71**,** 703–713

Weissert, H., and Lini, A., 1991. Ice age interludes during the time of Cretaceous greenhouse climate? In: Mueller, W. (Eds) Controversies in Modern Geology, Academic, San Diego, Calif., pp. 173– 191,.

White, T and Arthur, M.A., 2006. Organic carbon production and preservation in response to sea-level changes in the Turonian Carlile Formation, U.S. Western Interior Basin. Palaeogeography, Palaeoclimatology, Palaeoecology, 235**,** 223-244

Wignall, P.B., Myers, K.J., 1988. Interpreting benthic oxygen levels in mudrocks: a new approach. Geology, 16, 452–455

Wignall P.B., Twitchett R.J., 1996. Oceanic anoxia and the end Permian mass extinction. Science, 272, 1155-1158

Wilson, P. A., and Norris, R.D., 2001. Warm tropical ocean surface and global anoxia during the mid-Cretaceous period, Nature, 412, 425– 429

Zimmerman, H. B., Boersma, A., and McCoy, F.W., 1987. Carbonaceous sediments and paleoenvironment of the Cretaceous South Atlantic Ocean. In: Brooks, J., and Fleet, A.J. (Eds) Marine Petroleum Source Rocks, Geol. Soc. Spec. Publ., 24, 271– 286